Fabrication and Characterization of N-doped CVD graphene-based gas sensors for NO_2 gas sensing applications

Microelectronics Department, Faculty of EEMCS

ET4300: Master Thesis Electrical Engineering

Bram Kool

Delft University of Technology

TU Delft

Fabrication and Characterization of N-doped CVD graphene-based gas sensors for NO_2 gas sensing applications

Microelectronics Department, Faculty of EEMCS

by

Bram Kool

Student Name	Student Number
Bram Kool	4291492

Thesis advisor:	Sten Vollebregt
Daily supervisor:	Mudassir Husain
Project Duration:	June, 2024 - February, 2025
Faculty:	Faculty of EEMCS, Delft

Cover:	Artistic portrayal of gas sensors in their final application, created by Image Creator from Microsoft Designer
Style:	TU Delft Report Style, with modifications by Daan Zwaneveld

TU Delft

Acknowledgements

The process of graduation went with ups and downs for me as some people know, but a number of people really helped me stay motivated throughout the project, and I want to sincerely thank them for their support.

First of all I would like to thank Sten Vollebregt for the project offer, for the weekly meetings we had, and for the supervision and ideas when I got stuck with the research. Second, thanks to my daily supervisor, Mudassir Husain, for helping me out with a lot of cleanroom processes that I couldn't have done alone, especially the handling of chemicals that I'm certainly not an expert in.

Of course I'm really grateful for ECTM as a group and all of its wonderful people. Finding people to have lunch with was never hard, and if you wanted to have a laugh you could walk into the social room for a coffee and a talk. Especially the 'dilemma op dinsdag' was usually a heated topic of debate...

Special shout out to my office mates Koen, Maria and Jonas, who always made sure that something happened, from dank toilet memes to water guns, and from cleanroom frustrations to sharing victories. My thesis never felt like sitting alone in a dark student cave thanks to you!

Of course it was not just people from ECTM supporting me. First and foremost I want to express my gratitude to my girlfriend Leonoor, who was always there for me, could help me see the sunny side of things, and remind me that there is more to life than a master's thesis. I love you from the bottom of my heart!

My friends that I could always count upon, thank you for you support, and for doing the cool stuff that we did together. Special shout-out to Tim, Felix, Rutger, Henk, Maarten, Ruben, Jos, Jeroen, Levi, Joël, PC, William and of course Pieter. For all the electronics projects, tank related nerd stuff, fireworks madness, survivalrunning, drinking beer, bushcrafting, parkour, guitar jamming, motorcycle riding, and good stories about all of this we share. Let's never stop doing these!

To my room mates, that I have lived together with for almost two years now. Thanks for the many talks and stuff we celebrated together, the weekends away, and the stuff we had to repair in our shitty house. I'll never forget how taking a shower causes your fuses to blow, and how a broken roof window will make it rain inside your house. No worries, these will all become positive memories... after some-time :)

And last but certainly not least thanks to my family, my parents and my sisters, for their support and unconditional love during the last part of my studies. For always being available for a chat and for loving me the way I am. And of course for the Toyota wiper fluid tank you bought for me as a graduation present. Thank you!

Bram Kool
Delft, June 2025

Abstract

Air pollutants like NO_2 are harmful in small concentrations, and gas sensors are needed that can detect gases in such low quantities. A promising candidate for this is doping graphene, a single layer of carbon atoms, with nitrogen impurities, and using this material as a chemoresistor. This thesis investigates the fabrication and characterization of this nitrogen-doped graphene (NDG) in a low-pressure chemical vapor deposition (LPCVD) process. This is first tested with a mixture of methane and ammonia gas as carbon and nitrogen precursors respectively. After this is proven to be ineffective, a benzene-like liquid called pyridine is bubbled into the reactor to supply both the carbon and nitrogen, and grow graphene on both copper and molybdenum catalysts. The graphene is characterized by Raman spectroscopy, SEM, FTIR, EDX and XPS measurements. The CVD parameters are changed to optimize the quality of the grown graphene. The nitrogen doping couldn't be confirmed, but a CVD recipe is now available to grow graphene with pyridine, manufacture a gas sensor with this new material and conduct NO_2 gas tests to measure the sensor's sensitivity.

Contents

List of Figures

List of Tables

Nomenclature

Abbreviations

Abbreviation	Definition
NDG	Nitrogen Doped Graphene
PG	Pristine Graphene
CVD	Chemical Vapor Deposition
MHP	Micro Hot Plate
(r)GO	(reduced) Graphene Oxide
CNT	Carbon Nanotubes
BM	Aixtron Black Magic Pro
PVD	Physical Vapor Deposition
MFC	Mass Flow Controller
SSP	Single Side Polished
DSP	Double Side Polished
ORR	Oxygen Reduction Reaction
ARPES	Angle-Resolved Photo Electron Spectroscopy
STP	Standard Pressure and Temperature
(FE)SEM	(Field Emission) Scanning Electron Microscopy
EDX	Energy Dispersive X-ray analysis
XPS	X-ray Photoelectron Spectroscopy
TFP	Transfer Free Process
...	

Symbols

Symbol	Definition	Unit
V	Voltage	[V]
I	Current	[A]
Z	Atomic number	[# protons]
Q	Flow rate	[sccm]
E_G	Bandgap energy	[eV]
F	Volume flow	[sccm]
P	Pressure	[Pa]
q	Electric charge	[C]
...		
ρ	Resistivity	[Ωcm]
σ	Conductivity	[S/cm]
λ	Wavelength	[nm]
ϕ	Work function	[eV]
χ	Electron affinity	[eV]
...		

1

Introduction

Gas sensing has been a concern of humankind for two centuries now. The first gas detection systems were the canaries that coal miners would bring with them in the tunnels where they worked. If the canary would stop singing or even faint, the miners knew there would probably be a harmful gas in the air, like carbon monoxide or methane, and they could exit the mine quickly. In the 19th century the flame safety lamp was invented by sir Humphry Davy, where the height of a flame in an oil lamp would rise if a combustible gas, like methane, was present, and fall if the oxygen level was dropping. From the 20th century on, electronic systems that could detect gases and vapors started to enter the market, mainly focused on safety of plants and personnel, that could detect multiple combustible gases, and also monitor the oxygen level. Ever since, gas detection has been an important trade in society.

Nowadays, gas sensing serves a great variety of purposes, like laboratory safety, environmental monitoring, and in firefighting. A common use is to measure harmful air pollutants, like sulphur dioxide (SO_2), nitrogen dioxide (NO_2) and hydrogen sulphide (H_2S), which are caused by industry emissions and burning of fossil fuels. Those gases are toxic in small concentrations already, and bring risks for human health and the environment. In this context, this thesis will focus on NO_2 gas, since it acts as greenhouse gas, contributes to acid rain and can cause respiratory tract infections in humans. Being able to detect this gas in low concentrations is important, for even below 100 ppm, this gas can already pose health risks in the long term.

In this research, the focus is on achieving this low concentration gas detection with the help of a graphene-based gas sensor. Graphene is a promising material for such a sensor, because of its high specific surface area and large carrier mobility. To enhance the performance even further, the nitrogen-doping of graphene is studied to make it more sensitive for gas adsorption, and more selective towards certain gases. Such sensors can potentially be manufactured in a CMOS process, using the chemical vapor deposition technique, to achieve larger, continuous areas of nitrogen-doped graphene. When integrated in a larger array, this enables us to achieve an e-nose device, which makes the detection of a variety of different gases possible via pattern recognition.

A lot of work has already been done on the nitrogen-doping of graphene. A recent literature review has been written on this topic by G. Deokar et al. [1] and this thesis will build on top of that work. We will mainly focus on optimizing the CVD process for growing large area nitrogen-doped graphene, fabricating the sensor with this material, and testing and characterizing both material and sensor for the NO_2 sensing performance.

The following chapter gives background information for gas sensing and why graphene is a promising material for this. Chapter three contains experimental information on the processes used in the cleanroom, and why certain CVD parameters were chosen. Chapter four explains the different characterization techniques used for testing the grown graphene, and how they work. In chapter five and six, we elaborate on the measurement results and show the data. This is followed by a discussion, conclusion and future work chapter.

2

Background information

This chapter will give information on the mechanics of gas sensing, list some of the materials that are already being used for it, state why graphene is a good candidate to replace those materials, and explain why doping the graphene with hetero atoms might improve its performance.

2.1. Gas sensing

There are different methods to achieve the goal of gas sensing, which is to measure a given amount of gas, and turn it into a signal containing information about the presence, concentration, and ideally also the type of gas. To name a few, one can use optical, surface acoustic wave, electrochemical, catalytic and chemoresistive (semiconductor) sensors[2]. In this thesis the focus is on the chemoresistive type, since graphene falls in this category. The electrochemical and chemoresistive types sometimes get mixed up because of the name resemblance, but they are definitely two distinct types of gas sensing.

The classical operation of chemoresistive gas sensors is shown in figure 2.1. It relies on chemical interactions between the surface material and the gases in ambient air. When a gas sensitive material is heated to a few hundred degrees, oxygen molecules will adsorb to its surface and generate surface bonding states. It is this adsorbed oxygen that the introduced gas interacts with, giving rise to electron transport between the oxygen and the semiconductor material. Gases can be divided in oxidizing and reducing gases, and the semiconducting material can be of the n- or p-type. Based on the combination of those, gases that react with the oxygen will either increase or decrease the electrical resistance of the semiconductor, which can in turn be read out with electronics.

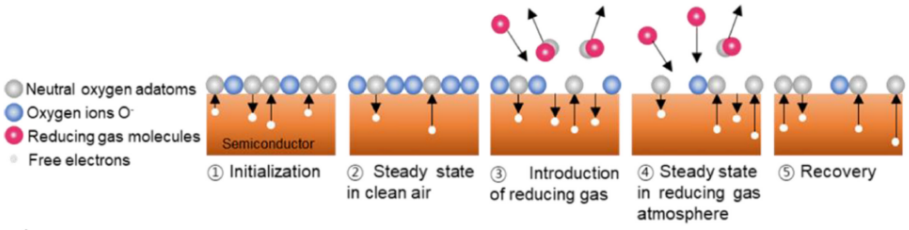

Figure 2.1: The steps in chemoresistive sensing. Picture taken from [2]

Next to this method, one can also use gas sensors based on field effect transistors [3]. Here, the sensitive material is used as the active layer for the device, and a gate is added to influence the current by means of gate bias. The gate is usually a back-gate, so that the gas-sensitive surface is completely open to gas reception. This method offers very high sensitivity, but the gate voltage needs to be driven with several tens of volts, which poses some problems for device integration. This method will be used later on for material characterization, since it will show n-type or p-type doping.

2.2. Gas sensitive materials

There are already a wide variety of semiconductor materials being used for gas sensing. In this section the most common ones will be listed, together with some of their characteristics. It's by no means an exhaustive list, since the amount of materials tested for their gas sensitive properties is rather big. All the same, this will give us an idea about what can still be improved by using different materials.

2.2.1. Metal oxides

The biggest group of materials being used is that of the metal oxides (MO_x) [4]. From this group, the most well known material is tin oxide (SnO_2) [5], which is an n-type semiconductor. It is sensitive to a wide variety of gases, including ammonia, ethanol and acetone vapour. The main drawbacks are that it is only sensitive to gases at higher temperatures, generally in between 200 and 500 °C, and that it shows a very similar reaction to a lot of different gases, and thus is not very selective.

Another abundantly researched metal oxide is Zinc oxide (ZnO), also an n-type semiconductor. It is sensitive to multiple gases as well, including carbon monoxide, formaldehyde and methanol. The list of detectable gases overlaps for a large part with that of SnO_2. The n-type characteristic means that this material is mainly sensitive to reducing gases [6].

Examples of p-type semiconductor metal oxides are nickel oxide (NiO) and cobalt oxide (Co_3O_4), which are better in sensing oxidizing gases. On their list are toluene, ethanol, isopropanol, ammonia and NO_2. All of those metal oxides have to be heated up by a micro hot plate (MHP) to make them sensitive to ambient gases, and thus are quite power hungry, easily consuming hundreds of milliwatts, which makes them not really suitable for portable devices. Furthermore they have to be decorated with nanoparticles, like platinum (Pt) or palladium (Pd), to make them selective to certain gases.

2.2.2. Nitrides

Another group of materials are the binary nitrides (MN_x) [4]. A common example of a nitride gas sensing material is boron nitride (B_3N_4), which is a III-V compound. Interestingly enough, it's also called "white graphene", since it has the same honeycomb crystal lattice as graphene, with sp^2-hybridized bonds between the B- and N-atoms. This material has been tested to be sensitive to LPG, with impressive response and recovery times (55s and 40s respectively) [7]. Next to that it can also be used as humidity sensor, mainly in the lower regions of RH (10-40% RH).

There is another interesting material in this group, called graphitic carbon nitride (g-C_3N_4), which is a polymeric and crystalline semiconducting material [8]. This CN allotrope looks remarkably like graphene doped with nitrogen, and is also a 2D material, where many of the layers can be held together by van der Waals forces to form a bulk material, just like graphene. It has been found to be sensitive to ethanol and NO_2, the latter of which makes it even more interesting, since our graphene-based gas sensor is aimed at the same gas. However, to get to the separate layers, this material is synthesized in bulk and must then be exfoliated, which is not a scalable process.

2.2.3. Metal sulfides

This group is relatively new, and not a lot of materials have been reported to be useful for gas sensing yet, but there are some promising candidates. Three important ones are Cadmium sulfide (CdS), Copper sulfide (Cu_2S) and Zinc sulfide (ZnS) [4]. Cadmium sulfide is a II-VI n-type semiconductor, with a bandgap of approximately 2.42 eV. It can be produced by CVD among others, and is sensitive to ethanol, isopropanol and NO_2. Combined with nanoparticles on its surface it can be made selective to a specific gas.

Zinc sulfide is a II-VI semiconductor as well, but with a much larger bandgap at 3.66 eV. It has two crystalline forms, of which only one (face centered cubic) is stable at room temperature. Just like CdS, this material offers quite some detectable gases, such as NO_2, gasoline (vapor), n-butanol, acetone and formaldehyde. It's mainly been synthesized hydrothermally, but thermal co-evaporation is also possible. This material has vacancies on its surface which promotes the adsorption of oxygen, which enhances its gas sensing ability.

The main advantage of metal sulfides over graphene-based gas sensors, is that they have a bandgap, making transistor applications possible. Next to that they can also work at room temperature, use abundant materials, and have the potential to be sensitive to a lot of polluting gases. Just like the metal oxides, these materials have been decorated with nanoparticles to make them more selective to specific gases.

2.2.4. Transition metal dichalcogenides (TMDs)

A closely related group to metal sulfides are the TMDs. Those materials use a metal in between two chalcogen elements, which is the group of oxygen, and further contains sulfur (S), selenium (Se) and tellurium (Te). They form a hexagonal lattice, and are layered 2D materials, where the layers are bound by weak van der Waals forces, just like graphene. Three notable materials in this group are SnS_2, MoS_2 and WS_2, which can all be fabricated by use of the CVD method, and have a tuneable bandgap. These specific three materials are obviously also sulfides, and are therefore sometimes also included in that group, like in [9]. Here, it is shown that MoS_2 can be doped with metal impurities to change the adsorption energy towards different gases, and hence make the sensors more selective.

2.3. Graphene

In this thesis the focus will be on carbon nanomaterials, more specifically on graphene. It is one of the allotropes of carbon, other notable ones being diamond, carbon nanotubes (CNTs) and fullerenes [10]. Graphene is a single layer of graphite, and with that a 2D material, where C-atoms are bonded together in a honeycomb lattice. The bonds in one graphene layer are strong covalent bonds, while the bonds between layers are weak van der Waals bonds. Carbon has an atomic number of 6, and 4 valence electrons in its outer shell, just like silicon (Si), which is a well known semiconductor. These 4 valence electrons are the cause of the many possible allotropes of carbon.

2.3.1. Hybridization

To understand the specific bonding of graphene better, we have to look at a concept known as electron orbitals. This model builds on top of the Bohr model, where all the electrons are moving in circular orbits around the nucleus, with different radii, and a different number of electrons fitting in each shell. Orbitals are, strictly speaking, functions describing the location and wave-like behavior of an electron in an atom. They are probability based, and specify where an electron can likely be found around the nucleus. Those orbitals are usually depicted as a certain shape in which the electron moves, and there are four (known) types, called s-, p-, d- and f-orbitals. They will also be filled with electrons in this order with increasing atomic size, which is due to the required energy for the electrons to be in a certain orbital. A graphic overview of the orbitals is given in figure 2.2.

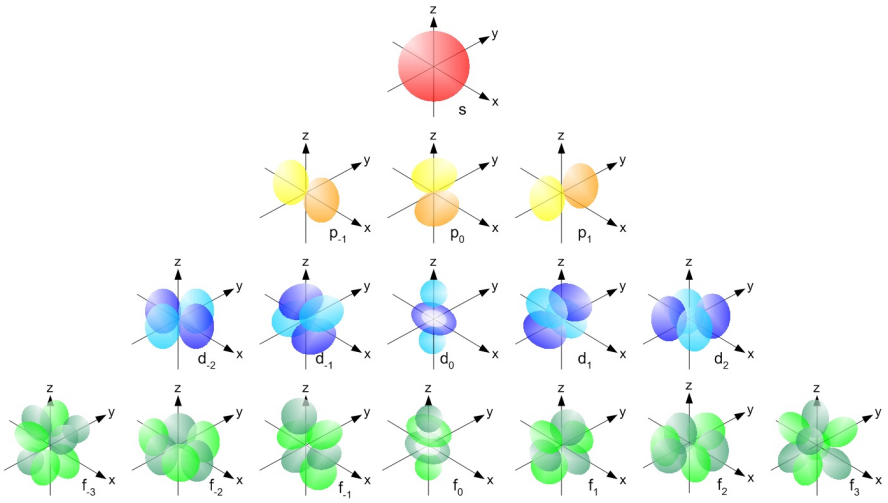

Figure 2.2: The possible orbitals electrons take around the atomic nucleus.

The number of the orbitals in this image is not arbitrary. It corresponds to the elements in the periodic table. Each of the orbitals depicts two spots that can be taken up by electrons, one with spin up, and one with spin down. This means that s-, p-, d- and f-orbitals have 2, 6, 10 and 14 electron vacancies respectively, no more, no less. To make things more complicated, not each atomic shell has all 4 types of orbitals, and some orbitals of the next shell will fill up before the current shell is completely full. This gives rise to the s-, p-, d- and f-blocks in the periodic table not being in that order from left to right. The first shell has only s-orbitals (2 vacancies), the second has s- and p-orbitals (2 + 6 = 8 vacancies), the third shell has s-, p- and d-orbitals (2 + 6 + 10 = 18 vacancies) and the fourth shell has s-, p- d- and f-orbitals (2 + 6 + 10 + 14 = 32 vacancies). From the fifth shell onward, more orbitals should exist in which electrons can move, but those orbitals will only fill up after the seventh shell, and no elements are known after that shell, so these orbitals are irrelevant in this discussion.

Going back to graphene, carbon has 2 electrons in its first shell as s-orbitals ($1s^2$), 2 electrons in the second shell as s-orbitals ($2s^2$), and 2 electrons in the second shell as p-orbitals ($2p^2$). This leaves 4 p-orbital electrons to be filled up to complete the shell, after which you would end up with the noble gas neon (Ne). The electron configuration in the outer shell of an atom largely governs how that atom bonds to other elements to form molecules. These electrons are called valence electrons. But since the s-orbitals in the second shell are completely filled, this would mean that carbon has only 3 p-orbitals that are trying to bond with other atoms, 2 half-filled (only spin up or spin down occupied), and 1 completely empty, adding up to 3 valence electrons, which is not in compliance with the molecules carbon forms. This can be explained by the concept of hybridization.

As mentioned, carbon has 4 valence electrons, so all electrons in the second shell play a role in the molecular bonds that are formed. When this happens, electrons are said to be hybridized, and in case of carbon they do this in one of three forms, **sp, sp^2 or sp^3** hybridized forms. In the second case, one s-orbital electron and two p-orbital electrons (hence the name) all fill a similar shaped orbital which is a hybrid between an s- and a p-orbital. This means it has slightly higher energy than an s-orbital, but lower energy than a p-orbital. The result is an atom with three sp^2 orbitals and one remaining, half-empty p-orbital. In graphene, the three sp^2 hybridized electrons form a planar honeycomb structure, where each C-atom is σ-bonded to three neighbouring C-atoms, see figure 2.3. The remaining p-orbital (shown in purple) is π-bonded and gives rise to electric conduction. Multiple layers of graphene can be held together by van der Waals bonds, which forms graphite. In contrast, sp^3 hybridization can be found in diamond, where each C-atom bonds 4 of its neighbours, all with σ-bonds, forming a really strong, tetrahedral crystal lattice. On the other hand, sp hybrids can be found in the triple bonded acetylene for example, where two of the three bonds are π-bonds, and the remaining σ-bond is made up of two sp hybridized electrons.

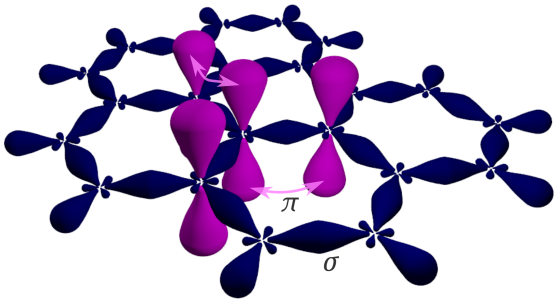

Figure 2.3: The sigma and pi bonds in graphene

2.3.2. Electronic properties of graphene

Graphene has some unique traits. First of all it's classified as a semimetal. This means that its electronic band structure shows no bandgap, but the valence and conduction band only slightly overlap, and the density of states is low at the Fermi level. This means it has good conduction like a metal, but this conductivity is governed by both electron and hole mobility. This also means the material can be doped to make it either n-type or p-type, depending on the dopant.

The electron mobility of graphene is high, with values reported well over $\mu_g = 12000 cm^2 V^{-1} s^{-1}$ [11]. Compare this for example with crystalline silicon, which has electron mobility of $\mu_s = 1400 cm^2 V^{-1} s^{-1}$, or common metals (Al, Au, Cu, Ag) which are in the range of $\mu_m = 10 - 50 cm^2 V^{-1} s^{-1}$. This means that graphene can have a very high conductivity, ρ, even though it has much less charge carriers available compared to a metal. The resulting resistance is heavily influenced by adsorption of other molecules on the graphene surface, but we'll come to that in the next section.

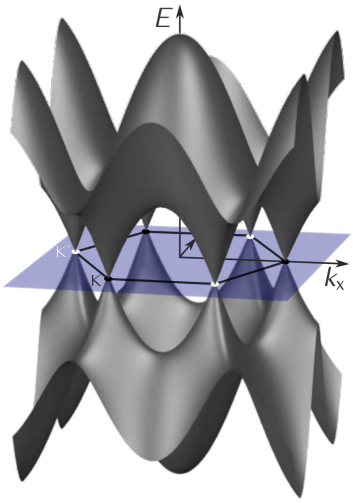

Figure 2.4: The electronic band structure of graphene in k-space.

We can dive a little bit deeper into the electronic band structure of graphene, and find that it has a hexagonal Brillouin zone, which is effectively the unit cell of the graphene crystal lattice. The six vertices of this Brillouin zone are called the Dirac points, and here the conduction and valence bands meet, making for the zero bandgap structure. Using the dispersion relation, shown in equation 2.1, one can calculate the energy of electrons as a function of their wave vector **k**, and plot this in three dimensions to obtain a visual of the electronic bands. This is shown in figure 2.4. The lattice constant for graphene is $a \approx 2.46$ Å, the nearest-neighbor hopping energy is $\gamma_0 \approx 2.8eV$, and the $\pm$ denotes the conduction and the valence band. This image can be thought of as the energy barriers electrons 'see' when moving through the graphene lattice [12].

$$E(\mathbf{k}) = \pm\gamma_0\sqrt{1 + 4cos(\frac{3}{2}k_x a)cos(\frac{\sqrt{3}}{2}k_y a) + 4cos^2(\frac{\sqrt{3}}{2}k_y a)} \quad (2.1)$$

2.3.3. Why graphene for gas sensing?

So what would be the benefits of using graphene for gas sensing applications? The biggest advantage of graphene is that it is a 2D-material, and since those materials are ideally only one layer of atoms thick, graphene has the best surface to volume ratio one can get. This also means that the impact on the electronic properties by adsorption of even a few molecules is quite large, because all charge transport has to go via the surface of the material, which is also where charge from adsorbates will be injected or extracted. This will give a graphene-based sensor superb sensitivity. To put this in numbers, limits of detection (LOD) for NO_2 and NH_3 gases have been reported at 5 ppb and 1 ppm respectively [13].

Next to that, graphene is highly conductive, but still a semiconductor/semimetal, which is also beneficial. If one were to use an insulator, there are hardly any free charge carriers available to interact with adsorbed gas species, and no signal will be obtained. On the other side, if a metal is used, there are so many free charge carriers, that the change in conductance won't be noticeable, it's like ladling water to the sea. Another advantage is that graphene is potentially sensitive to gases at room temperature, while, as mentioned in the previous paragraph, a lot of other materials need to be heated up first. This seems like a small deal, but heating costs time and energy, which makes a measurement both slow and power hungry, and thus impractical for portable or remote applications. Last but not least, CVD graphene can be made compatible with current CMOS processing, even though this is not trivial because of the high temperatures involved.

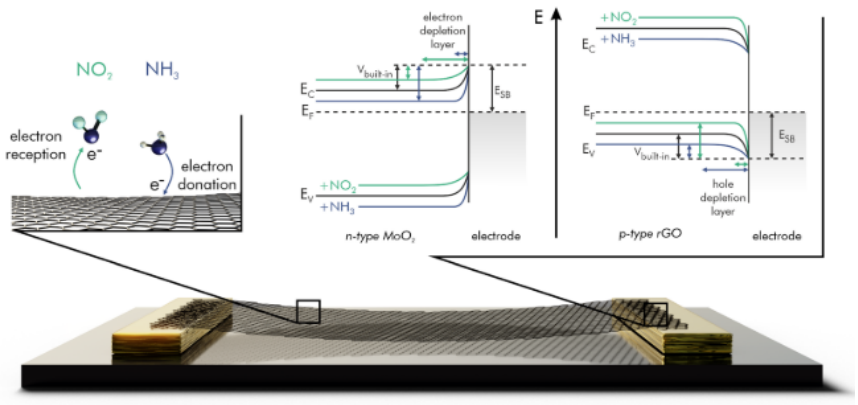

Figure 2.5: A graphene gas sensor, with reducing and oxidizing gases, and the corresponding band shift. Taken from [14].

For 2D materials like graphene, the gas sensing mechanism works different from the process described in section 2.1. The material doesn't need to be heated up to several hundred degrees, and oxygen doesn't play a role in the adsorption process. Instead, gas molecules adsorb to so-called active sites in the material, which are irregularities in the graphene lattice. These can be either defects, where the carbon is not bonded in the typical, hexagonal pattern, or impurities: other atoms that end up in the lattice during the graphene growth. The adsorbing gases cause a transfer of charge which effectively temporarily dopes the material n-type or p-type, as shown in figure 2.5. This will in turn cause the graphene Fermi level to shift, and hence cause the schottky barriers at the metal contacts to become either forward or reverse biased, further increasing the change of conductivity, but also making it non-linear.

A downside, however, is that gases and water molecules adsorbed to the graphene don't easily desorb at room temperature. That's why a micro hot plate (MHP) is still necessary to help with device recovery after a measurement [15]. This may seem like a big downside, since it brings heating back in the process, but the referenced heater only consumes 31mW, can be used to recover multiple graphene sensors at once, and only needs to be powered briefly after each measurement. Also the measurement accuracy is not dependent on the exact temperature of the MHP, eliminating the need for precise temperature control.

2.4. Doping of graphene

As explained before, graphene in its pure (pristine) form is not an ideal gas sensing device, as it has low adsorption energies for common pollutant gases. A way to improve this would be to dope the graphene with impurities like boron (B) or nitrogen (N). Graphene that either has a lot of defects in the lattice [16], or has been doped with hetero atoms, is much easier for gases to adsorb to. This was investigated using density functional computations [17], and afterwards proven by a lot of different research groups [1]. At room temperature, graphene exhibits p-type behavior, which is due to the adsorption of hydrogen (-H), oxygen (-O), hydroxyl (-OH) and carboxyl (-C(=O)-OH) functional groups among others [18]. These groups can be removed to a certain extend by thermal annealing in vacuum, but in ambient air the adsorption process will again take place. This p-type doping is apparent from a shift of the Dirac point, which is visible in I_{ds}-V_{gs} curves, where this point will shift towards positive voltages (more on this in section 4.5). By doping the graphene with nitrogen, the material becomes n-type, and the Dirac point shifts towards negative values. This doping has great potential to make the graphene much more sensitive to polluting gases like NO_2 and NH_3 [14]. The material being n- or p-type doesn't mean it will be more sensitive to either reducing or oxidizing gas, but the specific material chosen will usually make the sensor more selective to certain gases.

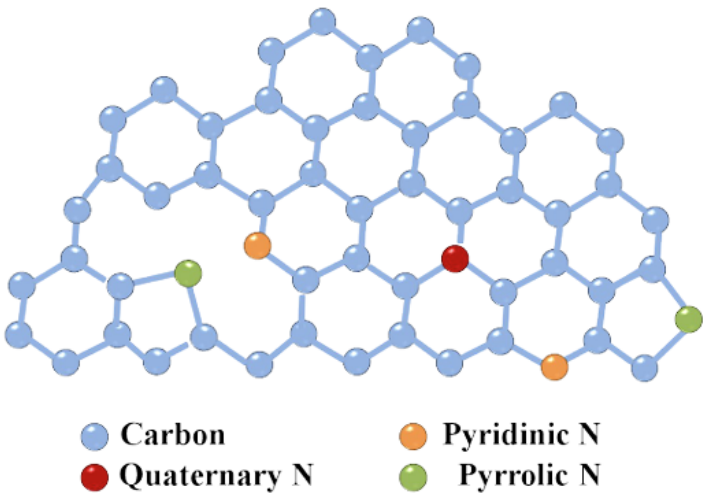

Figure 2.6: The three types of N-bonds in graphene: graphitic (or quaternary), pyridinic and pyrrolic

Nitrogen doping has been tested in a CVD process with pyridine in a horizontal quartz tube on a copper foil [19]. This was characterized with the help of FE-SEM in combination with EDX, XPS and Raman spectroscopy. Doping could indeed make the material n-type, but only if the incorporated nitrogen atoms assumed the graphitic bonding type (see figure 2.6). If the N-atoms become pyridinic or pyrrolic bonded in the graphene, it will exhibit p-type behavior. This will still improve the gas sensing performance of the graphene layer, because more active sites are present for gas adsorption.

Boron doping is also a possibility and can be used to make the graphene material p-type. [20]. This was tested to work well for a reducing gas like NH_3, making it both more sensitive and selective for this gas. The method of synthesis was quite different from the one used for nitrogen, but it was still a CVD process, albeit with a solid precursor (in powder form) for boron. XPS was used to confirm the boron bonded to the carbon, and I-V measurements confirmed the shift of the Dirac point. This was also apparent in the fact that the resistance went up when a reducing gas was introduced into the gas test chamber.

Next to nitrogen and boron, many other heteroatoms have been used to try and dope graphene. Notable ones include sulphur (S), phosphorus (P), selenium (Se), oxygen (O), silicon (Si) and iodine (I) [20]. For our purposes though, nitrogen should be a good candidate to measure the NO_2 gas, so we will focus our efforts on incorporating N-atoms in the graphene lattice.

2.4.1. Ion implantation

When talking about the doping of impurities in semiconductor manufacturing, an easy step to take is to think of ion implantation. This process is used in a lot of fabrication steps in the silicon industry to make devices, since almost no devices use silicon in its pure (intrinsic) form. In this method, an ion source containing the desired impurity, is used to generate a plasma, where a high voltage is used to accelerate the ions of this plasma. Those ions are accelerated further in an acceleration tube where the final velocity of the ions can be set. They strike a silicon wafer in the process area, where they crash into the crystal lattice, ripping apart covalent bonds while traveling deeper into the material. Finally they will come to a stop at a certain depth in the lattice, after which they will need a thermal anneal to reform the covalent bonds, and become a part of the silicon crystal. An overview of this process is shown in figure 2.7.

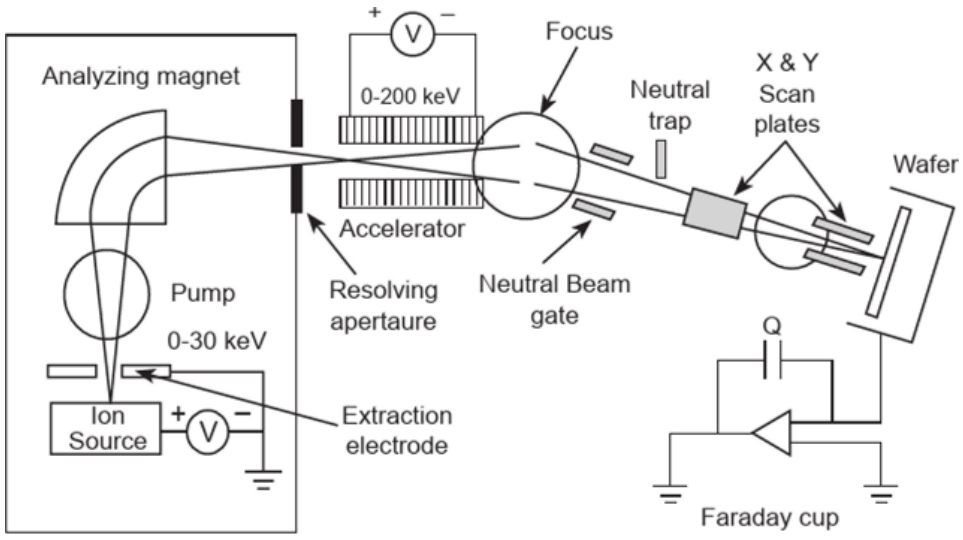

Figure 2.7: An ion implanter with its different sub systems. The ion source is on the left, and the process unit is on the right.

Characteristic for this system is that it produces an impurity profile in the semiconductor given by a Gaussian distribution, which can be described by the following formula [21]:

$$N(x) = N_p exp[\frac{(x - R_P)^2}{2\Delta R_P^2}] \tag{2.2}$$

Here, N is the implanted dose [cm^{-3}], x is the depth into the material, R_p is the mean value called *projected range* and ΔR_p is the standard deviation called *straggle*. The problem for graphene in combination with this technique is that it's really thin. Ideally, in the case of single layer graphene, the layer is one atom thick, and only a few tenths of nanometers across. When we look at standard settings for ion implantation systems, the projected range can go as low as a few tens of nanometers, which is a factor hundred bigger than our material. The straggle at that acceleration energy will be in the order of a few nanometers, which is still too wide for our purposes. This can also be understood qualitatively: the ions that impact the surface need something to slow them down, and the quicker they go, the more collisions it takes for them to come to a halt. At the same time, they need a minimum amount of energy to be able to separate the covalent bonds of the target, in order to achieve doping. In case of graphene this will mean that they will always fly straight through the target, possibly damaging the graphene in the process, but ending up in the catalyst material behind it, or even beyond that as well.

2.4.2. Doping by diffusion

Just like ion implantation, diffusion doping is an example of ex situ doping. This means that the material to be doped, usually a crystal, is grown first, and afterwards it's doped during a different process. For diffusion, this happens at high temperatures (900°C - 1200°C), and it can utilize solid, liquid and gaseous impurity sources [21]. The name 'diffusion' comes from the concentration gradient driven mass transport phenomena. There are a lot of concepts and formulas governing this transport, but in our case it's not very relevant since we're not interested in an impurity distribution over the depth of our material, since graphene is only one layer of atoms thick. What we are interested in however, is the methods used in this diffusion process, and if we can translate some of them to a practical way of doping in situ, i.e. during the growth of the graphene in the CVD process.

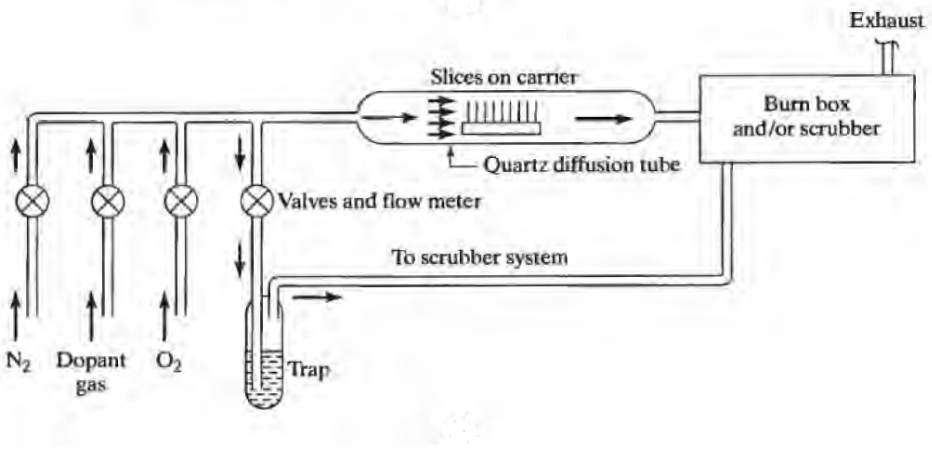

Figure 2.8: An open-furnace-tube diffusion system with a gaseous precursor. Picture taken from [21].

An example of a diffusion system is shown in figure 2.8, in this case with a gaseous precursor. This setup is actually really similar to a horizontal quartz tube CVD system, as we will see later on. For using a liquid precursor one would use a bubbling flask, and flow a carrier gas through it to the reactor chamber, to transport the vapor to the wafers. In case of solid precursors, an option is to produce the precursor in wafer form, and put them in between the process wafers. The high temperature will cause them to partially evaporate, and this gas is then transported to the silicon wafers.

Since our graphene is also going to be produced on silicon wafers, we can follow a similar approach to try and bring impurities into the graphene. However, in our case we are going to use a (cold wall) showerhead reactor instead of a horizontal quartz tube. More on this CVD system in the next chapter, but from the diffusion process we know we need three things for efficient doping: a high temperature, a steady supply of the precursor and enough time to let the dopant atoms incorporate into the graphene lattice. In the next section we will first take a look at what has already been tried in literature.

2.5. State of the art

A lot of literature has already been written on doping graphene with nitrogen atoms. There are different methods of synthesizing the pristine graphene, and some of them can be altered to produce doped graphene. Next to the already mentioned CVD process, a few notable ones include high temperature annealing, arc discharge, hydrothermal, solvothermal and pyrolysis [1]. We'll briefly go over those alternatives here, and end with a more elaborate discussion about CVD results and the pros and cons of that process.

Thermal annealing in this case means a process where a piece of graphite is brought in contact with a transition metal catalyst, for example nickel-copper layers, and heated up to high temperatures, usually somewhere between 600 and 1000 $^{\circ}C$. Carbon atoms will dissolve into the metal at these high temperatures, and precipitate out to form a graphene layer at cooldown. An example of this process can be found in [22], where Mo is used as a catalyst layer. If a nitrogen precursor, like melamine ($C_3H_6N_6$), is added into this process, it becomes possible to grow NDG [23]. The advantage here is that powdered graphene materials can be used, and that basically only an annealing oven is needed. The downside is that there is not much control over the final N content and doping configuration.

The arc discharge method uses an electrical arc between an anode and cathode to vaporize a carbon precursor, which can be either the electrode itself (graphite), or a hydrocarbon solution that the electrodes are immersed in. A third option is to fill the space in between the anode and cathode with a gas containing nitrogen, like NH_3, which can mix with the vaporized carbon and form NDG on the anode. However, this method produces a low doping level, and doesn't grand control over the nitrogen functionalities, making it an overlooked way of producing NDG [24].

Hydrothermal synthesis of graphene is mainly used in combination with graphene oxide (GO). The GO is manufactured in flakes, and dispersed in water using an ultrasonication process. For the actual doping a nitrogen containing chemical is added to the water, for example urea, and then the water is heated [25]. The doping process is quite slow, and in this particular example the solution was kept at 180 $^{\circ}C$ for 12 hours. The main downside is that this method works with graphene flakes, and it is not really suited to create large, continuous graphene sheets. Similar to hydrothermal synthesis, the solvothermal method also uses a solvent with reagents to produce the desired material, but in this case it's not water. For example, in [26], lithium nitride dissolved in tetrachloromethane was used and kept at 250 $^{\circ}C$ for 10 hours. Both methods could produce nitrogen-doped graphene with varying percentages of incorporated N, at relatively low termperatures.

Last but not least, pyrolysis is another method to produce NDG. It is a bit of a blend between the hydrothermal and CVD method, since it starts with GO dispersed in water, to which the nitrogen-containing precursor is added, in this case urea [27]. However, after this step the solution is dried by evaporating all water at a temperature of 55 $^{\circ}C$, and then a high temperature is used to break down the solids into their constituent elements, which is exactly what pyrolysis is. This is similar to CVD, but in CVD the precursors are always added as a gas or vapor to grow thin films (bottom-up synthesis), while here a bulk material is slowly being transformed into small pieces of NDG (top-down synthesis). Just like the hydro- and solvothermal methods, pyrolysis works with graphene derivatives in flake or powder form, and is not really suitable for growing large, continuous sheets on silicon wafers.

The method of choice for this thesis is that of chemical vapor deposition. CVD and its different forms (LPCVD, PECVD) already play a big role in current CMOS processing, and are excellent systems for depositing thin layers of a specified material on silicon wafers. A more elaborate explanation on the CVD process will be given in section 3.3, but for comparison here, CVD uses gas or vapor flows at high temperatures and low pressure, and can grow those layers in times ranging from a few minutes to a few hours. It is a true bottom-up method of graphene growth, and has the potential to incorporate impurity atoms during the growing process (in-situ) [28]. It is also possible to first grow graphene using the CVD method, and then dope it in a second step (ex-situ), for example by using an ammonia plasma in the same CVD reactor [29]. The first CVD grown graphene was already reported in 2009, and ever since, research groups have been trying to dope it with hetero atoms like nitrogen or boron. We will go over some of those reports in the remainder of this chapter.

In [30] M. Son et al. doped graphene with nitrogen atoms by using pyridine in a two-step CVD process. They distinguish between nucleation and lateral growth in those two steps, and add more carbon precursor in the second step to help with the lateral growth. For adding the pyridine liquid to the reactor chamber, a bubbler setup is used. The process is run at the low temperature of 300 $^{\circ}C$ under ambient pressure in a horizontal quartz tube CVD reactor. The group achieved relatively large areas of graphene, multiple square centimeters, and a high mobility of 1400 $cm^2V^{-1}s^{-1}$. The nitrogen content in the graphene was estimated at 1.6 % approximately.

The group of Zhai et al. grows graphene on glass substrates using a plasma process [31]. They bypass the use of a transition metal catalyst, and use inert N_2 gas as a dopant. On top of the plasma in the chamber, they also use hot filaments at a temperature of 2000 $^{\circ}C$ to help break down the nitrogen gas. The dopant level can be adjusted by controlling the N_2 gas flow. The main focus of this research is on making energy harvesting devices, and the NDG on glass can significantly improve those devices compared to pristine graphene. In their paper they state that the whole growing process on glass is a lot harder because the lack of a catalyst to help the dissociation reaction on the surface. The benefit of this method is that the graphene doesn't have to be transferred anymore after growth, since it's already on an insulation surface.

Another research project focused on the bonding types of nitrogen with graphene, targeting the pyridinic N bonding (see figure 2.6) specifically [32]. They use ethylene gas mixed with hydrogen, and add ammonia gas for doping. As catalyst copper foils are used. They could control the nitrogen content by adjusting the ammonia flow rate, and get the N content up all the way to 16 atom %. This was confirmed by both XPS and UPS measurements. The main focus here is to confirm that N-doping of carbon materials enhances their oxygen reduction reaction (ORR) activity, but this turned out not to be true however.

Large-area nitrogen doped graphene was produced by the group of Z. Jin et al. [33]. They produced centimeter scale sheets by using pyridine as a precursor, and copper foils as the catalyst material. Raman mapping shows that the graphene is uniformly monolayered. The N-content is confirmed with XPS, and mainly pyridinic and graphitic bonded nitrogen is present. Electrical measurements on back-gate devices are used to confirm n-type doping, and hence a Dirac voltage shift to the negative side is visualized, exceeding 20 volts difference. The pyridine is bubbled into the reactor by using argon, at a temperature of 1000 $^{\circ}C$ at approximately 7 torr pressure. The CVD system is a fused quartz tube, and growth times were around 10 minutes.

An ex-situ doping process with plasma is investigated by Y. Lin et al. [34]. Two different plasma sources are used in this case, a lab-scale microwave (MW) plasma, and an industrial radio-frequency (RF) plasma generator. The thickness of the graphene has an influence of the N-bonding type with graphene, with thicker graphene having relatively more graphitic-N bonding. The plasma will damage the graphene during exposure, and mainly for monolayer graphene the integrity is not well preserved. Bilayer graphene can be efficiently doped while staying intact, and the dirac point is shown to shift by approximately 0.45 eV using ARPES. Many defects can be repaired by a high temperature self-healing process after doping, thus making plasma treatment a viable option for doping graphene.

N-doped graphene was also investigated for the use in lithium battery applications [35]. In this research, PG was grown using hexane, and NDG was grown using acetonitrile, both liquid precursors. The use of a bubbler setup was not specifically mentioned, which means they could also have used the low pressure (0.01 Torr) of the quartz tube to draw the vapors in. The graphene is grown on copper foils, to simulate growth on large copper current collectors in lithium batteries. XPS is used to confirm N-doping, which is mainly of the pyridinic type, with also a fair amount of pyrrolic-N. Since the graphene would not have to be transferred after growth for this application, it would be a feasible way to improve the performance of contemporary battery technology.

In the next chapter we will look at our experimental process, the choices that will be made for our setup, and which CVD parameters we will use to get the best possible results.

3

Experimental

Now that the basics of gas sensing are clear, and it is known why one would want to use graphene as the sensitive material, we can move on to how we're going to produce the material for the sensor. For this we will use a chemical vapor deposition (CVD) process, specifically tailored for the growth of both graphene and carbon nanotubes. There are a number of choices to be made here, the biggest ones being the choice of growth catalyst, precursors and the CVD parameters.

3.1. Growth catalysts

Graphene will not just grow on a silicon wafer, neither will it grow on silicon dioxide. To facilitate this growth, a catalyst is needed that can serve as a reservoir for carbon and helps in breaking down the precursor into its constituent elements, but at the same time doesn't react with it. For this purpose usually a transition metal, i.e. the purple elements shown in figure 3.1, is used, and some common choices are Copper (Z=29) and Nickel (Z=28), and occasionally Cobalt (Z=27) is used [36].

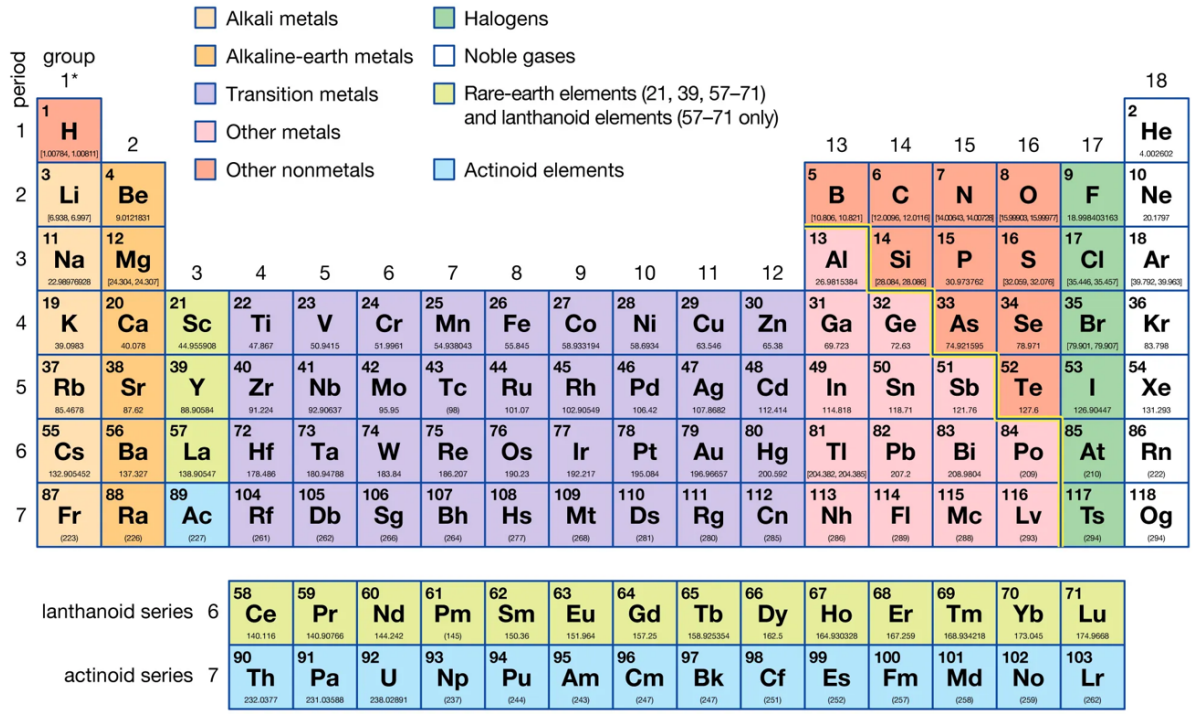

Figure 3.1: The transition metals outlined in purple. Cu, Ni and Co are often used.

However, another metal has also been proven to work well to create FLG and MLG: Molybdenum [37] [38]. This catalyst has a number of advantages over the more traditionally used transition metals. First of all it has a very high **melting point**, which will prevent the catalyst from becoming almost a liquid, and thus changing its shape during graphene growth. This is mainly an issue of copper, which has a melting point of 1085°C, only slightly above the temperatures used in CVD. Secondly, the **solid solubility** (in at% @ a given temperature) is much lower compared to that of nickel, which is usually an advantage, because a high solid solubility makes it harder to grow single layer graphene. This is because during the cooling phase, the carbon dissolved in the catalyst will precipitate out, and form additional graphene layers on the surface. Third, the **diffusivity** (in m^2s^{-1}) of carbon into the metal should be high, so the influx of carbon atoms won't saturate the surface of the catalyst, but permeates through the bulk. It is hard to give an exact number for this, since, like the solid solubility, the diffusivity is a strong function of temperature. Cobalt seems to have the higher diffusivity compared with nickel, since the permeability, which is the product of diffusivity and solubility, is on par.

The other choice to make for the catalyst is its thickness. The catalyst is deposited on the wafer by sputtering (PVD), and the layer thickness can be precisely controlled in this method. This thickness is a trade-off, which is shown in figure 3.5. A thinner catalyst usually makes the graphene growth process surface-mediated, where the graphene grows upon first contact with the precursor, since there is not enough bulk material to provide a significant carbon flux into the catalyst. It also makes for more manufacturable gas sensors, since one can opt to use the transfer free method (TFM), but in general it's harder to grow SLG. A thicker catalyst gives more bulk reservoir to carbon, which makes the growth process bulk-mediated where the graphene grows during the cooling step, because of the carbon precipitating out of the bulk [39]. In general this makes it easier to grow SLG, but the cooling process is much more critical in this case. A downside is that TFM becomes harder to perform with a thicker catalyst, and above 1μm the layer may even crack due to internal stresses in the material.

3.2. Precursors

To grow the graphene (pure carbon), and dope it with nitrogen, we need materials that contain those two elements. Additionally they should be suitable for use in a CVD reactor, so ideally they are gases, but liquids are also possible via bubbling.

3.2.1. Carbon

The first option for a carbon-containing gas would be to use methane (CH_4) [28], see figure 3.2. Another often used gas is ethylene (or ethene, C_2H_4) [32], and even acetylene (or ethyne, C_2H_2) is sometimes used. In principal any gas with carbon content can be used, so even CO_2 is an option, but the catalyst would need a pre-treatment with hydrogen plasma in this case [40]. For our purposes it makes sense to go for the methane for a few reasons. Methane only has one carbon atom per molecule, so the deposition rate can be kept low, to prevent multilayer graphene growth, and promote single layer graphene. Next to that, methane is easy to handle since it's basically natural gas, and not super toxic. It's also readily available, since it's already been installed in the CVD tool, and can be used right away. During pyrolysis of methane, the molecule will split up into individiual atoms, of which the H atoms will bond to each other to form hydrogen gas (H_2), and the carbon will dissolve in the catalyst, see reaction 3.1. This process normally happens only with temperatures over 1200°C, but the presence of the catalyst brings it down to under 900°C.

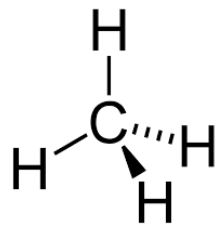

Figure 3.2: The skeletal formula of methane.

$$CH_4(g) \rightarrow C(s) + 2H_2(g) \tag{3.1}$$

An example of a liquid precursor would be benzene, an aromatic compound containing a hexagonal ring of carbon atoms. Other possibilities are ethanol, toluene and hexane. Especially benzene might still be useful for precision injection into the CVD reaction chamber via bubbling, since its carbon bonds are sp^2 hybridized, and its effective flow rate can be set much lower than the gaseous precursors. Those materials are most probably not needed, since graphene was already successfully grown on molybdenum before using methane gas [41]. Still, they might come in useful for the precision injection.

3.2.2. Nitrogen

The most straightforward choice to make here would be to use ammonia gas (NH_3) [28]. Sometimes actual nitrogen gas (N_2) is being used, but this has a triple bond between the nitrogen atoms, which makes them harder to separate [31]. During pyrolysis in the CVD reactor, NH_3 will split up in its constituent elements, which is very similar to the same process for methane. The only difference is that the produced carbon is a solid, and the nitrogen will bond to each other to form nitrogen gas (N_2).

$$2NH_3(g) \rightarrow N_2(g) + 3H_2(g) \tag{3.2}$$

Since this process only takes place at the metal catalyst, this formation of nitrogen gas is really close to where the actual graphene grows, so this process is still different from just flowing N_2 in the reaction chamber. Here, the nitrogen has a chance of bonding to the carbon before bonding to another N-atom, so the nitrogen can be substituted in the graphene lattice. The hydrogen gas that is produced from both the methane and ammonia gas actually helps the graphene synthesis, by keeping the surface clean, and is easily pumped away afterwards. Ammonia is shown in figure 3.3, notice the lone pair.

There are other nitrogen containing gases that would theoretically be possible to use as a dopant. Two options would be to use either NO_2 or N_2O. Those gases are totally different in nature and their uses, but they both contain nitrogen and oxygen. They could be tested for pyrolysis in a CVD reactor chamber to see if the gases decompose. If this works, the main question is of course if the oxygen as a byproduct is going to aid in graphene nucleation. For a catalyst like Cu it is beneficial to have a small amount, but for other metals, like Ni, Pd, Ru and Rh it is detrimental [42]. For molybdenum it is still unknown.

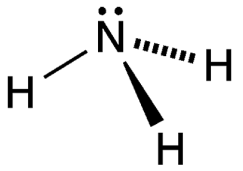

Figure 3.3: The skeletal formula of ammonia.

Next to those, one could use a gas like $(CN)_2$ (cyanogen), which has carbon atoms triple bonded to nitrogen. This could be very interesting, since cyanogen can form a polymer called paracyanogen [43], which has a hexagonal structure consisting of C and N with different types of bonds, and looks a bit like graphene. Unfortunately this gas is very toxic, and should be handled with uttermost care. For now, we will choose ammonia gas as our first choice in combination with methane gas.

3.2.3. Carbon and nitrogen

There are also substances containing both carbon and nitrogen atoms that could be used in CVD reactors as precursors. For example, pyridine (C_5H_5N) is demonstrated to create nitrogen doped graphene under the correct circumstances [30]. Its structural formula is shown in figure 3.4.

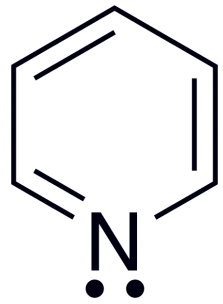

Figure 3.4: The skeletal formula of pyridine.

This liquid can be bubbled into the reactor chamber by use of a carrier gas like Argon or Nitrogen. It is quite flammable, so care should be taken, but it is not as dangerous as cyanide gases in toxicity, which makes it a whole lot easier to handle. The main advantage of using a liquid is that lower partial pressures of the carbon- and nitrogen-containing substances can be obtained by the bubbling process. The disadvantage is that usually a higher oxygen content in the grown graphene is obtained (because of air in the bubbling flask), which is undesirable. An obvious downside to using a compound like pyridine is that we cannot change the C:N ratio directly by changing the relative flow rates anymore. However, this can still be controlled with other parameters, such as the temperature and gas flow [44]. The pyrolysis of pyridine at elevated temperatures is a lot more complex than that of methane or ammonia, and is outside the scope of this thesis.

Other options include acetonitrile (CH_3CN), dimethylformamide ($HC(=O)-N(-CH_3)_2$) and monoethan -olamine (C_2H_7NO), but they don't really have an advantage over the already mentioned precursors,

and are more complex to work with. For this reason we will stick to the pyridine as backup precursor, in case that the process with ammonia doesn't produce the wanted results.

3.2.4. Flows and gas mixture

The next question is: what gas mixture do we want to use in the reactor chamber? To answer this we need to understand the function of all gases present during graphene growth. Next to the already mentioned precursors, these include Argon and Hydrogen. Argon is the inert gas and hydrogen is a reducing agent. The gas mixture will differ throughout the different stages of the CVD process, which consists of heating up, growth time and cooling down. More on this in the next section.

Argon (Ar) is used to fill the bulk of the reactor chamber, in order to flush any unwanted gases that are present. It is a noble gas which will not contribute to any reaction during the CVD process. The precursor gases will be diluted by the argon, because if one was to use only precursor gases, the dose would be way too high. As such, the argon helps to control the pressure in the chamber that is regulated by the pressure controller, and will create the right flow dynamics of the gases along the catalyst.

Hydrogen (H_2) is also added to the mixture, and has different functions. During heating of the chamber, before the precursor gases are injected, it will clean the catalyst surface. The metal catalyst has been exposed to air at this point, and a thin layer of metal oxide will have formed on the surface. This is undesirable for the graphene growth, and the hydrogen will reduce the surface oxide in the preanneal step. During growth it can help to activate the hydrocarbon radicals, in case of using those as a precursor, and promote graphene formation. And even during the cooldown phase it has a function. Here it can etch the thicker parts of the graphene to have some control over the eventual layer thickness. An elaborate study of hydrogen in all parts of the graphene growth process has been done in [45].

Later on we will use a bubbling setup, with nitrogen gas (N_2) as the carrier gas. The main requirement for a carrier gas is that it is inert, i.e. does not readily undergo chemical reactions. For this reason Ar could also have been used here, but N_2 was chosen since it was already installed.

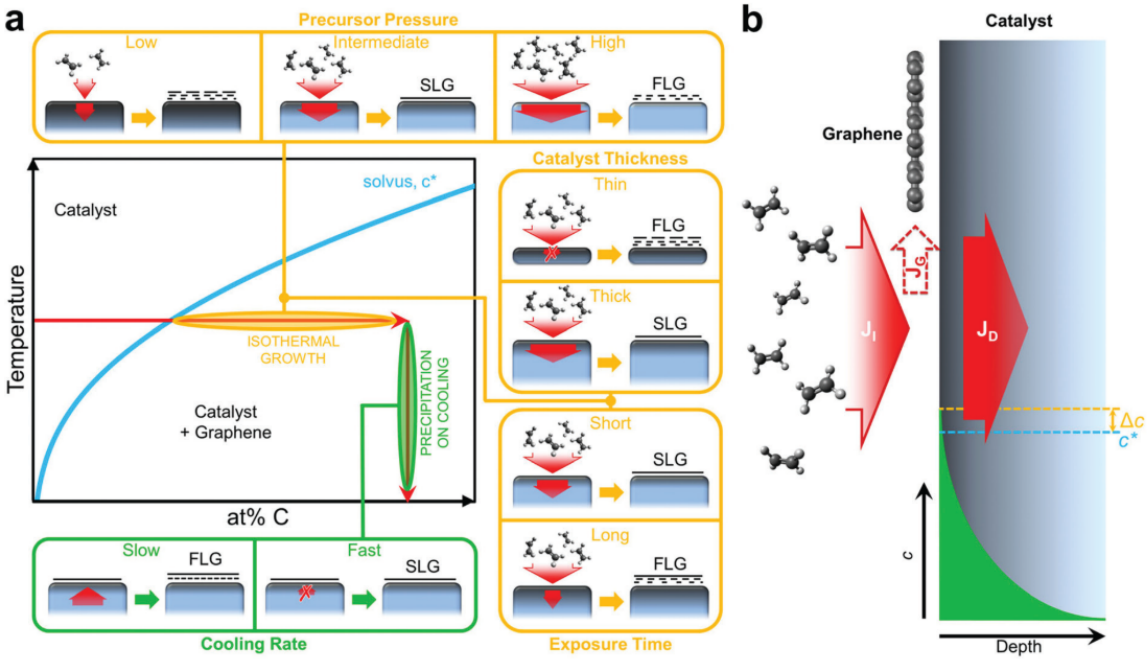

Figure 3.5: The possible growth methods of graphene on a transition metal catalyst. Picture taken from [36]

.

Since the exact gas mixtures are not the goal of this study, we will mainly stick to already proven recepies that have been used for growth of pristine graphene. This means we will use argon to flush

the chamber, H_2 to do the preannealing of the catalyst, and a mixture of the two with mainly argon during the graphene growth (960/40 sccm Ar/H_2). During cooldown we will use only argon for now.

3.3. The CVD system

This section aims to give a basic understanding of how a CVD system works, the terminology used for it, and the equations governing its behavior. The CVD is a research topic of its own, and we can dive very deep into this topic, but that's not the purpose of this thesis. For the interested reader who wants to know more, the book of Dobkin and Zuraw is recommended for further reading [46].

3.3.1. Measuring gases

A good point to start is to do some calculations on the stuff that is making the process happen: the gases. For this the most important equation that we need is the ideal gas law:

$$PV = nRT \tag{3.3}$$

Here, P is pressure, V is volume, n is the number of moles, R is the universal gas constant and T is the absolute temperature. The gas flows going into a CVD system are often expressed in standard cubic centimeter per minute (sccm) or standard liter per minute (slpm), which is a volume flow. However, using the ideal gas law, we can see that, if the pressure and temperature are given (which they usually are), the volume flows translate into a molar flow, and we know exactly how many atoms or molecules of gas enter our system.

Next to that, the CVD reactor systems usually don't operate under standard pressure and temperature (STP) conditions, but under low pressure and high temperature. If equation 3.3 is solved for the volume, we can see that both those factors will increase the volume tremendously. To give an example, let's consider a gas flow of 300 sccm at STP going into our reactor. The reactor operates at a temperature of 800 $^\circ C$ and a pressure of 1 mbar. From the ideal gas law it follows that the volume expands to 1000 mbar / 1 mbar = 1000 times because of pressure, and even further by 1073.15 K / 273.15 K $\approx$ 3.93 times because of temperature, which means the volume flow in the reactor chamber will be 19.6 liters per second! Suffice it to say that those volume changes shouldn't be ignored.

A final note about the gases is that the concentration of any constituent of the gas mixture is equal to the ratio of that gas flow to the total flow, multiplied by the total concentration. This is an intuitive result, but unfortunately it only holds as long as the gases are ideal. With heavier gases, like refrigerants, the results will become inaccurate, so this is something to keep in mind when working with pyridine vapor.

3.3.2. Kinetic theory

Next, we will briefly touch upon kinetic theory: the study of the motion of molecules in gas. In a CVD process we're mainly interested in the molecules that strike the surface of our wafer or sample, since those are the molecules that will contribute to film deposition. From kinetic theory, a flux can be calculated that tells us how many molecules strike a given surface area per unit time. With the help of the ideal gas law, this can be expressed as a function of temperature and pressure, known as the Knudsen equation:

$$J = 3.51 \cdot 10^{22} \frac{P}{\sqrt{M \cdot T}} \tag{3.4}$$

Where J is the molecular flux, P is pressure, M is molar mass (in grams/mole) and T is temperature. This formula puts an upper bound on the rate at which deposition can happen. For us, the deposition rate, R in Å/min, is not really interesting, since we're not looking to deposit a film of a few hundred nanometers on our wafer, but just a single layer of graphene. Still, to grow graphene, the molecules need to strike the surface, and from this equation we now know that this flux goes down with higher temperature, lower pressure and higher molecular mass. The flux is indicative for how fast a layer will grow, so we can use it to estimate if growth times need to be longer or shorter. For example, when changing from smaller methane molecules to bigger pyridine molecules, we would expect the time to grow the same number of graphene layers to increase, and hence we can change the recipes to grow the same amount of layers.

3.3.3. Reactor types

Let's conclude this section by looking at the two most encountered CVD reactor systems: the tube and the showerhead reactor. The tube reactor is shown in figure 3.6.

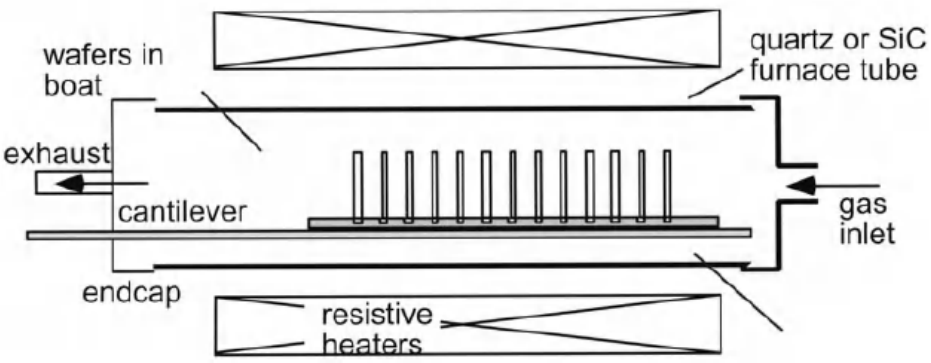

Figure 3.6: A schematic drawing of a CVD tube reactor. Image taken from [46]

This is a hot-wall reactor, and the reactor volume is nearly isothermal. Multiple wafers can be loaded on a 'boat', and they will all be processed simultaneously. This means that high throughput can still be achieved, even if processing times are long. This kind of reactor is normally used for **front end** processes: the layers that are deposited before the first metal layer, which means high temperatures can still be used. For us the throughput is not such a big deal, since we're only doing experiments, but in case of processing whole wafers, the thermal uniformity is a big advantage.

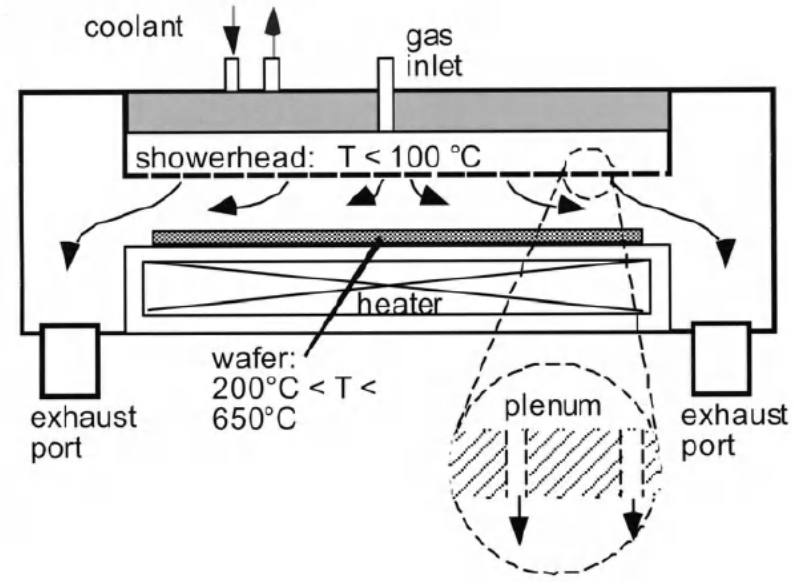

Figure 3.7: A schematic drawing of a CVD showerhead reactor. Image taken from [46]

The showerhead type reactor is shown in figure 3.7. This type of reactor is a cold-wall reactor, since it's being heated from the inside and the reactor walls are relatively cool. Only one wafer can be loaded at a time. This type of CVD reactor is mainly used in **back end** processes: the layers deposited after the devices are made in the silicon. The main benefit is that a plasma generator can be used, which usually enables deposition to occur at lower temperatures, to prevent deposited metal layers from melting. Another advantage is that the wafer chuck can also support pieces of wafer, which enables us to try multiple different recepies with the same wafer by dicing it in many smaller pieces.

3.4. CVD parameters

For the graphene growth we will use the Aixtron Black Magic Pro system (BM), situated in the EKL cleanroom at the TU Delft. This device has a showerhead type CVD reactor, with optional plasma generator, and a variety of gases that can be used. It can be programmed using recipes, on which more details can be found in appendix A.

3.4.1. Temperature

Growth of graphene happens at high temperatures, usually in the range of 800 °C - 1000 °C. However, this temperature is dependent on both the catalyst and the precursor choice. One needs a minimum temperature to achieve pyrolysis of the precursors, and this temperature is lowered to some extend in the vicinity of the catalyst. A good starting point would be 915 °C, which has already been used for graphene growth on Mo, both with methane [37] and in combination with amorphous carbon [22]. The basic trade-off in temperature is growth-rate. One should not choose the temperature too low or the graphene won't grow at all, but neither should it be chosen too high or one will only get MLG, and it will be difficult for the N-atoms to incorporate into the graphene lattice [47].

3.4.2. Growth time

Growth time is another trade-off in the CVD process. This parameter is usually in the range from 10 minutes to an hour, but can even be multiple hours in some extreme cases. Since the graphene takes time to nucleate, and will grow easier at the edge of existing graphene (rather than a bare spot on the catalyst), it will start to grow in flakes. When the growth time is too short, the flakes will be isolated domains, and no complete graphene coverage of the sample is achieved. On the other side, when growth time is rather long, additional layers of graphene will grow underneath the first layer. Just like temperature, this is a function of the catalyst and precursors choice.

3.4.3. Cooling rate

The cooling rate after the growth time is also important, and can be set in the temperature profile of the BM. The effect this has is strongly dependent on the catalyst, mainly on its solubility and diffusivity. Carbon that diffused into the catalyst during growth time may precipitate out to form additional layers during cool down. If SLG is desired it is helpful to choose a fast cooling rate, to prevent this outflux of carbon. However, according to [36], this effect "is only minor as a result of the rapid decrease in carbon diffusivity with temperature".

3.4.4. Pressure

For the growth of graphene roughly two different pressures are being used: either atmospheric pressure, or pressure in the order of a few (tens of) mbar. Lower pressures (deep vacuum) are not really possible, since process gases are added during growth. The main benefit of the atmospheric growth is a more simplistic system, since a vacuum pump, a pressure vessel and a vent valve don't have to be present, making it cheaper. Working at lower pressures however, has the benefit of having more control over the partial pressures of the precursors, and growing higher quality graphene. Since the BM system had a vacuum system, and can not operate at atmospheric pressure, we will work at low pressure. The range of pressures is 1-90 mbar, but we will mostly use 25 mbar during graphene growth, and 10 mbar during cooldown.

3.4.5. Plasma

The BM has a plasma generator that can be used in the CVD process of graphene. This method has been used in the literature to dope graphene with nitrogen ex situ [48] [29]. However, this method also seriously damages the produced graphene, which is visible in the increased D-peak of the Raman spectrum. Some defects in the lattice are beneficial for gas sensing, but since the plasma in the BM is quite violent, and too many defects will lower the mobility of the FLG significantly, we will not use this plasma for now.

3.4.6. Bubbler setup

The Black Magic system already has a bubbler flask installed which was previously used for adding water vapor during CNT growth. This setup can be used for transporting liquid precursors to the reactor

chamber in a controlled manner via an MFC. An important thing to note is that in this setup the MFC is installed downstream from the bubbler flask. It is helpful to have a basic idea how such a vapor flow compares to the flow of a gas line that is directly connected to a similar MFC. For this we need the following formula [49]:

$$F_{v,out} = F_{c,in} \frac{P_v}{P_{head} - P_v} \tag{3.5}$$

Here, F denotes a volume flow, and P denotes a pressure. More precisely, $F_{v,out}$ is the flow of vapor to the MFC, $F_{c,in}$ is the flow of carrier gas into the bubbler flask, P_{head} is the pressure in the headspace (the part in the bubbler flask that's not the liquid) and P_v is the vapor pressure. Now, let's insert some numbers here. $F_{c,in}$ is the flow we can set using the MFC, for methane an often used value is 25 sccm. P_{head} is equal to the carrier gas pressure, which is 2 bar in this case. The vapor pressure is dependent on the liquid present in the bubbler flask, and is always a strong function of temperature. For pyridine we can look it up in the following graph:

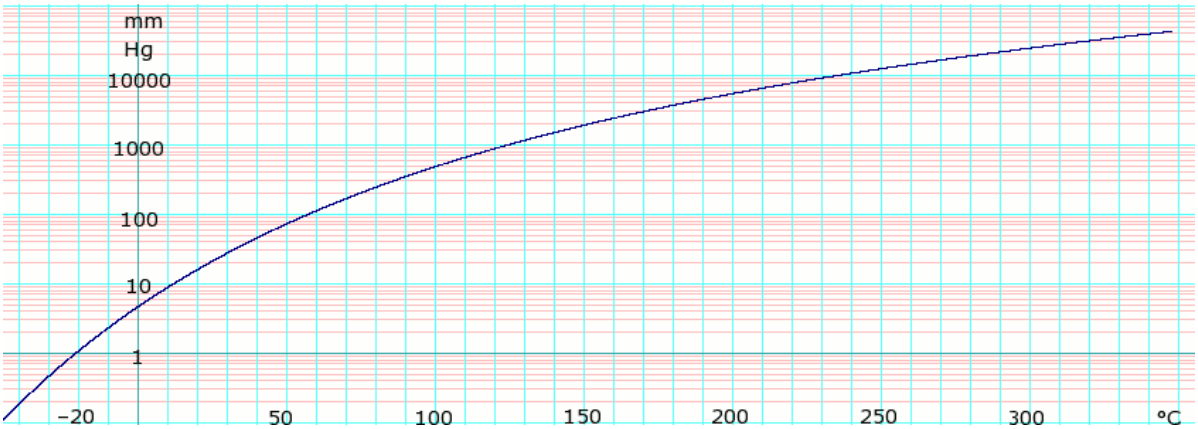

Figure 3.8: The vapor pressure of pyridine as a function of temperature.

In the cleanroom the temperature is regulated at $21°C$, and we find a value of 17 mmHg for that, which is approximately 22 mbar. This vapor pressure is the part of the liquid that is vaporized, exerting pressure on the chamber walls of the bubbler flask. When a carrier gas enters the flask from below, it will flow upwards through the liquid in bubbles (hence the name), and mix with the vapor in the headspace before exiting through the outlet valve. In this way it will carry the vapor to the reaction chamber. Now that we have all the numbers, we can put them into equation 3.5, and find a vapor flow of approximately 0.278 sccm for pyridine. This is the part of the total carrier gas flow, in this case 25sccm of nitrogen gas (N_2), that's contributing to the deposition reaction in the CVD chamber: a bit over 1%. That means that we have much less precursor concentration with a bubbler setup, compared to directly flowing gaseous precurors to an MFC. This result will be used extensively in chapter 6.

4

Characterization

After having manufactured the nanomaterial, we need a way of characterizing it, to say anything about the quality, amount of layers, effective doping, etc. Since we can not tell those properties by simply looking at the graphene, some more sophisticated methods are needed here. In this chapter we take a look at the used characterization techniques.

4.1. Raman spectroscopy

A well known measurement for detecting graphene is Raman spectroscopy, which is performed in almost all papers discussing graphene and its variants. It is an optical technique, that illuminates a sample with a laser beam, and detects the photons that have Raman scattered from the sample. This Raman scattering, in contrary to Rayleigh scattering, changes the wavelength of the incident light, which in turn creates a spectrum that acts as a kind of fingerprint for a material. In this spectrum the shift in wavelength is plotted versus measured intensity, to create a number of peaks for specific vibrational modes in the material. Graphene produces a number of those peaks, of which three are dominant, called the D-band, G-band and 2D-band [50]. They are shown in figure 4.1 from left to right. A lot of information can be obtained from such a spectrum.

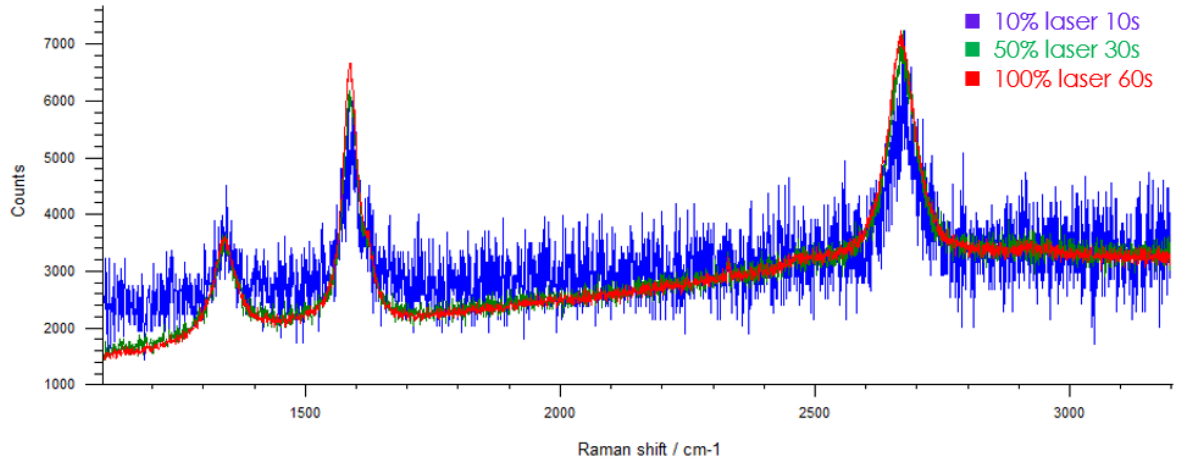

Figure 4.1: An example of a Raman spectrum of a graphene sample produced in ESP lab.

The most notable of the three bands is the G-band, which is present for both graphite and graphene. It is caused by resonance of the sp^2 bonds between carbon atoms, of which those materials are build. The position of the G-band is sensitive to the number of graphene layers, and will shift to lower wave numbers as the layer count goes up [50]. Care has to be taken with estimating layer count, since the position of this band is also sensitive to chemical doping. It can be found at approximately 1582 cm^{-1}.

Then we have the D-band, which can be found at Raman shift $\approx$ 1350 cm^{-1}. This band is due to a so-called 'breathing mode' of sp^2 bonded carbon rings, which are only active when the ring is next to a defect of the lattice, or near the edge. It is usually the weakest band in graphite spectra, and will only show up in graphene spectra when there are a lot of defects. Its intensity is the main indicator of how many defects are present. When growing pristine graphene this band is ideally very low, but after chemical doping, where the impurities introduced are defects themselves, the D-band will become quite well visible.

Lastly, there is the 2D-band, or sometimes called the G'-band. This band is an overtone of the D-band, and is the result of a two phonon lattice vibrational process. Unlike the D-band, it is also active when not next to a defect or the edge of the lattice, and its intensity is usually high in graphene materials. While it is also present in graphite spectra, the intensity in graphene is usually higher than that of the G-band, while in graphite it is the other way round. It can be found around 2685 cm^{-1}.

In the setup in the ESP lab, a Renishaw Raman Invia is used, for which two lasers are available, 532nm (green) and 633nm (red). The system has a built-in microscope with 5x, 20x, 50x and 100x magnification objective lenses. For the laser choice, the decision was made to go for the 633nm laser, since for graphene it doesn't matter a lot. NIR lasers wouldn't have been a good option, because they might cause fluorescence with the underlying Si or SiO_2. As for the measurement itself, the two main parameters are the laser intensity and the exposure time. In figure 4.1 a few combinations of the two can be seen. We can keep the laser power at 100% since it will produce the highest Raman signal, and the only reason to tune it down would be in case the laser damages the sample, which it doesn't. An exposure time of 10 seconds is sufficient for a quick check if graphene is present, but for quantitative measurements we need a longer measurements time, like 60 or even 90 seconds.

For the interested reader, a deeper dive in the graphene Raman spectrum and the solid state physics that govern this behavior can be found in [51] and [52].

4.2. Scanning electron microscopy (SEM)

A Hitachi Regulus 8230 SEM system was used to create high magnification images of the different samples that were made. The main advantage here is that, while graphene is transparent and not well visible with optical techniques, it is visible with an electron beam. Next to that, because of the high magnification it is possible to tell something about the quality of the produced graphene. Unfortunately we won't be able to show if nitrogen is incorporated in the graphene lattice from those micrographs.

Operating the SEM, there are quite a number of parameters to set and processes to fine tune. The most important one is probably the acceleration voltage of the electron beam. As a general rule, the higher this voltage, the more energetic the incident electrons and the deeper the beam will penetrate into the sample. The range can be chosen from 0-30 kV, but since we are mainly interested in the surface of our samples, going higher than 5 kV will not give us any useful information. When we go below 1 kV there is also an option of deceleration, in which the sample itself is given a (negative) voltage to slow the electrons down before they hit the sample. This gives us the benefit of a higher acceleration voltage, which will give us a more accurate beam to work with, but also electrons which will catch only the uppermost sample information because of the lowered landing velocity [53]. This will be our mode of choice in most cases.

Other important settings are the working distance, magnification, contrast/brightness, focus, detector type and configuration and scanning mode. Since this thesis is not about how a SEM works, we won't go into detail here, but let it be clear that for most of those parameters there is an optimum (working distance, focus, contrast/brightness, scanning mode) and with others we can experiment to see different things (magnification, detector type and configuration). An example micrograph is shown in figure 4.2. The settings used to capture it are shown in the bottom, in order being the name of the system, acceleration voltage (with optional deceleration mode), magnification, used detectors, and a scale bar for sizing. This particular sample has graphene on top, but the visible grains are probably molybdenum carbide crystals, which form during the CVD graphene growth process.

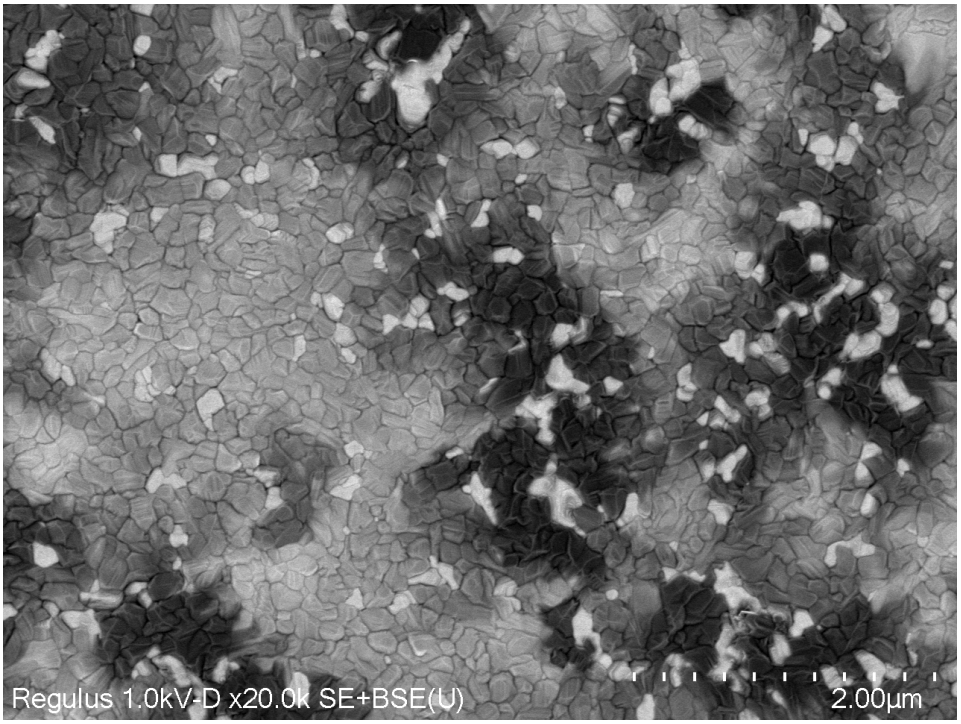

Figure 4.2: A graphene sample on a Mo catalyst, grown for 5min with 25sccm of methane.

4.3. Fourier transform infrared spectroscopy (FTIR)

The next step is to find ways to detect and measure the amount of nitrogen incorporated into the graphene lattice. The method that is most often used for this is XPS (more on this in section 4.6), but this is not directly available in the lab, and ideally we would have a cheaper and quicker process to give a first indication if nitrogen is present in the sample or not. An option for this would be FTIR, in which the transparency of the sample to infrared light is measured over a range of wavelengths. Peaks in this spectrum translate to specific functional groups, having a very precise frequency at which they have bending or stretching vibrations of molecular bonds, absorbing part of the energy of the incident light at that wavenumber. To conduct these measurements, a Thermo Electron Nicolet 5700 FTIR spectrometer is available, with the standard transmission accessory, and on top of that a HATR module (more on this in paragraph 4.3.2). In this section we will explain the process, and in the next chapter elaborate on the results.

There is limited literature available on CVD nitrogen doped graphene, that is characterized by use of FTIR. The studies either focus on graphene oxide (GO) and its reduced variant (rGO) [54], or on carbon nanotubes [55]. The former gives an explanation on how to interpret the resulting spectra, which is shown in fig 4.3, and serves as an example on what to expect. Mainly the peaks at 1187 and 1571 cm^{-1} are important, since they correspond to C-N and C=C stretching bonds respectively. This suggests that we will only see the peak at 1571 cm^{-1} when graphene is present, and the one at 1187 cm^{-1} when there is nitrogen incorporated into the lattice, or if it is only attached to the graphene. This is an important difference that we have to be careful with while evaluating the produced spectra.

The latter article uses absorbance spectra instead of transmission, which basically results in an upside-down spectrum, but the same peaks should be present. In this research CNTs were grown using a CVD method with methane and hydrogen for the pristine variant, and ammonia gas was added during the growth to dope it with nitrogen impurities. The focus for nitrogen doping is mainly on two peaks at 1250 (C-N) and 1372 (N-CH_3) cm^{-1}, but the two previously mentioned peaks are not present in the spectra. This might be due to the fact that in this paper CNTs are considered instead of rGO, which would mean that the allotrope of carbon that is measured, has a strong influence on the resulting spectrum.

To this end it would be helpful to have an overview of the different carbon based nanomaterials, and their respective FTIR spectra, with explanation of the peaks observed at different locations. An elaborate research paper was found that discusses exactly this, and also different types of vibrations (i.e. stretching, bending, rocking) are taken into account [56]. It lists both the peaks of the earlier mentioned graphene oxide samples and the nitrogen doped CNTs, next to synthetic diamond, diamond-like carbon (DLC), graphite, fullerenes and carbon quantum dots (CQD). This article will be consulted in the next chapter when we have our measured spectra of the CVD grown graphene samples.

To be able to conduct the correct measurements, it's very useful to have a basic understanding of how an FTIR spectrometer works. As already explained, the goal of the measurements is to illuminate the sample with a range of infrared frequencies, and measure the transmitted light intensity with a photo detector. The range of frequencies, usually denoted as wave numbers, is chosen from 400 till 4000 cm^{-1}, which is in the near- (NIR) and mid-infrared (MIR) region. At the heart of an FTIR system is a Michelson interferometer, of which a conceptual image is shown in 4.4. This optical device basically encodes all the frequencies present in the IR light source with spatial information by means of interference. The moving mirror causes the two reflected beams of light to have a different optical path length, causing interference when the two beams recombine. The result is an interferogram which is measured by the detector. With the help of the Fourier transform, this interferogram is converted to a spectrum, with all the measured frequencies and their corresponding intensities. This method is much quicker than the older, scanning method, in which all frequencies had to be passed through the sample after each other [57].

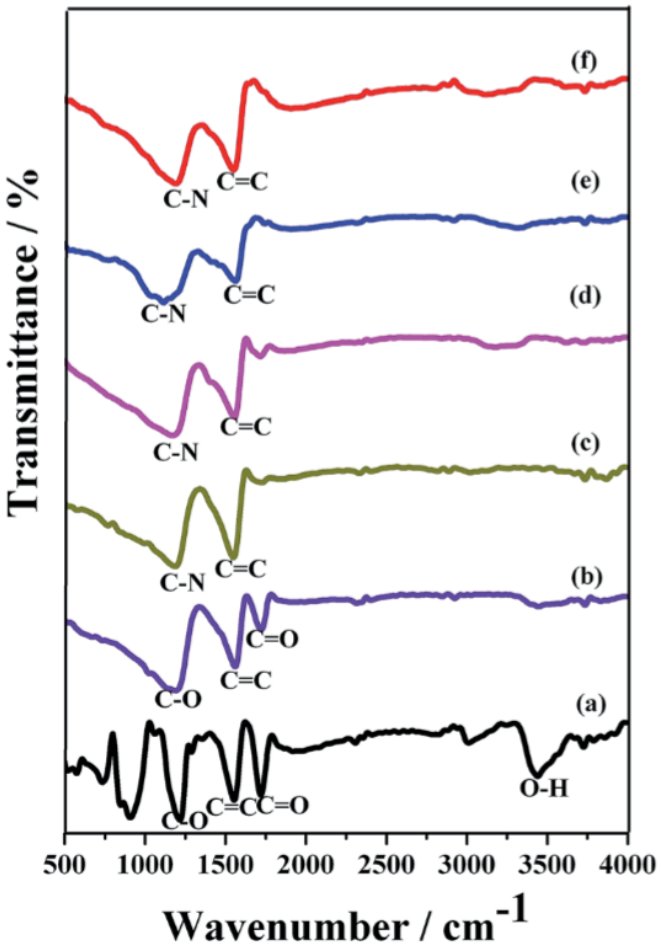

Figure 4.3: FTIR spectra of different nitrogen doped rGO samples. Picture taken from [54]

A practical problem faced with while operating the spectrometer is that of sufficient signal at the detector. The Nicolet has a lot of self diagnostics that run while doing measurements, and thus can give an indication if the measurement results are valid. If the amplitude of the interferogram is too low it will notify the user, and explain that the acquired spectrum is probably not a correct representation of reality. This message was encountered a lot, and the reason is that the metal layer, used as a catalyst for growing the graphene, is opaque to infrared radiation. A thin layer (a few tens of nanometers) of metal will already stop most of the incoming radiation, because the frequency is so high (12 - 120 THz in this case). This leaves us with two options if we still want to get accurate measurement results: get rid of the metal by transferring the graphene to another sample, or perform reflective FTIR measurements in the HATR accessory. We will explain both here.

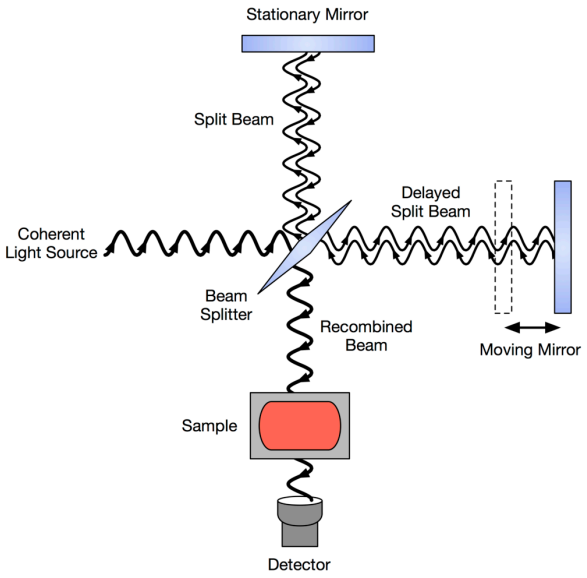

Figure 4.4: The principle of a Michelson interferometer, with a fixed and moving mirror.

4.3.1. Etching the catalyst

For etching the Mo catalyst a solution of 30% hydrogen peroxide is used. This process is similar to that used in [37], but they use phosphoric acid instead. Etching with nitric acid is a much faster process, and the 50nm Mo will be gone in a matter of seconds. The peroxide is more controlled, and easier to work with, but takes minutes to etch the catalyst away. This is still an acceptable time window, and combined with quicker setup of the etching step, and easier cleaning afterwards, this was the method of choice.

The advantage here is that the Mo catalyst allows for transfer free process (TFP). During the etching the graphene stays in place, and will float down to land on the SiO_2 passivation layer. This means we don't have to use a polymer to attach to the graphene, and transfer it to a different wafer, which leaves a lot less room for error, and there's usually very little loss of graphene quality after transfer. This doesn't work for all catalysts however, and also becomes harder as the Mo is thicker, so in that case we have to find another way.

4.3.2. The HATR module

Another possible way of getting accurate infrared measurements is to use reflective instead of transmission measurements. The metal layer on the wafer will, next to absorbing, also reflect a part of the incoming infrared light. If we can measure this light in the detector, which has passed twice through the sample, we might be able to see absorption peaks generated by the graphene. In this way we wouldn't have to etch the catalyst away, and no other sample preparation is needed, which would be ideal. Unfortunately, the spectrometer that is available cannot conduct such measurements, as it is only suited for diffuse reflectance infrared Fourier transform spectroscopy (DRIFTS).

Figure 4.5: The Pike HATR accessory

However, a third option is possible: ATR or attenuated total reflection [58]. Here, The sample is placed on a crystal that is transparent to infrared light, for example diamond, germanium or zinc selenide. The 'total reflection' refers to the total internal reflection (TIR) that occurs in this crystal for the infrared light. The infrared light enters the crystal at an angle greater than the critical angle, and bounces back from the surface where the sample is. The 'attenuated' comes from the fact that the material, a powder, solvent or pliable film, put on top of the crystal will attenuate the infrared light, creating the characteristic spec-

trum in the end. In our case a HATR, horizontal ATR, is being used, simply meaning that the infrared light bounces up and down multiple times inside the crystal, each time undergoing TIR, so the same amount of infrared light enters and leaves the crystal. The accessory used is a Pike HATR, with a Zinc Selenide crystal of 4mm thick, so the light beam bounces exactly 10 times up and down. A press is used to make sure there is good contact between the crystal and the sample. The accessory is shown in figure 4.5.

The next question is how the sample can interact with the infrared beam, if it's on top of the crystal, while the infrared beam stays inside of the crystal. This happens with a so-called evanescent wave, that is created outside the crystal, orthogonal to its surface [59]. A visual representation is shown in figure 4.6. The sample can interact with this wave, and absorb some of its energy. To have an idea of the height of this wave, we can look at the depth of penetration:

$$d_p = \frac{\lambda}{2\pi(n_1^2 sin^2(\theta_1) - n_2^2)^{1/2}} \tag{4.1}$$

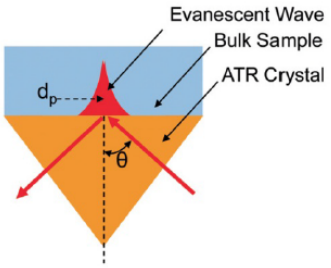

Figure 4.6: Total internal reflection, and the associated evanescent wave.

Where n_1 is the refractive index of the crystal, n_2 the refractive index of the sample (or air when no sample is present), λ is the wavelength of the IR light, and θ is the angle of incidence of the IR beam. If we fill this in for a glass plate (ZnSe: $n_1 = 2.4$, $\theta = 45°$, $n_2 = 1.4$, $\lambda = 4000cm^{-1} = 2.5\mu m$), we end up with a penetration depth of 0.414 µm. For graphene and Mo, the refractive index is both complex (the complex part is called the extinction coefficient), and a strong function of wavelength, hence this depth of penetration will be different. The conclusion however is still clear, the contact between the sample and the crystal must be really good, or we will just measure the air in between.

4.4. Energy-dispersive x-ray spectroscopy (EDX)

Another, readily available measurement method is EDX (sometimes also called EDS). This is a system that works in conjunction with an electron microscope, either SEM or TEM, since it needs an electron bundle to interact with the sample. The electrons from the high energy beam strike the surface, and will occasionally knock out an electron from its shell in the atoms that make up the sample. This means that a vacancy for an electron opens up, and because lower energy states are filled up first, an electron from a higher energy shell will fall back. In this process x-rays are emitted, with energy equal to de difference in electron energy before and after the jump. Those x-rays, called characteristic x-rays, are specific to the element they are emitted from. This process is visualized in figure 4.7.

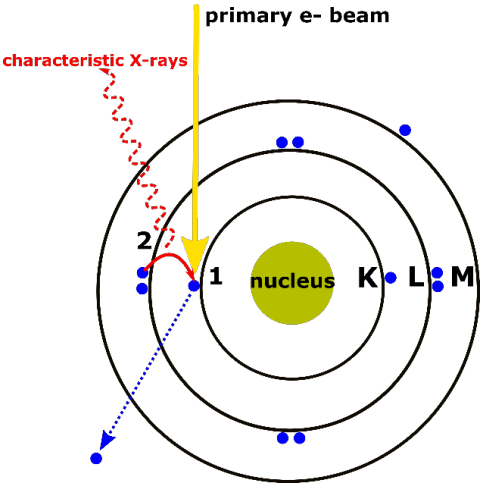

Figure 4.7: The process of emitting x-rays in EDX.

The EDX detector itself is an x-ray detector that will count the number of incoming x-rays, together with their energy, usually measured in kilo electronvolt (keV). From this information, the accompanying software will generate a histogram, where the elements are mapped from an energy chart, a periodic table where all the elements are listed with their specific energies. It should be noted here that, for bigger elements with more electron shells, more energies are available, and thus more peaks will show up in the histogram. This is because instead of just jumping from the L to the K shell, electrons can now also jump from M to L, N to M, or even skip shells to go from M to K or even N to K. This usually produces much higher energy x-rays, and so the elements can still be distinguished from one another. The energy chart is added in appendix [ref]. An example histogram is shown in figure 4.8. Note how the software already maps elements to the peaks to make it more readable.

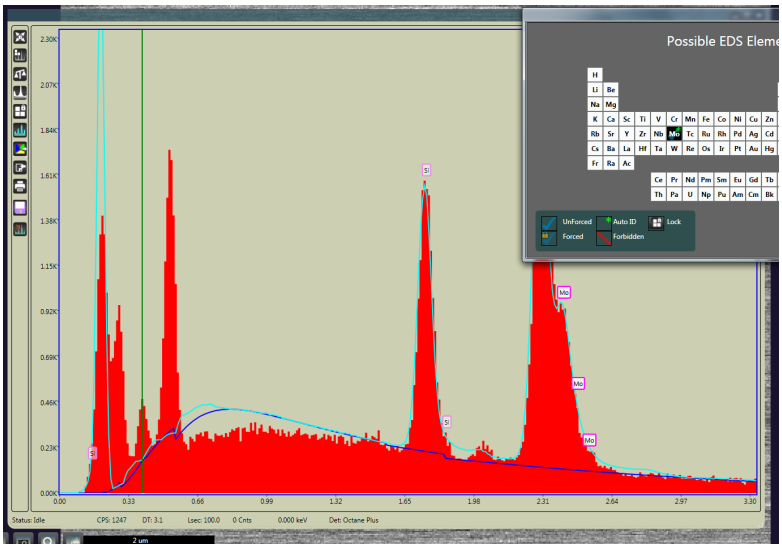

Figure 4.8: A histogram produced by an EDAX system, showing Si, Mo, C, N and O.

Operating the EDX system, there is one important parameter to choose, that was already mentioned in section 4.2, namely the acceleration voltage of the electron beam. This was also important in producing good images with a SEM, where the emitted electrons are detected to produce a 2D image. In this case we are detecting x-rays, and to generate them we need a higher acceleration voltage, starting from 5 kV. For heavier elements we need an even higher voltage, and a rule of thumb is to use twice the expected energy peak. As an example, for iron (Fe) we would expect a peak at 0.705 keV and at 6.403 keV, so we would use at least 14 kV for the electron beam. The downside here is that, as a general rule, the more energetic the electrons are, the deeper they penetrate into the sample. Since graphene is really thin, ideally we would like to image only the surface of the sample, and thus we want to use an acceleration voltage that is as low as possible. Unfortunately, this turns out to be unfeasible, as even for the lowest voltages electrons travel a few hundreds of nanometers into the sample, which is already way beyond the graphene thickness. If we look at the shape of the interaction volume in figure 4.9, this would mean almost no x-rays would originate from the graphene layer.

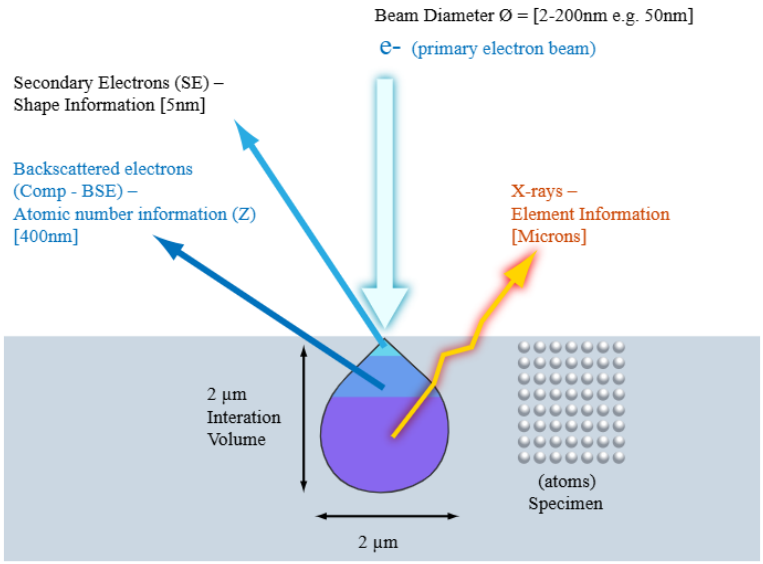

Figure 4.9: A side view of the electron beam interacting with a sample volume.

Where the interaction volume increases with higher acceleration voltages, it decreases as the sample material either has heavier atoms, or if the atoms are packed closer together. In other words, if the density is high, the electrons will penetrate less deep into the sample. Transition metals, used for the catalyst material, have one of the highest densities in the periodic table, with Mo ($10.2 g/cm^3$) coming in not far behind lead ($11.342 g/cm^3$), and thus will stop a lot of the incident electrons. This means we can use the EDX method to analyze the catalyst for dopant atoms. Albeit not a proof of doping on its own, if the histogram shows nitrogen, it could be an indication of nitrogen doping in the graphene layer.

4.5. Back-gate measurements

Just like with semiconducting materials like silicon and germanium, doping graphene with impurity atoms will cause its electrical properties to change. This can be investigated by doing electrical measurements in a FET geometry, with graphene as the channel material. For this a back-gate transistor is usually fabricated, where graphene is transferred onto a Si/SiO_2 sample, with heavily doped silicon acting as a back electrode. This back electrode can be used as a gate, and will affect the conduction in the graphene channel by sweeping the voltage across it. A device like this is shown in figure 4.10, the contacts are usually made of a noble metal, like palladium or gold. Just like a silicon FET it has a width and length, and contacts called gate, drain and source.

A transistor would normally use a semiconducting material as a channel. The bandgap, E_G, of this material is important as it determines a lot of properties of the transistor. Pristine graphene doesn't have a bandgap, as it is a semimetal, and so it will always conduct, like a metal. In other words, we cannot turn it on or off, which is exactly what we want to do in a transistor. Doping it with impurities can cause a bandgap to open by suppressing the density of states near the Fermi level [28]. This bandgap is hard to measure directly, but it can be estimated from the on/off ratio of the drain currents when sweeping the gate voltage. Bandgaps of common semiconductors are 1.08 eV for silicon, 0.66 eV for germanium and 1.42 eV for gallium arsenide. To get sufficient I_{on}/I_{off} for use in CMOS logic structures, a bandgap of at least 0.4 eV is required [60]. This bandgap is proportional to the atomic percentage of impurities incorporated in the graphene lattice. For a concentration of 3.13% N-atoms this is estimated to be 0.21 eV using DFT calculations. For 12.5% doping the bandgap would rise to 0.6 eV [61].

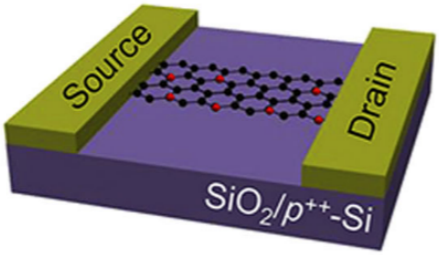

Figure 4.10: A graphene back-gate transistor device. Image taken from [1].

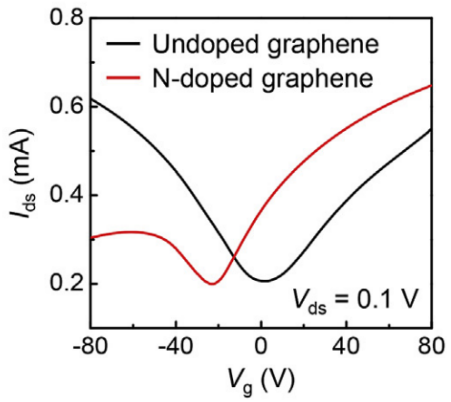

Figure 4.11: I_{ds}-V_g characteristic of pristine and nitrogen-doped graphene. Image taken from [30].

Next to the bandgap, p-type and n-type doping can be measured in graphene. This can be seen by a shift in the dirac point, as shown in figure 4.11. The dirac point is where the conduction and valence bands meet in graphene, and for pristine, undoped graphene it can be found at zero gate voltage (black curve in the figure). However, if the material is doped, either electron (n-type) or hole transport (p-type) becomes dominant. The Fermi level will shift into the conduction or valence band, and we need to apply a voltage to find back the dirac point. For N-doped graphene, which will most likely become n-type, we need to apply a negative voltage to repel the negatively charged electrons from the channel to find the point of lowest conductivity, which is the dirac point. This is shown in the figure with the red curve. Similarly, for p-type graphene the v-shape would move into the positive, right half of the graph. Note that, for PG, the V-shape of the graph is very symmetrical, but for the NDG, the left side quickly saturates. This is because we have both

electron and hole mobility for graphene, and for undoped graphene the electron and hole concentrations are in the same order of magnitude. For n-type graphene however, there are much more electrons (majority carriers), but much less holes (minority carriers), because each hole that is created will quickly recombine with an electron and vanish. For this reason, we can only get limited conductance with the minority carriers, and hence the drain current will saturate much quicker.

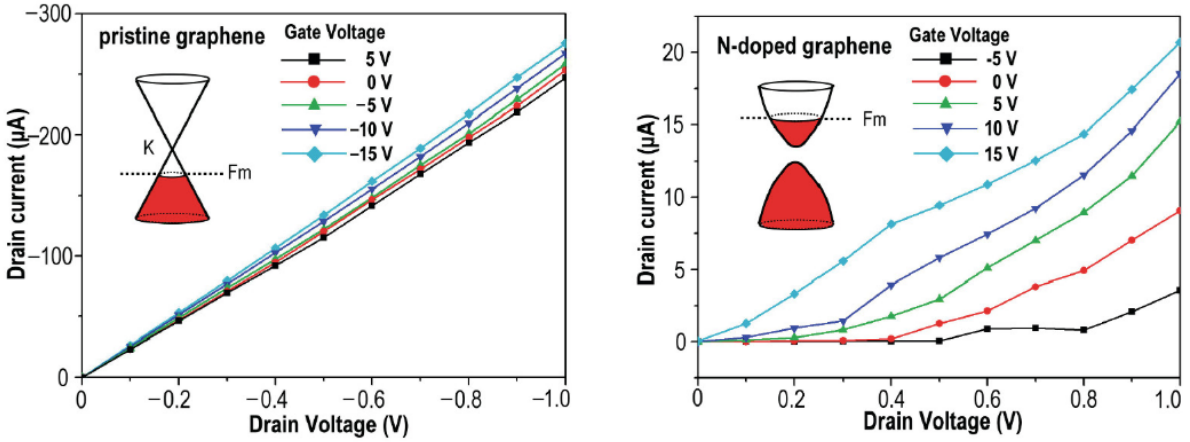

Figure 4.12: I_d-V_{ds} characteristic of pristine and nitrogen-doped graphene, together with the presumed band structures. Image taken from [28].

A different measurement is to sweep the drain voltage for different gate voltages, as shown in figure 4.12. This shows very clearly that for pristine graphene the channel acts as a resistance, with very linear behavior for different drain voltages. The N-doped graphene however is showing more complex behavior, starting to act more like a semiconductor, with slopes being dependent on both the drain and the gate voltage applied. By doing those measurements we can actually prove that we have effectively doped graphene, and changed its electrical properties.

4.6. X-ray photoelectron spectroscopy (XPS)

This technique is based on the photoelectric effect, meaning that light striking on a surface causes emission of electrons. In this context light means an electromagnetic wave, and in order to have sufficient energy to knock out electrons, we need to be in the X-ray frequency region. In a sense this technique is the opposite of the EDX technique (section 4.4), where an electron beam is directed onto a sample where it will knock out electrons from orbit, which will emit X-rays when higher energy electrons fall back to lower orbits. Also the information contained in the output signal bears similarities to that of EDX: we can identify the chemical elements in the sample, starting from lithium, and we can estimate the atomic concentrations of those elements. However, XPS has two significant advantages over EDX:

1. The technique uses low energy X-rays that will not penetrate very far into the sample material. This will result in a very shallow imaging depth of only a few nanometers.
2. Next to elemental identification the output signal contains information on chemical bonding to nearest neighbors. This means we can say something about the valence state of the atoms.

Those are significant advantages for the characterization of graphene, because point 1 will help us to mainly measure the graphene instead of the catalyst with EDX, and point 2 will help us determine the type of N-bonds (graphitic, pyridinic or pyrrolic) we have, if any.

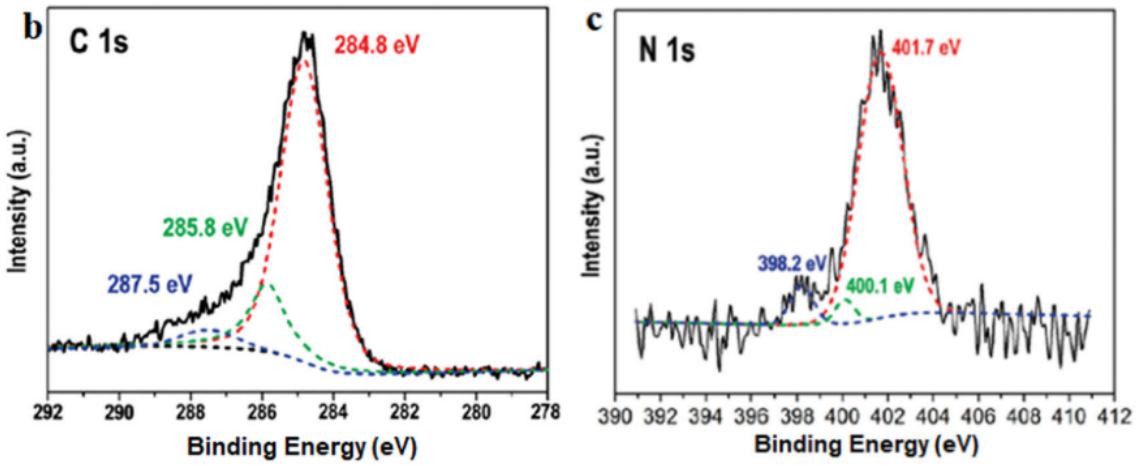

Figure 4.13: The C1s and N1s spectrum peaks of nitrogen-doped graphene. Image taken from [1].

A typical spectrum for nitrogen-doped graphene is shown in figure 4.13, where we already zoomed in on the two most important peaks, carbon and nitrogen. The peaks are not simply Lorentzians, but rather have a complex shape consisting of multiple peaks molten together. To get information on the chemical bonding a deconvolution is needed, which is also shown in the image. For carbon, we have the big peak at 284.8 eV, which are the sp^2-hybridized C atoms, bonded to other C atoms, that make up the graphene lattice. The two smaller peaks at 285.8 and 287.5 eV correspond to sp^2-hybridized and sp^3-hybridized C atoms that bond with N-atoms respectively.

For the N1s peak, there are also three smaller peaks present. Those correspond to the three bonding types of nitrogen we discussed earlier. In this case the big peak at 401.7 eV is graphitic-N. The two smaller ones are located at 400.1 eV for pyrrolic-N, and at 398.2 eV for pyridinic-N. Since the kind of N-bonding with graphene varies wildly with the synthesis method used, and with process parameters, it is really important to make sure this deconvolution is done correctly. For example, in [33] an XPS analysis is performed as well, and the main doping configurations are pyridinic and pyrrolic N-atoms.

To calculate the nitrogen content in the sample, one needs to find the areas under the peaks, and divide them by the total area. The number found will be the atomic percentage, which will usually be a few percent at max. Figure 4.13 might be misleading in this, since the intensities are plotted in arbitrary units, and the peaks are shown with the same size. To give an idea of the peak size, a full spectrum is shown in figure 4.14. Here it also shows the y-axis in counts per second, similar to EDX, which makes different figures easier to compare. Unfortunately, in most of the literature the arbitrary units are used.

This technique will be used as a final proof of doping, and show the type of N-doping. The results will be presented in the next chapter.

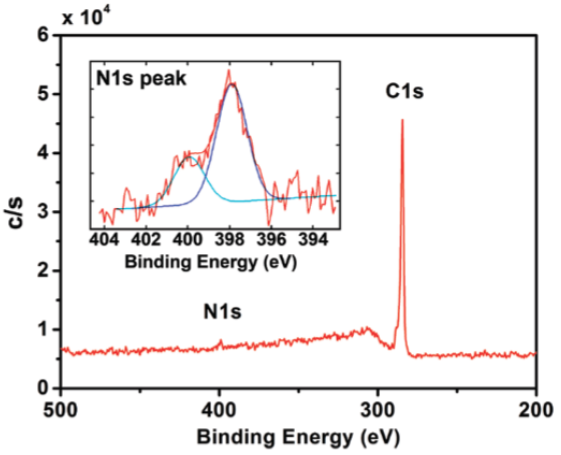

Figure 4.14: Full XPS spectrum of NDG. Image taken from [33].

5

Results with ammonia

This chapter will show and discuss the results found after the experimental and characterization work with ammonia and methane as precursor. It will also show the experiments that didn't work or were not performed in the correct manner, to indicate important details that should be taken into account. The lab work was done in batches, each consisting of a small number of wafers, that were prepared for graphene growth. This involves thermal oxidation of the silicon to form a silicon dioxide passivation layer, sputtering a metal catalyst for graphene growth, and optionally patterning this catalyst to make the transfer free process easier. After this, the wafers were diced, so that many smaller pieces of silicon wafer were obtained, and a lot of different graphene recepies could be run from a single wafer. This makes it possible to investigate a variety of different process parameters.

5.1. First batch

The first batch consisted of a 100 mm p-type, single side polished, 525 μm thick wafer with ρ = 1 - 5 Ωcm. The SiO_2 passivation layer was grown at 600 nm, and the molybdenum (Mo) catalyst was sputtered 50 nm thick. It was diced in 8 pieces, conveniently numbered 1 till 8, to grow different pristine graphene and nitrogen-doped graphene samples. The CVD plan is shown in table 5.1.

Table 5.1: The CVD recepies for the pieces of the first wafer.

Sample (#)	Pristine or nitrogen-doped	Temp. ($^\circ C$)	Pressure (mbar)	Growth time (min)	CH4 flow (sccm)	NH3 flow (sccm)	Ar / H2 (sccm)
M1.1	PG	935	25	20	25	0	960 / 40
M1.2	NDG	935	25	20	25	20	960 / 40
M1.3	PG	935	25	5	25	0	960 / 40
M1.4	NDG	935	25	5	25	100	960 / 40
M1.5	NDG	935	25	5	25	20	960 / 40
M1.6	NDG	935	25	5	25	10	960 / 40
M1.7	NDG	935	25	10	25	10	960 / 40
M1.8	NDG	885	25	10	25	10	960 / 40

The parameters for sample M1.1 have already been tried and tested in the Else Kooi laboratories, and this sample serves as a reference for the measurements. The recipe has been added in appendix A, along with some explanation of the code. This recipe was used as a starting point to find a recipe suitable for nitrogen doping. Next to adding the nitrogen precursor, only one parameter was changed per sample, so that we could make sure that resulting changes in the graphene quality, electronic properties and possible doping, were due to that specific change. The BM creates log files of all its setpoints and actual values after each run, which were closely monitored to make sure that what happened inside the reactor is in alignment with the programmed recipe. Each run, including heating up and cooling down, took approximately 2 hours to complete.

Table 5.2: The curve-fitting results of the 5 samples from the first batch containing graphene.

Peak fittings D, G, 2D	Sample M1.1	Sample M1.3	Sample M1.6	Sample M1.7	Sample M1.8
Intensity	0.38	0.56	0.42	0.18	0.49
(normalized	0.99	0.98	0.98	1.00	0.99
to G-peak)	0.89	0.92	1.26	0.85	1.06
Center	1339	1341	1338	1335	1336
location	1587	1590	1588	1584	1588
$[cm^{-1}]$	2671	2675	2670	2668	2671
FWHM	44	42	41	40	46
$[cm^{-1}]$	35	36	35	29	38
	62	65	63	65	66

5.1.1. Raman measurements

All samples were measured in a Renishaw Raman Spectroscopy setup using a 633nm laser, and with the obtained spectra it is possible to tell the difference between graphene or no graphene. In the case of no graphene, just a flat, noisy line was obtained with very low counts. In case of graphene, the three distinct peaks, explained already in section 4.1, were visible. In this batch, the samples containing graphene were M1.1, M1.3, M1.6, M1.7 and M1.8. The spectra of those are shown in figure 5.1.

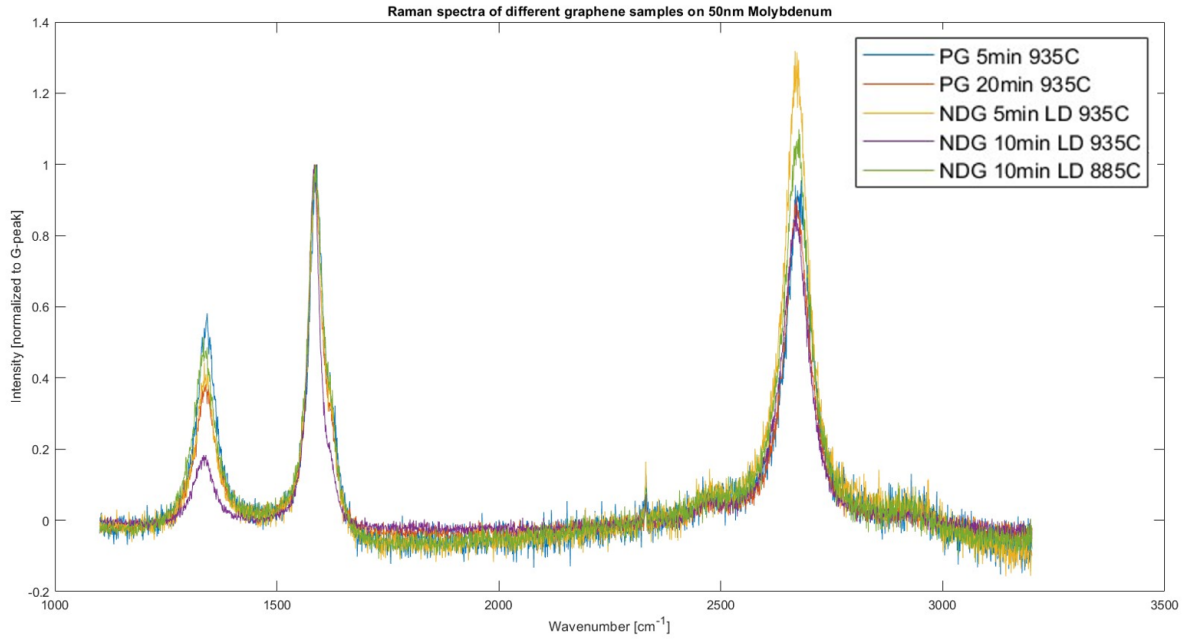

Figure 5.1: The results of the first batch of graphene samples, the baseline is corrected.

On top of that, a curve fitting script was used to be able to make a comparison. In this script, the baseline of the graphs is corrected, and 3 lorentzians are used to locate the three characteristic peaks. In this way it is possible to extract the exact location, intensity and full width at half-maximum (FWHM) of the peaks. The results of this are shown in table 5.2. The script itself is attached in appendix B.

It should be noted that the intensities of the peaks are seldom used to judge the graphene quality. Rather, the ratios of the intensities relative to other peaks are used, with the two most used ones being I_D/I_G and I_{2D}/I_G. This is because multilayer graphene will give a stronger Raman signal, and produces higher peaks, but is not desirable over single layer graphene. The I_D/I_G ratio indicates how defective the graphene is (higher values meaning more defects), and the I_{2D}/I_G ratio gives an indication on the layer count (single layer graphene produces large values). In the table the intensity values are normalized to the G-peak, so the value for D is close to the I_D/I_G ratio, and the value for 2D is

approximately the I_{2D}/I_G ratio, which makes them easier to compare.

From these results an important conclusion could be drawn. All samples that saw more than 10 sccm of ammonia gas, have no graphene on them. This means that, in one way or another, the introduction of ammonia gas next to methane, impedes the growth of graphene instead of doping it with nitrogen. The next logical step would be to go to lower flow rates of ammonia compared to methane.

5.1.2. SEM micrographs

The main point of using the SEM is to spot structural differences in the morphology of the catalyst surface. Seeing the graphene itself proves to be difficult because it's so thin. Even with low beam acceleration voltage, and with a deceleration option for lower landing voltage, the graphene only shows up when it has multiple layers. Still, because the graphene grows on the interface with the catalyst, by imaging that surface we can still tell something about the graphene growth process. For this batch, the most interesting question to ask is whether there is a visual difference between the samples containing graphene, and the ones that don't.

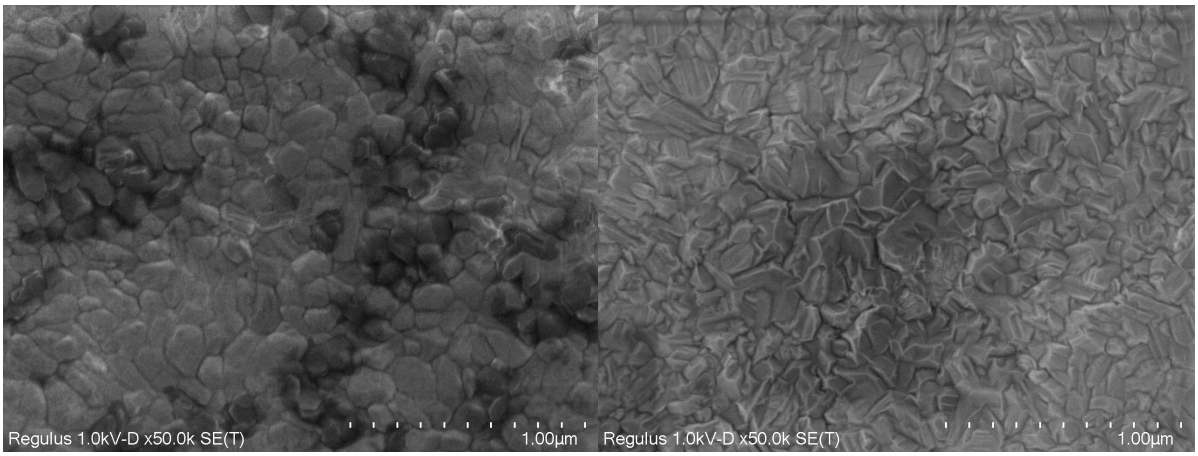

(a) Sample M1.5 without graphene 50k times magnified **(b)** Sample M1.7 with graphene 50k times magnified

Figure 5.2: Comparison of two samples without and with graphene. Left is grown with 20 sccm NH_3, right with 10 sccm.

The images in figure 5.2 are taken with the same electron beam settings, magnification and detector. They look a bit different, with the left picture having more rounded grains, and the right one sharper, more defined grains. This might however also be because of a slightly different focus, contrast or brightness setting. At least the grains are there in both cases, they're about the same size and in both cases there are darker regions as if clouds are drifting over it. In contrast, sample M1.4, where a lot more ammonia gas was used, is a lot harder to image, and at 22k magnification, getting a sharp image was already a challenge. Usually this is an indication of a smoother surface: if there are no clear structures or sharp lines present, focusing is difficult. This could also be why figure 5.2a is less sharp than 5.2b. The hypothesis here is that, before graphene growth, the methane interacts with the catalyst to form molybdenum carbide (either MoC or Mo_2C), which are the visible grains. Graphene can then grow on top of the carbide layer. Introducing ammonia during this reaction slows the formation of these crystal grains, or stops it altogether if the flow is sufficiently high. To test this, we need to run more recepies in the next batch (see section 5.2).

5.1.3. FTIR results

To conduct transmission measurements with the FTIR setup, the metal catalyst needs to be etched away, as explained in section 4.3. This was however not a trivial task, and a mistake was made which caused most of the grown graphene to be lost. Still, measurements were conducted with different background samples (silicon, SiO_2 and without sample), but the results didn't show any new peaks, and the self-diagnostics showed that too little signal was reaching the detector. For now, the decision was made to move to a second wafer, grow new graphene samples, be more careful with the etching,

and then do measurements again with the FTIR to see if we can get better results.

5.2. Second batch

The second batch, like the first batch, consisted of a p-type, single side polished (SSP), 525 μm thick wafer with ρ = 1 - 5 Ωcm. However, this one was diced in 12 pieces to allow for more process variations, while still maintaining sufficient sample size to use them in the measurement tools. The CVD plan is shown in table 5.3. Note that the first sample wasn't processed at all. This is because we need to have a bare Mo sample for using as a background in the HATR measurements, as explained in paragraph 4.3.2. Also, the temperatures here are lower than in the first batch, which is because the quartz around the bottom heater in the BM was replaced, and good quality graphene could be obtained at lower temperatures. The main focus of this batch is to try some more combinations of growth time, methane flow, and ammonia flow to find the limits for when graphene will or will not grow.

Table 5.3: The CVD recepies for the pieces of the second wafer.

Sample (#)	Pristine or nitrogen-doped	Temp. ($^\circ C$)	Pressure (mbar)	Growth time (min)	CH4 flow (sccm)	NH3 flow (sccm)	Ar / H2 (sccm)
M2.1	none	-	-	-	-	-	-
M2.2	PG	915	25	15	25	0	960 / 40
M2.3	PG	915	25	15	50	0	1920 / 80
M2.4	PG	915	25	60	25	0	960 / 40
M2.5a	NDG	915	25	15	25	10	960 / 40
M2.5b	NDG	915	25	15	25	5	960 / 40
M2.6a	NDG	915	25	15	50	20	1920 / 80
M2.6b	NDG	915	25	15	50	10	1920 / 80
M2.7a	NDG	915	25	60	25	20	960 / 40
M2.7b	NDG	915	25	60	25	15	960 / 40
M2.8a	NDG	915	25	15	25	10*	960 / 40
M2.8b	NDG	915	25	60	0	100	960 / 40

* *The ammonia was turned on 5min after the methane was introduced in the reactor.*

5.2.1. Raman measurements

For this batch, the Raman setup was used a bit differently. Since in the previous batch it was found that ammonia seems to impede the graphene formation, the challenge here was to grow graphene with lower flow rates of ammonia, and then compare the different Raman results against the pristine graphene samples. Hence, the goal of this measurement was to check if there was graphene on the samples at all. This was quickly done by using 50% laser power, with an accumulation time of 10s, and checking if the three peaks would show up. From this it was clear that sample M2.1, M2.6a and M2.8b didn't contain graphene. For M2.1 and M2.8b this was not surprising. For M2.6a, which we grew longer and with relatively more methane than sample M2.5 of the first batch, it was though. For sample M2.7a, which did grow longer but with less methane, there was graphene, so judging from these results, the graphene growth process takes more time to start up when there is ammonia present in the gas mixture.

Before comparing the Raman results quantitavely, the log files of the BM were consulted, and it turned out that, below 20sccm of NH_3 flow, the MFC that was responsible for controlling this flow, didn't open at all. This was found to be common behaviour for MFCs: they specify in their datasheets that operating them in the lower 2% of their full range will give inaccurate results. In this case the range is 10-1000sccm, so we shouldn't operate it below **20sccm**. This meant that most of the produced samples in this batch are just pristine graphine, and only M2.6a and M2.7a would be interesting to compare. Unfortunately, the former doesn't contain graphene while the latter does, so it's hard to compare them by using Raman measurements. Nonetheless the Raman fitting was applied, and the results are shown in table 5.4.

Table 5.4: The curve-fitting results of the 9 samples from the second batch containing graphene.

Peak fittings D, G, 2D	Sample M2.2	Sample M2.3	Sample M2.4	Sample M2.5a	Sample M2.5b	Sample M2.6b	Sample M2.7a	Sample M2.7b	Sample M2.8a
Intensity	0.57	0.50	0.30	0.30	0.36	0.64	0.52	0.36	0.33
(normalized	0.99	1.00	0.97	1.00	0.93	0.96	0.97	0.99	0.97
to G-peak)	0.87	0.67	0.62	1.79	0.72	1.23	0.94	0.83	1.34
Center	1340	1338	1338	1337	1337	1339	1337	1338	1337
location	1589	1588	1586	1587	1587	1588	1587	1587	1587
$[cm^{-1}]$	2668	2668	2670	2670	2670	2664	2668	2671	2669
FWHM	41	45	43	40	42	45	43	44	41
$[cm^{-1}]$	38	38	31	31	32	40	38	33	31
	64	72	68	41	63	57	57	56	51

It can be read from the table that the intensities vary quite a lot, but the peak positions and widths are all close together. The variations of the peak intensities also depend on the exact spot on the sample, which is visible in the large 2D peak difference between sample M2.5a and M2.5b, even though they are virtually the same recipe. This means multiple points on a sample should be measured and averaged to be able to make a good comparison. The width of the 2D peak also varies quite a bit, but when the spectra are plotted on top of each other it becomes visible that this difference is mainly because of the differences in peak height, as can be seen in figure 5.3. Note also that the growth time (15 or 60 minutes) doesn't have a significant impact on the graphene quality. Furthermore there is no significant difference between the values of the previous batch (see table 5.2). We will use those values as reference when moving to different catalysts or precursors.

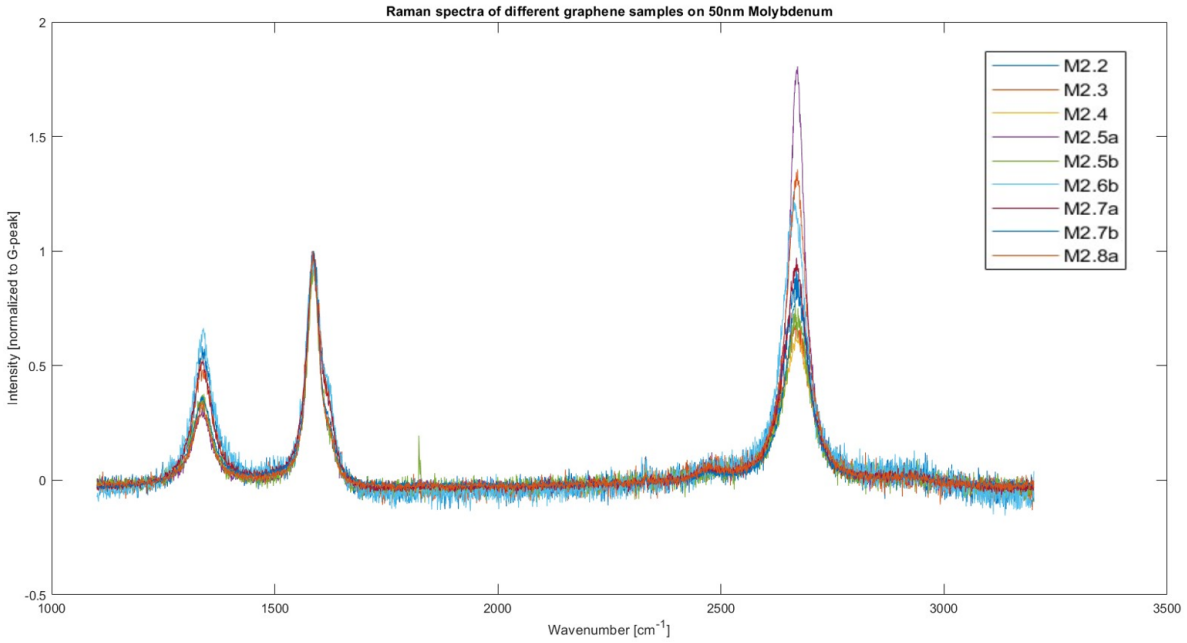

Figure 5.3: The results of the second batch of graphene samples, the baseline is corrected.

5.2.2. SEM micrographs

There is however still an interesting sample to study with the SEM in this batch, namely M2.8b, which was deliberately only treated with ammonia without any methane. The prediction is that, if we can pretreat the Mo catalyst with nitrogen, by bringing it in contact with ammonia gas at high temperatures, we should be able to grow graphene on it afterwards. The nitrogen contained in the catalyst could then diffuse out during the graphene growth, and get stuck in the graphene lattice, replacing some of the carbon atoms. To see if the ammonia had any effect at all on the Mo, SEM scans were made, and shown in figure 5.4. It is compared with a methane only sample.

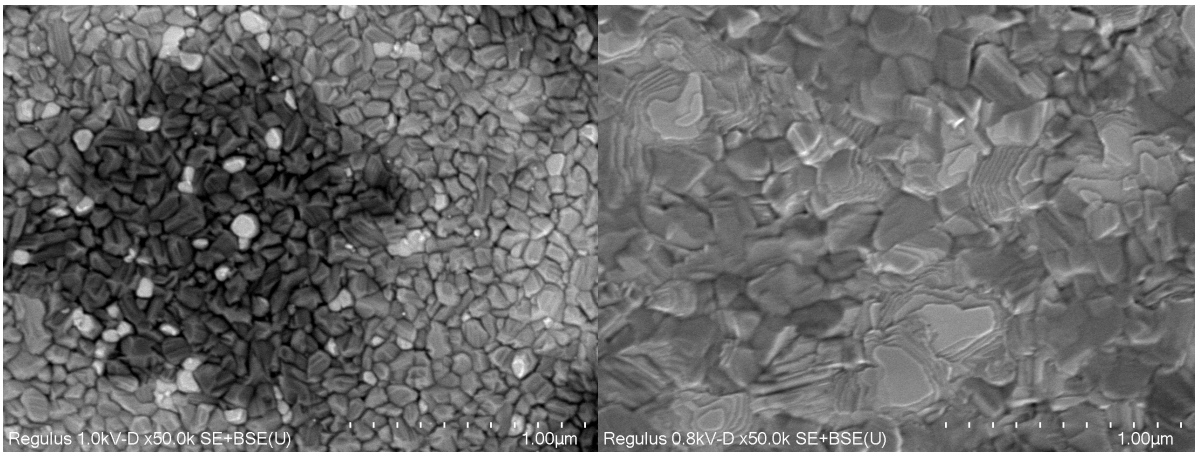

(a) Sample M2.6b with graphene 50k times magnified

(b) Sample M2.8b with ammonia 50k times magnified

Figure 5.4: Comparison of two samples' catalyst grains. Left is grown with 25 sccm CH_4, right with 100 sccm NH_3.

As can be seen, there is quite some difference. In figure 5.4b, the grains are much bigger, and seem to create 'terraces' where the crystals are stacked on top of each other. Also the 'clouds' (the darker part in figure 5.4a) drifting over the sample are gone, and there appear to be a lot more depth differences as if the sample was etched. To confirm a different chemical composition of the catalyst, we need to use an EDX setup, this will be discussed in section 5.2.4.

5.2.3. FTIR results

For this batch, the decision was made to use the HATR module as explained in paragraph 4.3.2, which was unavailable to us for the first batch. The HATR module doesn't need etching of the catalyst, and it should be more sensitive to surface materials since it interacts 10 times with it, instead of just passing through it once in a transmission measurement. The transmission accessory of the spectrometer was replaced with the HATR accessory, and the settings were adapted to use ATR correction on the interferogram. Samples were placed upside down on the module, with the graphene in contact with the ZnSe crystal, and then pressed down to ensure an intimate connection.

Unfortunately, not a single good measurement was obtained with the HATR accessory. The system gave errors about the measured signal being too low, and the peaks showing in the resulting spectra were very low. In example spectra the peaks usually go as far as 20% transmittance (which means 80% is either absorbed or reflected), and most of the expected peaks show up at at least 90%. Those rules are not set in stone, but in our case the magnitude of the peaks was most of the times not even 1% from the baseline, which makes these results doubtful to say the least. The error regarding signal magnitude was not the biggest problem, as it states in the HATR manual [59] that the energy throughput of this specific HATR module is around 15% of the throughput in an N_2 environment. Since we are working with a background-sample measurement method, just like with the transmission module, this should still give us valid results.

There are two explanations for this behavior. The first one is that the refractive index of the sample is too high to be measured with the ZnSe crystal. It is not trivial to find reliable numbers for the refractive index of graphene or Mo, but the numbers that can be found are usually above the index of ZnSe, preventing total internal reflection to happen. For another carbon material, diamond, the index is 2.417, which would also not work, so this could be a plausible explanation. The other reason could be that the HATR accessory is not made for these kind of samples. The sample holders are made for liquids, pastes and pliable solid films. Our samples are not pliable, and so will leave an airgap between it and the crystal, preventing the evanescent waves from reaching the sample. In either case, there is no simple solution we can utilize to make these measurements work, so we will move back to the transmission measurements for which we will need to etch the catalyst.

5.2.4. EDX spectra

As other characterization techniques proved to be insufficient to get a good picture of possible doping going on in our samples, an additional measurement tool was proposed to determine the chemical composition of the layers: EDX. As already explained in section 4.4, it works in conjunction with a SEM, since it needs an electron beam as input. For this technique, no sample preparation was required, but we could run a simulation up front to get an idea what we are actually measuring. This simulation was done in Casino [62], and the results are shown and explained below. After running this simulation, the actual measurement was performed, but a very low count rate was obtained from the x-ray detector, causing the results to be inaccurate. It turned out that the electron beam in the SEM needed alignment, since hardly any electrons were reaching the sample. This was a matter of time only, because the maintenance was already planned, so it was decided to leave this measurement for the next batch.

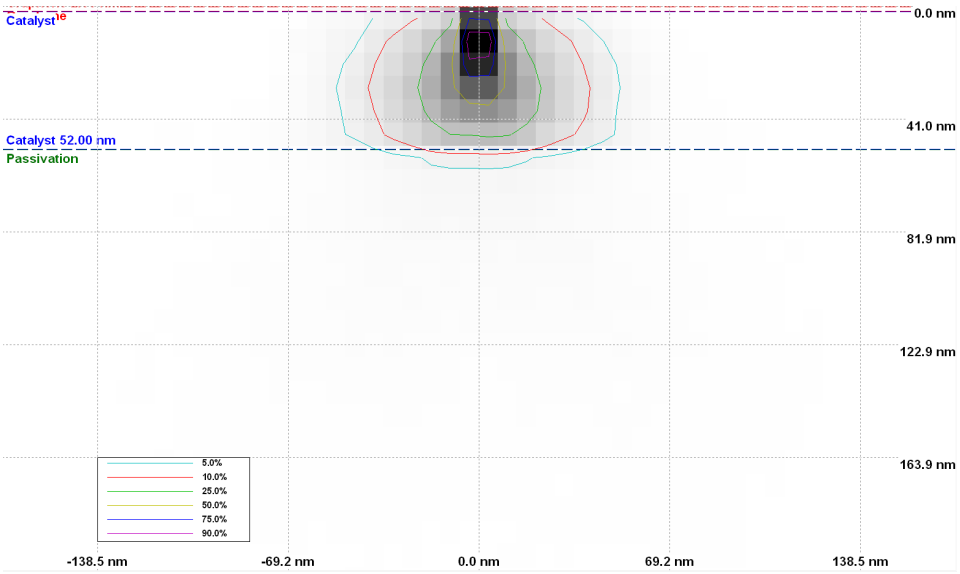

Figure 5.5: The energy by position chart generated by the Casino simulation.

The Casino simulation returns a lot of outputs, about the electron hits as a function of depth and backscatter angle. What we want to know is where the x-rays will be generated in the sample. In the simulation a stackup of material layers is made, in our case the wafer (Si), the passivation layer (SiO_2), the catalyst (Mo) and the graphene layer(s), made of carbon. Then an acceleration voltage is chosen (multiple can be simulated at once), and a monte carlo simulation is run. In figure 5.5 the result is shown for a 5kV electron beam. The colored lines show the penetration depths where the incident electrons have a certain amount of their energy left. The background squares with grayscale colors show the probability of generating x-rays at that location, with darker colors meaning a higher probability. This is a positive result, since it shows that most x-rays are generated in the catalyst near the surface, even for only 50nm of Mo. In section 5.3.3 the measurement results will be discussed.

5.3. Third batch

Before the third batch was produced, a new insight was gained while doing measurements on the FTIR spectrometer. The previously used wafers without any kind of processing were already blocking a large portion of the infrared radiation, and causing the spectrometer to give errors on too little signal received at the detector. This was probably caused by the low resistivity of those wafers, since skin depth, δ_s, is a function of conductance for electromagnetic waves in a lossy medium, with a higher conductance (lower resistivity) resulting in lower skin depth [63]. Another possibility is the unpolished backside of those SSP wafers, where the infrared light has to exit the wafer via a diffuse surface, causing scattering and thus a lot less radiation reaching the detector.

To combat both of them, for this batch p-type, double side polished (DSP) wafers are used with a thickness of 500 μm and $\rho > 1000\Omega cm$. Also the catalyst was patterned with 15x15 mm squares to make the etching process easier. This is because graphene can also grow on the side of the catalyst

and anchor to the SiO_2 layer, preventing the graphene from drifting away during etching. Two different thicknesses were used for the catalyst, 50nm and 200nm, to measure the impact on graphene growth. They are addressed with an 'a' (50nm) or 'b' (200nm) after the sample number.

The goal of this batch was specifically to try and find a recipe that would reliably grow graphene on Mo samples with the combination of CH_4 and NH_3, and collect their FTIR spectrum.

The wafers were again diced in 12 pieces, for which the CVD plan is shown in table 5.5. From the previous batch it turned out that graphene could only grow in combination with ammonia, if the recipe was run for longer times (60 minutes), so this was used as a standard in this batch. Only the first sample was grown shorter so the two PG samples could be compared against each other in the FTIR.

Table 5.5: The CVD recepies for the pieces of the third wafer.

Sample (#)	Pristine or nitrogen-doped	Temperature ($^\circ C$)	Pressure (mbar)	Growth time (min)	CH4 flow (sccm)	NH3 flow (sccm)	Ar / H2 (sccm)
M3.1	PG	915	25	15	25	0	960 / 40
M3.2	PG	915	25	60	50	0	960 / 40
M3.3	NDG	915	25	60	50	20	960 / 40
M3.4	NDG	915	25	60	50	40	960 / 40
M3.5	NDG	915	25	60	100	20	1920 / 80
M3.6	NDG	915	25	60	100	40	1920 / 80
M3.7	NDG	915	25	60	50	20*	960 / 40
M3.8	NDG	915	25	60	50	40*	960 / 40
M3.9	NDG	915	25	60	50	100*	960 / 40
M3.10	NDG	915	25	60	25**	100	960 / 40
M3.11	NDG	915	25	60	50**	100	960 / 40
M3.12	NDG	915	25	60	100**	100	1920 / 80

** The ammonia was turned on 15min after the methane was introduced in the reactor.*
*** The methane was turned on 30min after the ammonia was introduced in the reactor.*

5.3.1. Raman measurements

From the 12 samples, the first 6 were produced first and tested with Raman, so that changes could be made in the remaining recepies if necessary. This turned out to be a good choice, since only the first 2 samples contained graphene, while sample 3-6 surprisingly enough didn't. The difference could also be easily seen through the optical microscope in the Raman setup, this is shown in figure 5.6. Compared with sample M2.7a (see table 5.3) these samples have similar or higher methane to ammonia ratios, while the other parameters stay the same. To make sure a good conclusion could be drawn from this, the recepy of sample 7a was run again on a new Mo 50nm sample, to see if it would still produce graphene. This time it didn't, even though the only difference was a different wafer, and a patterned catalyst.

To dive deeper into this problem, two theories had to be tested: if already grown graphene would be etched away when exposed to ammonia gas at elevated temperatures, and if the ammonia can change the chemical composition of a catalyst without graphene on it, which seems apparent from figure 5.4. The former will be explained here, the latter is elaborated on in paragraph 5.3.3.

To try and etch the graphene on the first 2 samples, sample M3.1b was treated with 20sccm of NH_3 for 15 minutes, and sample M3.2b with 100sccm of NH_3 for 60 minutes. A Raman measurement was performed before the etching and afterwards to see changes in graphene quality. The results are shown in figure 5.7 and 5.8 for sample M3.1b and M3.2b respectively. All of them are taken with 100% laser intensity with the red 633nm laser. The different measurement points are chosen arbitrarily, but always include lighter and darker spots.

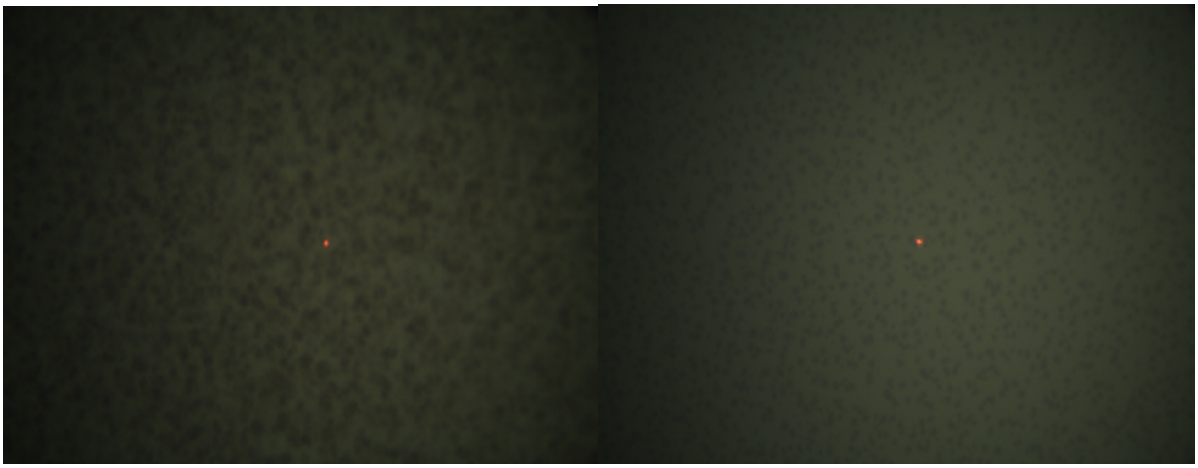

(a) Sample M3.2a with graphene 100 times magnified **(b)** Sample M3.4a without graphene 100 times magnified

Figure 5.6: Comparison of two samples with and without graphene. The density and size of the speckles differ.

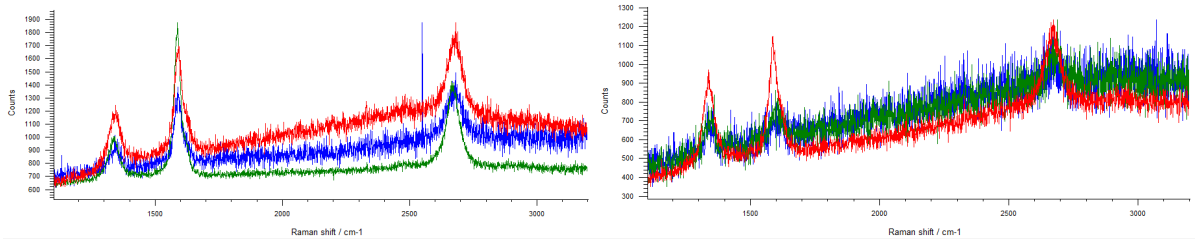

(a) Sample M3.1b before etch. Blue = 10s, green = 30s, red = 30s. **(b)** Sample M3.1b after etch. Blue = 10s, green = 10s, red = 30s.

Figure 5.7: Comparison of sample M3.1b before and after etch. The accumulation times are mentioned in the caption.

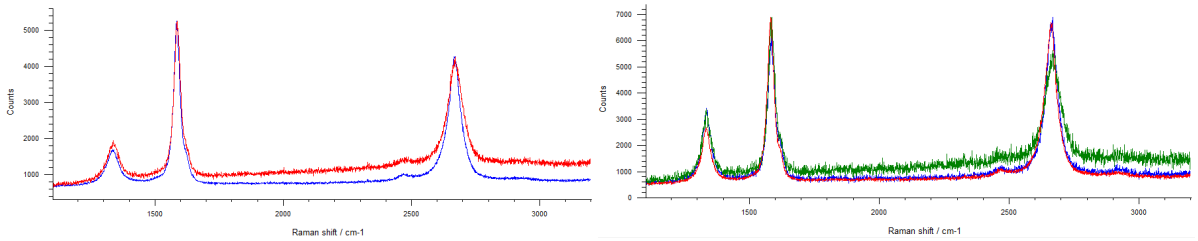

(a) Sample M3.2b before etch. Blue = 30s, red = 30s. **(b)** Sample M3.2b after etch. Blue = 10s, green = 10s, red = 30s.

Figure 5.8: Comparison of sample M3.2b before and after etch. The accumulation times are mentioned in the caption.

All vertical axes are that of count rates for 30s accumulation time. As explained, the peak intensities increase with multiple layers of graphene, but their ratios tell more about the quality. Still, a decline in the peak intensity could be an indication that the ammonia gas is removing graphene layers. In both cases the D-peak seems to have increased slightly, indicating more defects. For sample M3.1b the counts have decreased, but for sample M3.2b they increased. This comparison is not easy to make, since the count also varies with the position on the sample where the measurement is taken, which is not the same for the different measurements. The conclusion that can be drawn here is that NH_3 does not significantly etch grown graphene, but can induce more defects in the lattice.

5.3.2. FTIR results

With the new wafers we could finally perform FTIR transmission measurements. The plan is to use pristine graphene as a baseline, and see what peaks are present in its spectrum. Then the other samples will be measured, and any new peaks will be evaluated with the help of [56]. Samples M3.1a and M3.2a were etched with H_2O_2 to prepare them for the measurement, but in the meantime they were

stored in a single wafer carrier together with the other samples with 50nm of Mo. Unfortunately, some of the peroxide remained on the samples apparently, because a day later, all other samples (except for one currently in the reactor for a rerun of sample M2.7a of batch 2, see previous paragraph) had been etched as well. For now this meant that the ammonia samples yet to be produced, had to be made on the other wafer with 200nm of Mo.

The pristine graphene samples were successfully etched without losing graphene this time. As a background, both bare silicon wafers, and thermally oxidized wafers were used, both of the same DSP type with high resistivity. The expectation was that with the silicon wafers as background, peaks of silicon dioxide would show up in the spectrum, in addition to any peaks generated by graphene. With the dioxide wafers those peaks would be divided out, and we would be left with the graphene peaks. Furthermore, sample M3.2a has been in the CVD reactor for much longer than sample M3.1a, with more methane content. Therefore, it is expected that this sample will absorb more of the incoming infrared light, and thus create peaks with higher intensity, since there are more graphene layers. The results are shown in figure 5.9 and 5.10.

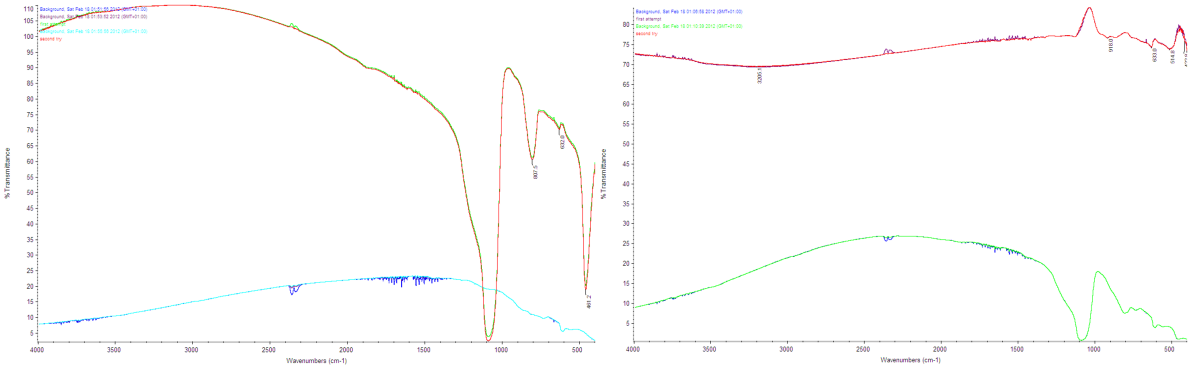

(a) Blue and lightblue = background, red and green = sample. **(b)** Green and blue = background, red and purple = sample.

Figure 5.9: FTIR transmission results of sample M3.1a with a silicon (left) and dioxide (right) background.

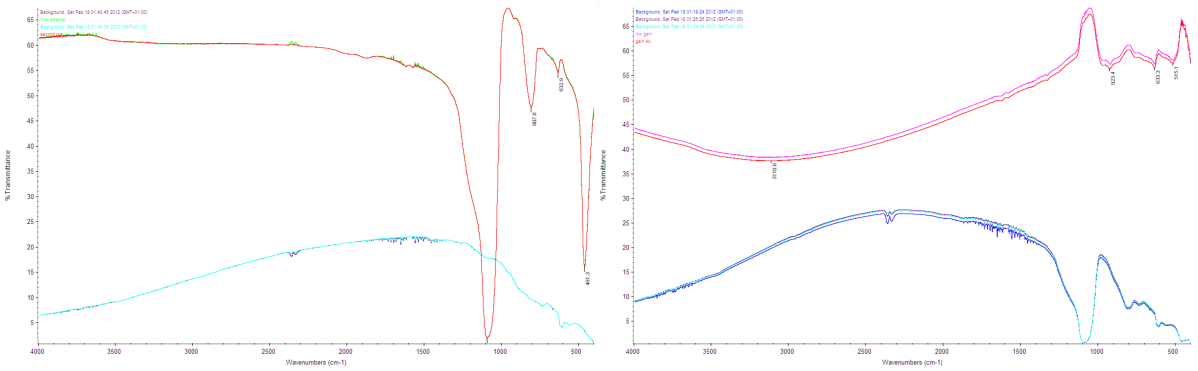

(a) Lightblue and purple = background, red and green = sample. **(b)** Blue, lightblue and purple = background, red and pink = sample.

Figure 5.10: FTIR transmission results of sample M3.2a with a silicon (left) and dioxide (right) background.

Figures 5.9a and 5.10a show three very clear peaks in the lower end of the spectrum, at wavenumbers 1092 cm^{-1}, 807 cm^{-1} and 461 cm^{-1} to be exact. Since they don't show up so clearly in figure 5.9b and 5.10b (except for the background spectrum), the first guess would be that they are related to the silicon dioxide. We don't have any libraries in the software of the Nicolet itself to compare spectra to, but a quick look online provides us with answers in [64], where they did FTIR analysis on a-SiO_2. The peaks at 1092 and 807 are asymmetric and symmetric stretching (ν) modes of Si-O-Si bonds respectively, and the peak at 461 is the bending (δ) mode of those same bonds. In multiple examples a large and broad peak around 3439 cm^{-1} is found which is due to Si-OH groups and adsorbed water, but since our samples are treated in a CVD reactor above 900°C, those bonds have been broken, and

they don't show up in the spectrum.

For the spectra with dioxide background, no extra peaks show up unfortunately. The only one that's sharp enough to count as a peak is the one at 633 cm^{-1}, but it's very small and also shows up in the silicon background spectra. No clear documentation can be found on what this peak might be a result of. However, since most carbon-carbon and carbon-oxygen bonds exist in the range from 1000 till 2000 cm^{-1}, this peak is of no interest to us, and we can conclude that pristine graphene is not IR active in this frequency range. An interesting thing to note is that, for sample M3.1a, a large part of the dioxide background spectrum is above 100% transmission, which is obviously not possible. This can be easily explained however, by looking at the refractive indexes of the different materials. $n_{air} \approx 1$ and $n_{c-Si} \approx 3.5$ for the infrared range (it's somewhat higher for the optical wavelengths). The index for silicon dioxide varies with frequency, but is in between those two indexes, and thus acts as an anti-reflective coating. In this way, more light can enter the sample, and leave it again at the back interface (where oxide is also present), giving rise to a higher signal at the detector, and thus a transmission above 100%, compared to the bare silicon wafer without anti-reflective coating.

5.3.3. EDX spectra

For the EDX measurements there are some interesting samples to inspect from both the second and the third batch. The samples we need to compare are pristine graphene, pristine graphene without catalyst (etched), graphene where ammonia was introduced, catalyst with only ammonia, graphene on pretreated catalyst and graphene with ammonia treatment afterwards. Those 6 spectra will be shown here, together with the corresponding SEM image and a brief explanation. A more elaborate discussion will be given at the end of this section. It should be noted that, for different points on the sample, different spectra can be obtained. The spectra shown are the most representative, and any significant deviations on different spots will be mentioned in the explanation.

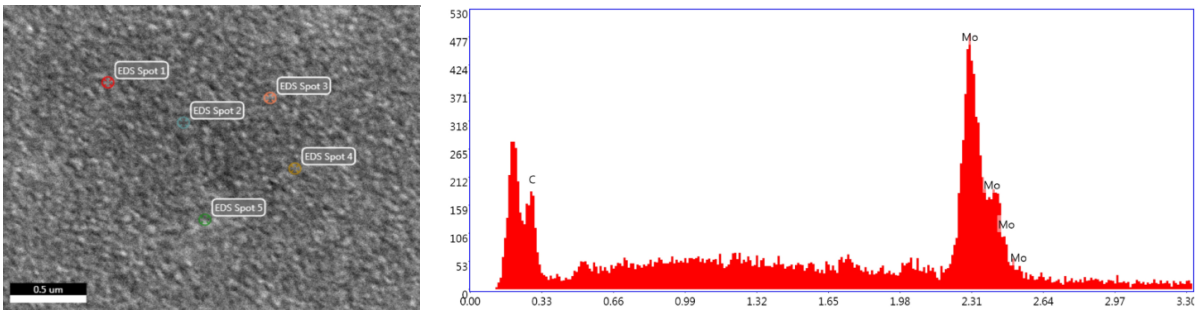

Figure 5.11: Sem image and EDX spectrum of graphene sample M3.1b grown with 25 sccm CH_4 for 15 min on 200nm Mo.

The first result is that of pristine graphene with the standard recepy in figure 5.11. The Mo (L α) peak is not surprising, but the carbon peak means that we can either detect graphene, or that carbon diffused into the catalyst, or even bonded with it. The peak left of carbon is the M-shell peak of Mo, which is always present next to the L α peak. Let's compare this to PG where the catalyst is removed by etching.

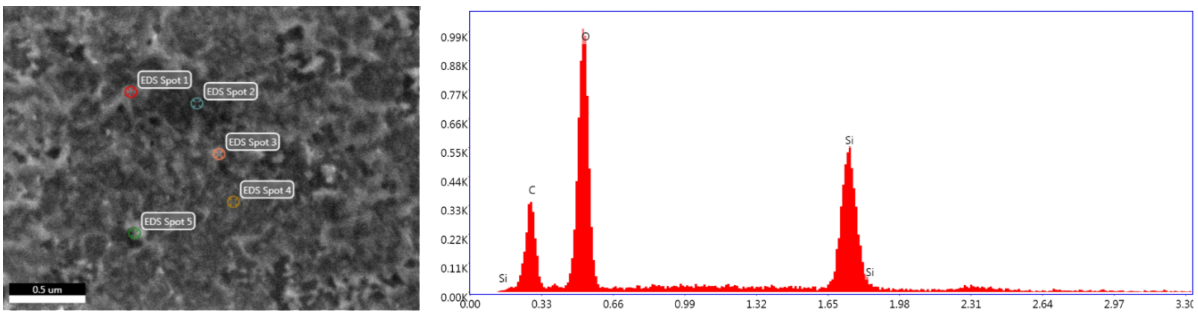

Figure 5.12: Sem image and EDX spectrum of the graphene sample with the catalyst removed by etching with H_2O_2.

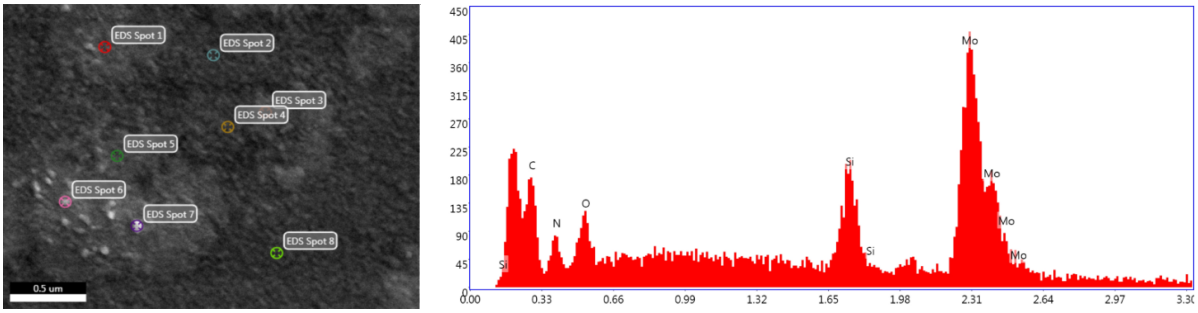

Figure 5.13: Sem image and EDX spectrum of the graphene sample grown with CH_4 and NH_3 simultaneously.

The result is shown in figure 5.12, which clearly shows a different spectrum. Since the graphene is now laying on the passivation layer, we can see the peaks for SiO_2 replaced the one for Mo. We can however still see a carbon peak, which must be the graphene. It should be mentioned that this particular sample was grown with 50 sccm CH_4 for 60 minutes, which means there are probably quite a few graphene layers. For the graphene that grew for 15 minutes with 25 sccm of CH_4 the carbon peak was harder to detect, but it was still there.

The next sample is M2.7a from the second batch, and the result is shown in figure 5.13. This is the first sample where nitrogen is detected, although this is only true for points 1, 3, 6 and 7. Those are the lighter parts in the SEM image, and they look very defective. Also, in all of the points of this measurement, SiO_2 can be seen in the spectrum. In contrast to figure 5.12 though, here it is not in the typical 1:2 ratio one would expect from the silicon oxide. This sample was hard to grow, and in repeated process runs there would be no graphene at all, as can be seen in the Raman results.

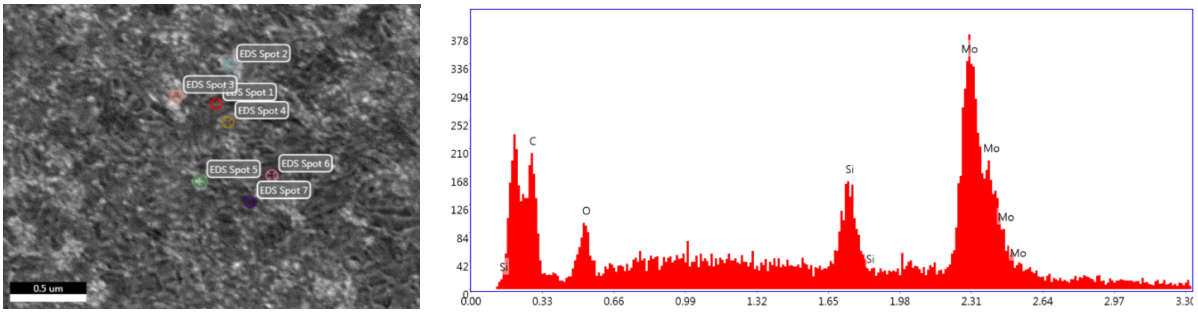

Figure 5.14: Sem image and EDX spectrum of the sample where the catalyst has been treated with only NH_3.

As mentioned in paragraph 5.2.2, an Mo catalyst sample treated with only NH_3 in the CVD reactor, shows different crystals on the surface than the graphene samples. Sample M2.8b was also measured with the EDX setup, and the results are shown in figure 5.14. This is an interesting result, since there is no nitrogen in the sample, but there is carbon, even though methane was not used here. It seems to suggest that the nitrogen can only bond to the graphene, but not with the Mo catalyst. For finding where the carbon content comes from, a good next step would be to measure a bare Mo sample that was never processed in the CVD reactor.

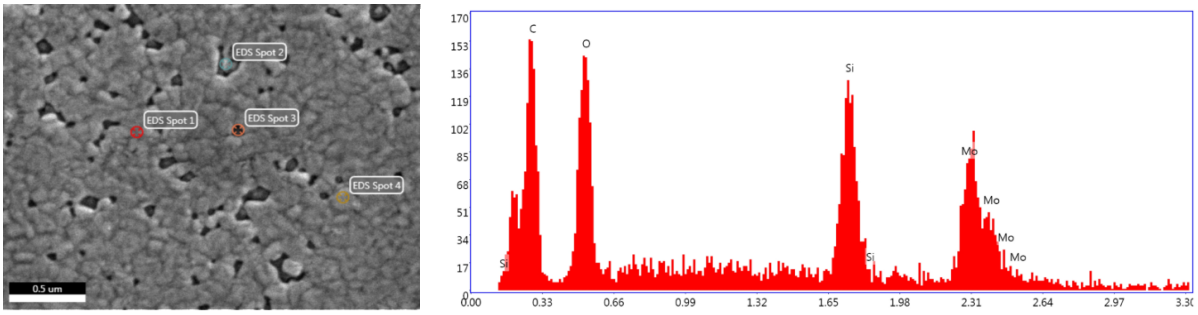

Figure 5.15: Sem image and EDX spectrum of the sample where the catalyst has been treated with NH_3 first, and then pristine graphene is grown on top.

This hypothesis seems to hold with the results of the next sample, M3.10b, shown in figure 5.15. Graphene still grew quite well on the catalyst, even for short times of 15 minutes. The spectrum shows that some of the Mo is consumed or converted to a form of molybdenum carbide, because the peaks of Mo get smaller, while those of Si and O get bigger. The carbon content stays more or less constant, which is not surprising since only a few layers of graphene will not show up significantly in the EDX spectrum.

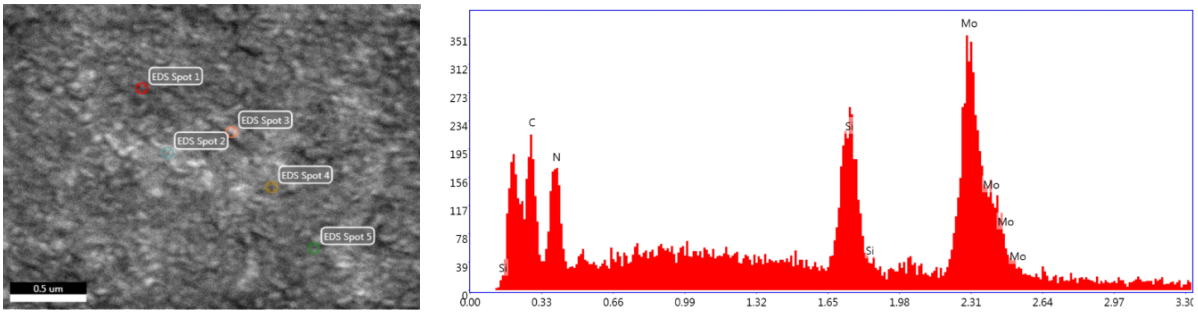

Figure 5.16: Sem image and EDX spectrum of the sample where pristine graphene is grown first, and afterwards the sample has been exposed to NH_3 under high temperature.

Doing those same process steps the other way round gives completely different results for sample M3.7b. In the spectrum shown in figure 5.16 no oxygen is present anymore, but there is a significant nitrogen peak. The Mo peak is also a lot bigger, but this is mainly because a thickness of 200nm was used here for the catalyst instead of the 50nm for the previous result. The results here differ a lot with the different points on the sample, but none of them show oxygen content. Something that does stand out is that the silicon peak scales almost 1:1 with the nitrogen peak. This might suggest that silicon nitride (SiN) is forming in places where the catalyst is thinner, or that the nitrogen is bonding with the graphene.

With all of those measurements combined there are a number of conclusions possible. It is quite plausible that the EDX measurement can pick up a signal from the graphene, since there was carbon visible after etching the catalyst away. Still, the carbon present in the sample that was only treated with NH_3 at high temperatures remains a mystery. It could be that carbon deposits that were present in the reactor chamber played a role, or that a contaminant at a later stage added the carbon. In any case it seems to be unlikely that molybdenum carbide forms, since for this usually a molybdenum source is used that has already been reduced by a strong oxidizer like oxygen or chlorine, forming MoO_3 and $MoCl_5$ respectively [65], rather than its pure form. From this, molybdenum carbide can then be synthesized more easily. This is confirmed by [66] where they use MoO_3 as well to prepare two different phases of molybdenum carbide: α-MoC and β-Mo_2C. The formation of molybdenum nitride (MoN) is even more unlikely, since in [65] it will be formed from molybdenum carbide, which we don't have in the first place. This conclusion is aided by the Mo sample treated in NH_3 sample not containing any detectable nitrogen.

The fact that nitrogen could be detected in those samples is a positive result, even though it only

happened in two of them. The sample where we introduced methane and ammonia simultaneously is hard to repeat, because the same recipe will not always grow graphene. Furthermore, the surface looks far from continuous, and the carbon and nitrogen don't really seem to coexist well. The other sample where we grew graphene first, and then used an ammonia post treatment is much more promising. It shows a higher nitrogen content, and is much more reproducible. Apparently, after the first nucleation of graphene, the further growth of graphene sheets is not so much inhibited by the ammonia anymore, and we might even try to combine it in one process where the ammonia is already introduced before the graphene growth is complete. However, it is still quite unlikely that this is actually nitrogen-doped graphene, as the nitrogen-carbon ratio is almost 1:1, which could never happen in doping.

For now, the next step is to compare the growth on Mo to the growth on Cu, because much more literature is available on this catalyst. This will be done in the next section. Furthermore, another transition metal catalyst will be used, Ni, which has a different growth mechanism of graphene. This is mainly caused by the different solid solubility for carbon in the two metals. This will be tested in section 5.5. Having those two metals to compare with, allows us to tell more about the actual growth mechanism in Mo. For molybdenum, the next step is to grow graphene using a different precursor that was already mentioned in chapter 3: pyridine. This will be explored in chapter 6.

5.4. Copper as catalyst

A lot of the literature found online on doping graphene with nitrogen uses copper as a catalyst, in most cases as a foil of $25\mu m$ thick [67]. Using a foil was not practical in out setup, but testing the doping process on a different catalyst would give some results for comparison. The trikon Sigma used for PVD could be fitted with different metal targets, and it was decided to test graphene growth on Cu and Ni films, since those catalysts are often used in the literature, but have a different process of graphene growth. These metals have a much lower melting point than Mo, and so the processing temperature is more critical here. We also need a thicker catalyst, as part of the metal will evaporate due to the heat. The following samples were made with a 550nm sputtered layer of pure Cu in the same aixtron Black Magic CVD reactor.

Table 5.6: The CVD recepies for the pieces of the copper wafer.

Sample (#)	Pristine or nitrogen-doped	Temperature ($^\circ C$)	Pressure (mbar)	Growth time (min)	CH4 flow (sccm)	NH3 flow (sccm)	Ar / H2 (sccm)
C1.1	PG	800	25	10	50	0	960 / 40
C1.2	NDG	800	25	10	50	50	960 / 40
C1.3	PG	880	25	10	50	0	960 / 40
C1.4	NDG	880	25	10	50	50	960 / 40
C1.5	NDG	880	25	10	50	20	960 / 40
C1.6	NDG	860	25	10	50	20	960 / 40
C1.7	NDG	860	25	10	50	50	960 / 40
C1.8	NDG	900	25	10	50	20	960 / 40

The starting point for these recepies was the paper of Wei et al. [28], where they use an equal amount of CH_4 and NH_3 to grow NDG for 10 minutes at 800°C. This was tested with samples C1.1 and C1.2, and afterwards Raman results were collected. Growing graphene at this temperature is working, although the quality of the produced graphene is quite poor. However, when we add NH_3 for sample C1.2, no more graphene can be detected, which is in line with the Mo results so far. The sample also appears to be damaged or etched in this case, and under the microscope the surface is full of black spots that appear to be holes in the copper.

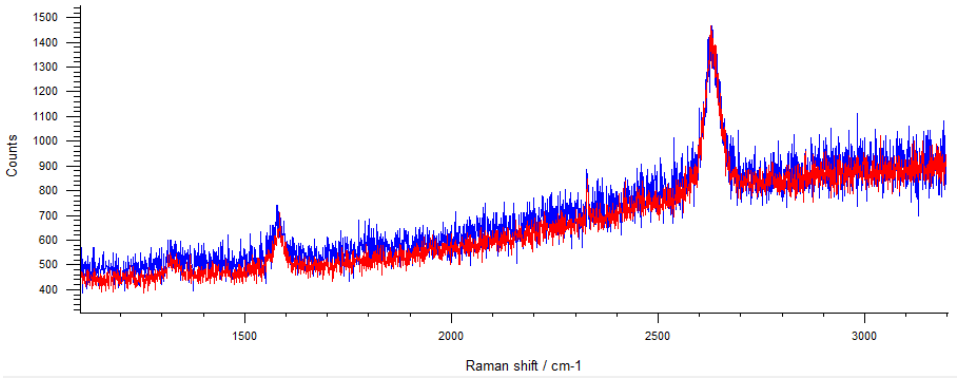

Figure 5.17: The Raman spectra of sample C1.3 with 100% laser intensity and 30s exposure time.

Because usually higher temperatures are used for copper, which promotes larger continuous sheets of graphene, the remainder of the samples were grown at higher temperatures. The starting point for this was 880 $^{\circ}C$, a bit lower than the temperature we use for the Mo, because the temperature for Cu is more critical as it approaches the melting point. The produced Raman spectrum for the PG sample is shown in figure 5.17. The overall shape of the spectra indicate good quality graphene, but the signals are relatively noisy, even for exposure times of 30 seconds and up. This is probably because the copper catalyst is interfering with the Raman signals, and it does so in a different way than molybdenum. To get a clean Raman spectrum we would have to transfer the graphene to a different substrate like SiO_2.

Unfortunately, it became clear really soon that when ammonia was added at these temperatures, the copper catalyst would be etched away rapidly, and after only 10 minutes, large areas of the underlying silicon dioxide would be visible. The images in figure 5.18 show what the samples looked like after they were taken out of the BM. This is an unwanted effect, not only because it hinders graphene growth, but also because the copper that is etched away might end up in the reactor chamber, and it can contaminate subsequently processed wafers.

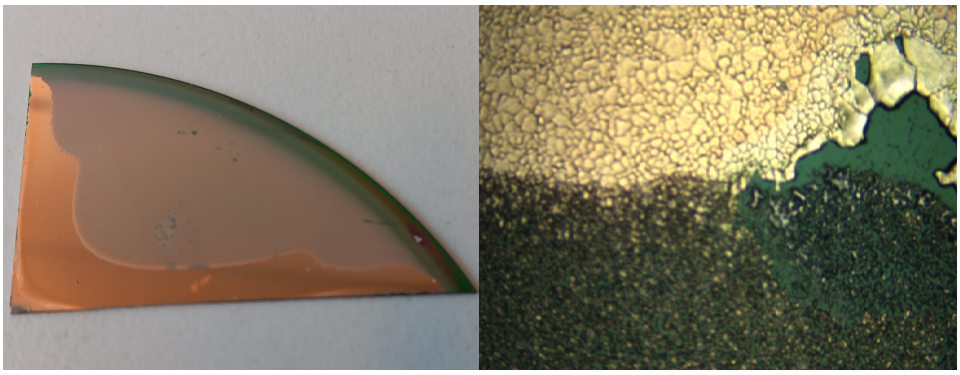

(a) Photograph of sample C1.2 after the CVD process **(b)** Micrograph 20x magnified on the edge of the copper

Figure 5.18: The remaining copper layer next to the edged part. The green layer is the silicon dioxide.

The samples that were subject to high temperatures, but no ammonia, didn't show this effect, so this could not be evaporation. Ammonia is playing an active role in the etching of copper at those temperatures. For now we can conclude that for these temperatures and gas flows, growing nitrogen-doped graphene on a copper film is not possible in our setup.

5.5. Nickel as catalyst

Similar to the copper samples, a number of samples were made on 500nm of sputtered Ni on 600nm SiO_2. The graphene growth process is quite different on a catalyst like nickel compared to copper, because of the differences in carbon solubility as already explained in section 3.1. Because molybdenum

is in between Cu and Ni in regard to its carbon solubility, it's useful to grow graphene on nickel as well to be able to see which growth process is most similar to that of Mo. In addition the effects of adding ammonia can be tested, to see if it will also inhibit growth for this catalyst. The following samples were made with a nickel coated wafer. The catalyst thickness in this case was chosen because a thicker catalyst makes it easier to produce SLG according to[36].

Table 5.7: The CVD recepies for the pieces of the copper wafer.

Sample (#)	Pristine or nitrogen-doped	Temperature ($^{\circ}C$)	Pressure (mbar)	Growth time (min)	CH4 flow (sccm)	NH3 flow (sccm)	Ar / H2 (sccm)
N1.1	PG	900	25	10	50	0	960 / 40
N1.2	NDG	900	25	10	50	50	960 / 40
N1.3	NDG	900	25	10	50	20	960 / 40
N1.4	NDG	880	25	10	50	20	960 / 40
N1.5	NDG	880	25	10	50	50	960 / 40
N1.6	NDG	920	25	10	50	20	960 / 40

In this case the article of Bao et al. [68] was used to choose appropriate parameters, in combination with an already existing nickel recipe to grow PG in the black magic. The first step was to test if we could grow graphene with just methane, and to use that as a reference. This was done with sample N1.1, and the resulting Raman spectra are shown in figure 5.19. Even for very short exposure times this sample gives a clean Raman signal, meaning that nickel is interfering much less with the Raman measurement when compared to copper. The 2D-peak relative to the G-peak indicates that this is multi-layer graphene, which we expected, since growing single- or few-layer graphene is much harder on nickel.

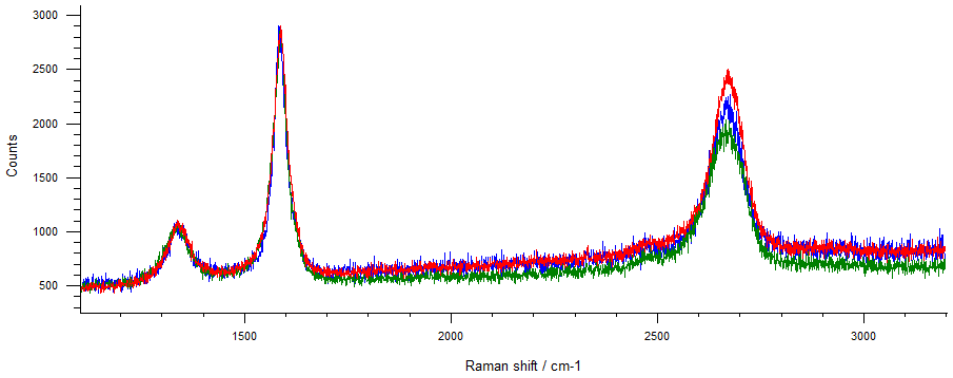

Figure 5.19: The Raman spectra of sample N1.1 with 100% laser intensity and 10s exposure time.

When adding ammonia to this recipe, the nickel samples showed similar behavior to the copper samples, where the catalyst material started to get etched away. Again, the temperature and ammonia flow rate was varied to see the effect on the etching, and samples N1.2 and N1.5 lost most of their metal layer, and didn't show graphene anymore. Samples N1.3, N1.4 and N1.6 still had a large part of their catalyst left, and on the parts that were not etched, the Raman measurement showed a graphene spectrum almost identical to that in figure 5.19. They can be found in appendix D. The three different temperatures used, didn't play a noticeable role in the etch rate.

This brings us to the conclusion of this chapter. Growing NDG on the catalysts that we used in this chapter is not possible in our setup for different reasons. The Mo samples won't grow graphene anymore when NH_3 is added, and the Cu and Ni samples get severely damaged by the ammonia. In the literature, foils are used most of the time, which makes the growth possible on Cu and Ni, because etching the thicker foils will take very long compared with the growth time. A possible solution to prevent the etching, is to use a different MFC in the black magic so that lower concentrations of NH_3 can be used, preferably below 10% of the CH_4 flow. This may also make the growth on Mo possible.

6

Results with pyridine

In this chapter we will elaborate on the results generated with pyridine. As already explained, pyridine is an aromatic compound that is a liquid at room temperature. To this end we will make use of a bubbler setup with the same Black Magic CVD system and nitrogen as a carrier gas. The vessel used for this is a 300 ml stainless steel bubbler flask. By passing the carrier gas through the flask, pyridine vapor is transported, via the nitrogen MFC, to the reactor chamber, where it can react at high temperature and low pressure to grow graphene. Again, wafers are broken into samples to be able to test different CVD parameters, and see how they effect the graphene growth and quality.

6.1. First batch

For pyridine the first batch is produced on 100 mm diameter p-type, single side polished wafers, with 600nm of SiO_2 on top, and a Mo layer of 100nm sputtered on the SiO_2. It was again diced in 12 pieces to have enough samples to run a variety of recipes, but keep the samples of sufficient size to perform measurements on after the growth. In table 6.1 the nitrogen flows are listed, but recall from paragraph 3.4.6 that the actual pyridine flow is just over 1% of that nitrogen flow.

Table 6.1: The CVD recepies for the pieces of the first pyridine wafer.

Sample (#)	Temperature ($^{\circ}C$)	Pressure (mbar)	Growth time (min)	N2 flow (sccm)	Ar flow (sccm)	H2 flow (sccm)	Graphene detected?
MP1.1	915	25	30	10	960	40	no
MP1.2	915	25	30	40	960	40	no
MP1.3	915	25	30	10	100	0	no
MP1.4	915	25	30	20	100	0	yes
MP1.5	915	25	30	40	80	20	yes
MP1.6	915	25	30	80	80	20	yes
MP1.7	915	25	30	40	100	0	no
MP1.8	915	25	30	80	100	0	no
MP1.9	915	25	30	20	80	20	yes
MP1.10	915	25	30	40	80	20	yes
MP1.11	915	25	30	160	0	0	aC
MP1.12	915	25	30	320	0	0	aC

The most important goal for this batch was to figure out if graphene could be grown on Mo with pyridine in the first place, since most papers using pyridine have copper as catalyst. To this end the main parameters to change here are the nitrogen flow rate, the chamber pressure, and the total gas mixture present during growth. Since the pressure controller is currently not giving accurate results (see figure 6.1), we will focus on the nitrogen, hydrogen and argon flow in this batch. The growth time and temperature will receive more attention in the next batch.

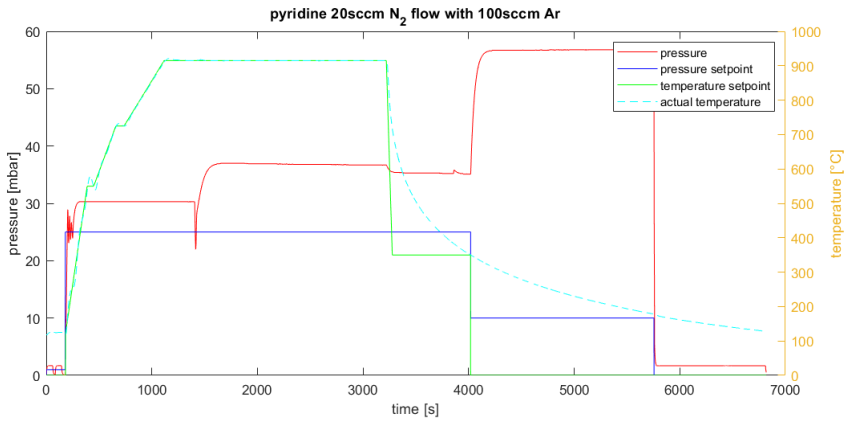

Figure 6.1: The chamber pressure showing a clear deviation from its setpoint in the BM.

For the first two samples the hydrogen and argon flow were kept the same as in the methane recipe, and the pyridine was introduced in relatively low flow rates of 10 and 40 sccm. No graphene was measured in the Raman setup, showing just a spectrum without visible peaks. A possibility for improvement here is to just increase the flow rate of pyridine, but the MFC is limited to 200 sccm, which means the vapor flow will still only be around 2 sccm which is low compared to methane. Another option is to look at the pyrolysis of pyridine, which is a lot more complex than that of methane [69]. That might mean that the radicals formed during pyrolysis need more time to be able to contribute to graphene growth. To get an idea of how much time the pyridine molecules stay inside the reactor with the current setup we can use the following formula [46]:

$$t_{res} = \frac{V}{F_{in}} \tag{6.1}$$

Here t_{res} is the residence time, the average time that a gas molecule spends in the reactor chamber, V is the volume of the reactor chamber, and F_{in} is the total volume flow into the reactor. Recall from section 3.3 that from the ideal gas law we know that gases coming from ambient conditions will expand tremendously because of the low pressure and high temperatures inside the CVD reactor. Doing a quick estimation, with argon and hydrogen adding up to 1000 sccm, our F_{in} will reach approximately 2.7 liters/sec for a temperature of 915 $^{\circ}C$ and pressure of 25 mbar. The volume of the reactor has to be estimated since no data is available, so an upper limit is taken of 30 liters. This gives a $t_{res} \approx 11$ seconds, which is really short if we compare it to the growth time. Since the volume of the reactor is a bit smaller in reality, and we didn't take into account other gases flowing into the reactor, this number is probably even below 10 seconds.

If we want to say something useful about this residence time, we need to compare it to the consumption lifetime, shown in equation 6.2, which estimates how quick a precursor molecule is incorporated into the deposited layer.

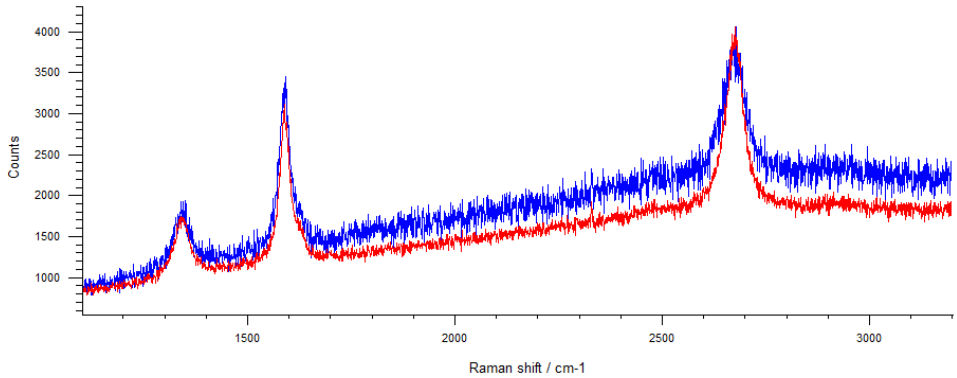

Figure 6.2: The result of sample MP1.9 with graphene growth on the surface.

Table 6.2: The curve-fitting results of the 5 samples from the first pyridine batch containing graphene.

Peak fittings D, G, 2D	Sample MP1.4	Sample MP1.5	Sample MP1.6	Sample MP1.9	Sample MP1.10
Intensity	0.42	0.46	0.52	0.48	0.93
(normalized	0.95	0.95	0.98	0.96	0.73
to G-peak)	0.86	1.03	0.80	0.74	0.62
Center	1339	1339	1336	1342	1347
location	1590	1589	1586	1590	1595
$[cm^{-1}]$	2674	2674	2665	2674	2678
FWHM	41	43	50	45	43
$[cm^{-1}]$	32	35	41	34	34
	58	57	60	64	74

Here, we have again the volume V of the reactor, the deposition rate K_S, and the surface area S. If this consumption lifetime is much bigger than the residence time, we're dealing with a differential reactor, and most of the precursor molecules are still present at the reactor exhaust. The surface reaction is the main limitation. If it's the other way round, we have a starved reactor, and the supply and transport of the precursor gas or vapor is the main bottleneck. Unfortunately, the consumption lifetime is a lot harder to evaluate, because K_S is not easily found, and depends on almost all CVD parameters, so for now we will just focus on increasing the residence time.

$$t_{con} = \frac{V}{K_S \cdot S} \tag{6.2}$$

To give the nucleation reaction more time, the remainder of the samples are only diluted with a total of 100 sccm of hydrogen and argon. Next to a higher t_{res}, this will also increase the relative concentration of pyridine in the chamber, which will in turn increase the surface reaction rate. Different N_2 flows and $Ar : H_2$ ratios were used, and it turned out that an N_2 flow rate of either 40 or 80 worked well if we would also add some H_2 to the mixture. The results of sample MP1.9 is shown in figure 6.2. The last two samples were used to see if we even needed the dilution of argon and hydrogen, by omitting those and increasing the nitrogen flow instead. This gave only amorphous carbon as a result, which shows the importance of the other process gases. The fitting results are shown in table 6.2.

An interesting thing to note, is that there is a significant difference in the samples with 80/20 Ar/H_2 ratio and the ones with only argon. The samples with only argon either don't contain graphene at all, or the graphene only grows in flakes near the edge of the sample. The samples with hydrogen have a bigger process window, and, while their graphene is far from perfect, at least all the samples contain detectable graphene.

Table 6.3: The CVD recepies for the pieces of the first pyridine wafer.

Sample (#)	Temperature ($^\circ C$)	Pressure (mbar)	Growth time (min)	N2 flow (sccm)	Ar flow (sccm)	H2 flow (sccm)	Graphene detected?
MP2.1	915	25	30	20	0	100	yes
MP2.2	915	25	30	40	0	100	yes
MP2.3	915	25	30	80	0	100	yes
MP2.4	915	25	30	160	0	100	yes
MP2.5	915	25	30	40	0	100	yes
MP2.6	915	25	30	80	0	100	yes
MP2.7	900	25	30	40	0	100	edge only
MP2.8	900	25	30	80	0	100	yes
MP2.9	915	25	15	40	0	100	edge only
MP2.10	915	25	15	80	0	100	yes
MP2.11	900	25	30	40	0	100	yes
MP2.12	915	25	60	40	0	100	yes

6.2. Second batch

The second batch is processed on a similar wafer as the first batch, with the same catalyst thickness. Now that we know that graphene growth on Mo using pyridine is possible, this batch was used to find a suitable growth time and temperature for this growth process, but also some changes in the gas mixture were still made. The table with all the processed samples is shown in 6.3.

The first thing to notice is that we switched from mainly using argon during the growth time, to only using hydrogen. This was done because the samples produced with hydrogen from the last badge gave better results in the Raman spectrometer. With the 100 sccm of H_2 used in this batch we obtained even better results. One explanation for this could be that hydrogen is much lighter than argon, and will help in pushing the much heavier pyridine vapor down to the chuck where the process wafer is, increasing surface reaction rate. Another option is that hydrogen is acting as a catalyst in the pyrolysis of pyridine, assisting in breaking down pyridine into smaller molecules or radicals. From [45] we know that for methane growth on copper hydrogen gas is also necessary for graphene growth. In [70] the roles of hydrogen as a surface activator for carbon, and that of an etching reagent that controls the graphene size are mentioned. They use 200-400 times the partial pressure of hydrogen compared to that of methane, which would translate to approximately 80-160 sccm for a 40 sccm flow of N_2.

The process window for pyridine flow is not terribly large, as 20 sccm of N_2 flow will give hardly any Raman result, and 160 sccm is beginning to look more like graphite. That's why the remainder of the samples are run with either 40 or 80 sccm flow rate, because those values gave the best results. Sample MP2.5 and MP2.6 were used to check repeatability of the recipes, and they showed very similar Raman spectra to sample MP2.2 and MP2.3 respectively. The fitting results are shown in table 6.4. No significant differences were found in either table 6.2 or 6.4 when compared to the methane fittings in tables 5.2 and 5.4, so nitrogen doping cannot be confirmed from the Raman spectra.

Table 6.4: The curve-fitting results of the 10 samples from the second pyridine batch containing graphene.

Peak fittings D, G, 2D	Sample MP2.1	Sample MP2.2	Sample MP2.3	Sample MP2.4	Sample MP2.5	Sample MP2.6	Sample MP2.8	Sample MP2.10	Sample MP2.11	Sample MP2.12
Intensity (normalized to G-peak)	0.78 0.78 0.72	0.47 0.97 1.11	0.63 0.98 1.09	0.66 0.93 0.68	0.70 0.89 0.67	0.47 0.95 0.66	0.58 0.96 1.35	0.65 0.92 0.75	0.54 0.98 1.23	0.28 0.98 1.17
Center location $[cm^{-1}]$	1339 1596 2661	1341 1587 2671	1341 1589 2670	1344 1592 2676	1343 1593 2680	1343 1590 2676	1339 1589 2673	1341 1591 2661	1342 1591 2676	1340 1587 2671
FWHM $[cm^{-1}]$	38 29 66	43 33 50	46 40 55	44 44 65	46 35 61	47 35 67	51 37 53	45 34 71	42 34 51	39 31 52

A lower process temperature of 900 $^\circ C$ was tried, since in [44] different temperatures are tried, for which their lowest temperature (930 $^\circ C$) could incorporate the most nitrogen at 3 at.%. This means that ideally we would like to grow at the lowest temperature possible. It turns out the recipe at 900 $^\circ C$ will still produce graphene, but the quality is worse than with 915 $^\circ C$. Since a higher temperature is not a possibility with the setup currently, we will stick to the 915 $^\circ C$. The growth time had quite an impact on the graphene quality, except for the edges of the sample. In the centre, a better Raman signal was obtained with increasing growth time, but at the edges there was graphene of lower quality that didn't improve with longer growth time. In the end, sample MP2.12 was found to have the best quality graphene, and its Raman spectra are shown in figure 6.3. The recipe for this sample is going to be used to grow the graphene for both the back-gate transistors in section 6.4, and for measuring the elemental composition with XPS in section 6.5 to confirm doping.

The next step, just like with ammonia, is to compare this growth with the growth on copper, since most of the literature uses a copper catalyst.

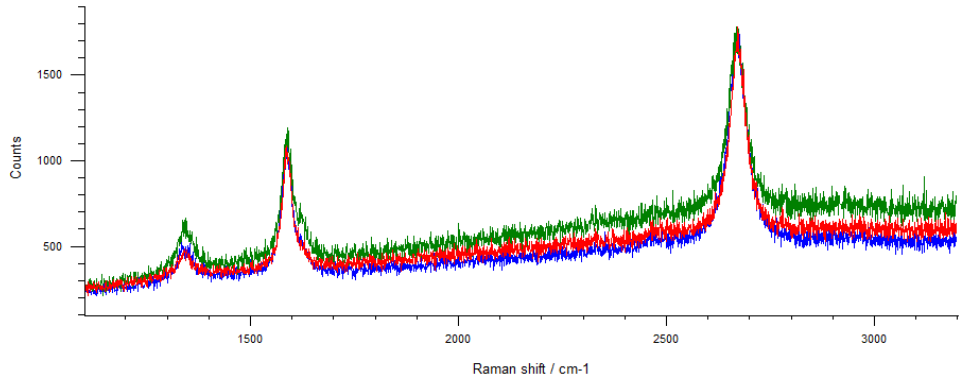

Figure 6.3: The results of sample MP2.12 measured in the centre of the sample piece.

6.3. Copper

A wafer sputtered with 600nm of pure copper was used, since a very thin layer would likely evaporate before the end of the growth time. Growing graphene on copper will allow us to verify the CVD setup by comparing Raman and SEM results to literature outcomes. Moreover, a lot of research groups use a copper foil of 25 μm thick to grow their graphene. With these experiments we will see if we can also grow on films using pyridine. Lastly, having different samples for the XPS measurements will tell us something about the influence of the catalyst material on nitrogen being incorporated into the graphene lattice. Table 6.5 shows which samples were produced with copper.

Table 6.5: The CVD recepies for the pieces of the copper coated wafer.

Sample (#)	Temperature ($^\circ C$)	Pressure (mbar)	Growth time (min)	N2 flow (sccm)	Ar flow (sccm)	H2 flow (sccm)	Graphene detected?
CP1.1	880	25	30	40	0	100	yes
CP1.2	880	25	30	80	0	100	yes
CP1.3	880	25	15	40	0	100	yes
CP1.4	880	25	15	80	0	100	yes
CP1.5	880	25	60	40	0	100	yes
CP1.6	880	25	60	80	0	100	yes
CP1.7	900	25	15	40	0	100	yes
CP1.8	900	25	15	80	0	100	yes
CP1.9	900	25	30	40	0	100	yes
CP1.10	900	25	30	80	0	100	yes
CP1.11	880	25	30	20	0	100	yes
CP1.12	900	25	30	20	0	100	yes

After the growth Raman measurements were performed, and all of the samples showed a graphene spectrum. The optical micrographs showed a wrinkled structure, with the different nucleation sites coming together in dark, vein-like structures, which is similar to the growth using methane gas. This is shown in figure 6.4, where it can be seen that the graphene domain size is bigger with the pyridine, which is beneficial for making devices with graphene. The copper grains where the different flakes come together are usually places where the defect density is high, they are formed because the copper is partially molten at the high growing temperatures, and they are not showing up in either molybdenum or nickel graphene samples.

The Raman spectra reveal that the quality of the produced graphene degrades with higher pyridine flow rates and with longer growth times. Samples CP1.5 and CP1.6 have an I_D/I_G ratio over 2, which is really poor for growth on copper. The samples produced with 80 sccm of pyridine flow show a I_D/I_G ratio of over 1 which is also subpar for copper samples. The samples grown with 40 sccm have this ratio below 1, usually around 0.5, and don't show a significant difference for the used growth temperatures. The best samples are CP1.11 and CP1.12 with the lowest pyridine flow we can get with this MFC. The Raman spectra of all those samples can be found in appendix D.

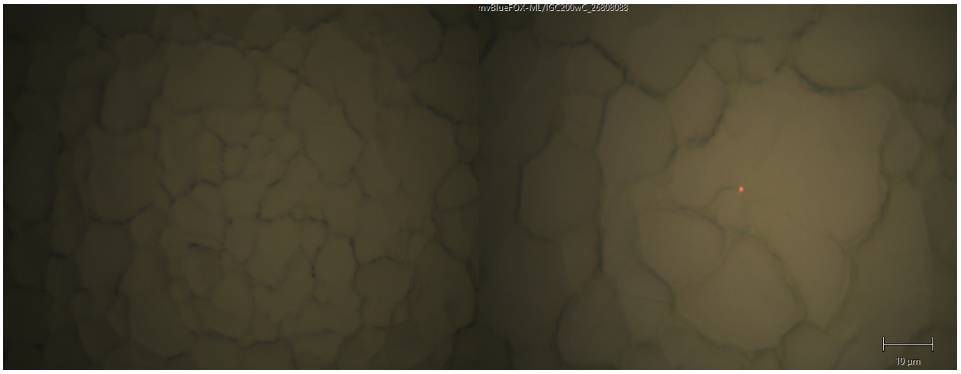

(a) Micrograph of the growth on copper with CH_4 **(b)** Micrograph of the growth on copper with C_5H_5N

Figure 6.4: 100x magnification of the copper surface after graphene growth.

The spectrum of sample CP1.11 is shown in figure 6.5. It's D-peak ratio is below 0.5, and the 2D ratio is over 2. This sample will also be used for XPS analysis to compare it with the molybdenum sample. In this way, we will be able to verify if nitrogen doping of graphene can be achieved in our setup. The process window is quite different for copper and molybdenum with respect to growth time, pyridine flow and even temperature, but this was expected since the growth process is surface mediated for copper, and most probably bulk mediated for molybdenum, just like nickel. Nickel itself wasn't tested because of time constraints, but is also proven to work, even at lower temperatures in ultrahigh vacuum [71].

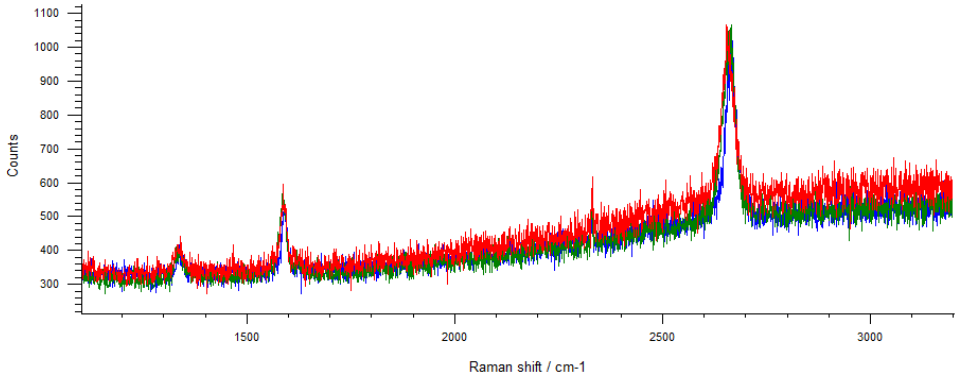

Figure 6.5: The results of sample CP1.11 measured in the centre of the sample piece.

6.4. Electric measurements

For the electric measurements we need to make some structures on the graphene layers, both to get well defined shapes to be measured, and because the graphene needs to be contacted by metal in order to do the measurements. A well-known example of such a structure is a van der Pauw test structure, which is a symmetrical shape of the layer to be measured, with four contact points on the edge of that structure [21]. These structures specifically are a good way to measure the sheet resistance, R_s, of a layer. In our case, measuring just the sheet resistance is not really useful, for two reasons. First, we know that the sheet resistance is a function of the doping concentration, but it doesn't tell us the type of doping, either n- or p-type. Second, the sheet resistance is also a strong function of graphene quality, and will change with the amount of defects and/or graphene layers. For this reason, we need to do the back-gate measurements as described in section 4.5.

Six wafers were prepared with bars of 50nm Mo of 20 by 200 μm. The graphene will be grown on top of the Mo structures in the same Black Magic CVD oven, and afterwards metal contacts will be evaporated onto these structures to do a four-point probe measurement. The silicon wafers themselves will act as the back-gate, since the silicon has already been doped with boron to have a conductivity $\rho = 1 - 5\Omega cm$. The molybdenum will have to be etched before doing the measurement, because it is a metal and thus a good conductor, so it would influence the measurement heavily. The thermally grown

oxide in between the graphene and back-gate is 600 nm thick. A SEM micrograph of the patterned Mo bars is shown in figure 6.6a.

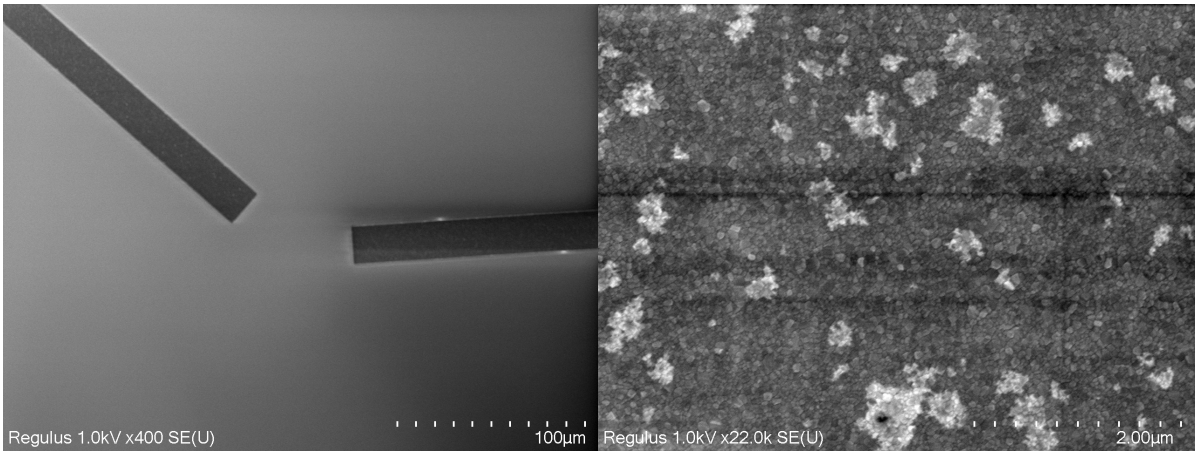

(a) Micrograph of the patterned Mo substrate. **(b)** Micrograph of the Mo surface of one bar.

Figure 6.6: SEM micrographs of the patterned wafer after graphene growth.

The idea was to process the six wafers with different CVD recipes, to be able to measure the influence on different process parameters. The first wafer was processed with the same recipe as sample MP2.12, with the only differences being the patterning, a slight difference in catalyst thickness (50 nm vs 100 nm) and the sample size now being a full-wafer instead of a diced 2x2cm piece of wafer. After doing the Raman it turned out that there was no graphene on the Mo surface that we could detect. The influence of the different catalyst thickness was quickly ruled out by trying the same recipe on a remaining 50nm Mo piece of wafer without patterning, which worked out fine. To test the wafer scale growth of graphene, a 300 nm Mo sputtered wafer was used, because at this moment in time no wafers with either 50 or 100 nm Mo were available to us. This also worked out, although the Raman signal showed a worse graphene quality than sample MP2.12, and was different when measuring on the left, right, top, bottom or centre of the wafer, which was probably because of temperature gradients in the reactor. This left us with the conclusion that the patterning was the main problem preventing graphene growth on the microstructures. To make sure the process wafers themselves were not the issue, the standard methane recipe was used to grow graphene on them. After doing Raman the structures showed a clear graphene signal, ruling out the wafers as the problem here.

SEM scans were made of sample MP2.12, the full wafer with 300 nm Mo and the patterned wafer, and they are shown in figure 6.7a, 6.7b and 6.6b respectively.

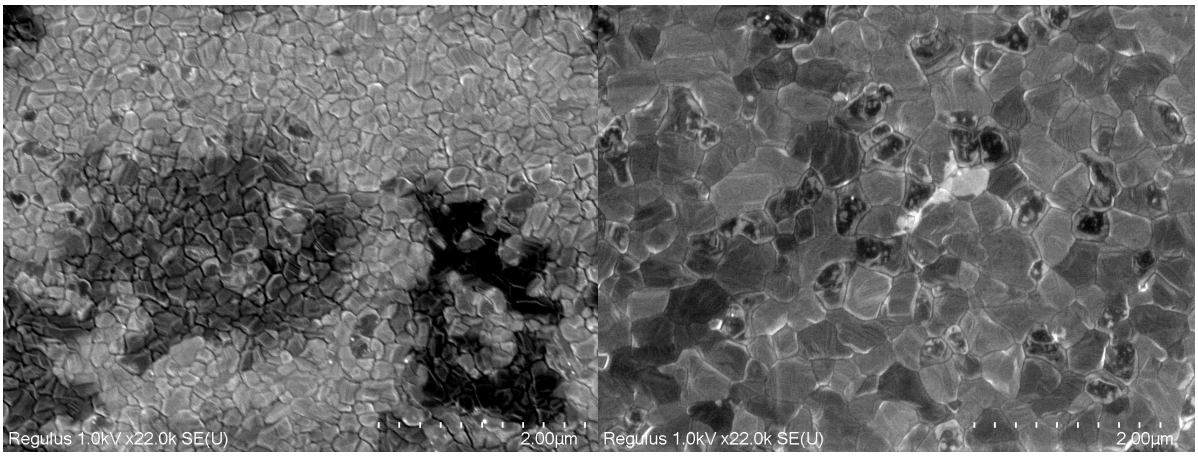

(a) Micrograph of sample MP2.12 after graphene growth. **(b)** Micrograph of the 300 nm Mo full wafer after growth.

Figure 6.7: Micrographs of the wafers without prepatterned catalyst.

Here it is interesting to see that all of the processed wafers show the molybdenum grains, which are not visible before processing. The grain size seems to increase with catalyst thickness, which is a process not occuring with methane as a precursor. This implies that the growth process is different for those three samples, and hence we would need three different recipes. Another thing to notice is the white stains on top of the patterned sample in figure 6.6b, which are not present on the unpatterned samples. Measuring those stains in the EDX setup could give us a clue about other surface reactions going on.

The hypothesis is that the pyridine recipe should be changed depending on the surface where graphene needs to grow, and the thickness of the catalyst. More surface means more pyridine flow, and a thicker catalyst means more growth time and vice versa. This would suggest that the patterned wafer is being processed for too long with way too much pyridine, but this is statement has to be tested. To this end a wafer with pre patterned catalyst was again diced in 12 samples, which were processed with different recipes and measured with the Raman spectroscopy setup. The results are shown in table 6.6.

Table 6.6: The CVD recepies for the samples with pre patterned Mo catalyst.

Sample (#)	Temperature ($^\circ C$)	Pressure (mbar)	Growth time (min)	N2 flow (sccm)	Ar flow (sccm)	H2 flow (sccm)	Graphene detected?
MPP1.1	935	25	15	20	0	100	yes
MPP1.2	935	25	30	20	0	100	yes
MPP1.3	915	25	15	20	0	100	yes
MPP1.4	915	25	30	20	0	100	yes
MPP1.5	900	25	15	20	0	100	minor
MPP1.6	900	25	30	20	0	100	minor
MPP1.7	915	25	30	40	0	100	yes
MPP1.8	915	25	30	80	0	100	yes
MPP1.9	915	25	60	40	0	100	no
MPP1.10	915	25	60	80	0	100	yes
MPP1.11	915	25	15	40	0	100	yes
MPP1.12	915	25	15	80	0	100	yes

After the first six samples the hypothesis is redefined with the role of the growth time and precursor flow swapped. Hence the recipe should be changed to grow for longer when more catalyst surface area is present, and the precursor flow should be increased with a thicker catalyst. This seems to make more sense, since the growth times of 15 and 30 minutes don't show much difference on the produced samples. It would also be an intuitive result, since the lateral growth of graphene only happens at a certain speed, and thus for larger catalyst areas with only a finite number of nucleation points, it will take time to cover the whole surface. The partial pressure of the precursor determines the flux into the catalyst material (see figure 3.5), and a thinner catalyst will become saturated much sooner, so we will need a lower influx, and hence lower precursor flow to prevent all the carbon from precipitating out during cooldown. This hypothesis holds quite well for the first 8 samples.

Sample MPP1.9 and MPP1.10 are grown using the exact same recipes as the processed whole wafers with a prepatterned catalyst, hence we would expect that no graphene will grow on those samples. For sample MPP1.9 this holds and we get an almost flat Raman spectrum, but for sample MPP1.10 a Raman spectrum is still obtained. This is suggesting that there is a reaction going on that's different for processing samples and whole wafers. This might be worth investigating in another research project, but for now we will pick the two best Raman spectra from the table, and process two other patterned wafers with those recepies.

6.5. XPS

The last measurement to be conducted is the XPS analysis, as discussed in section 4.6. This measurement has two stages of analyzing a sample. The first stage is the full survey, in which the whole spectrum range from 0 till 1100 eV is analyzed for electron emission. Similar to FTIR and EDX, peaks will show up corresponding to the kinetic energies of detected electrons. In the second stage, the peaks of interest can be selected, and a high resolution is run on those peaks only, because the full spectrum would take weeks to complete. Scanning only the peaks will still take over 10 hours. Additional details can be found in appendix C.

Two samples were chosen to be measured, a Cu and an Mo sample, more specifically MP2.12 and CP1.11 which had the best quality graphene according to the Raman spectra. Their full survey spectra are shown below.

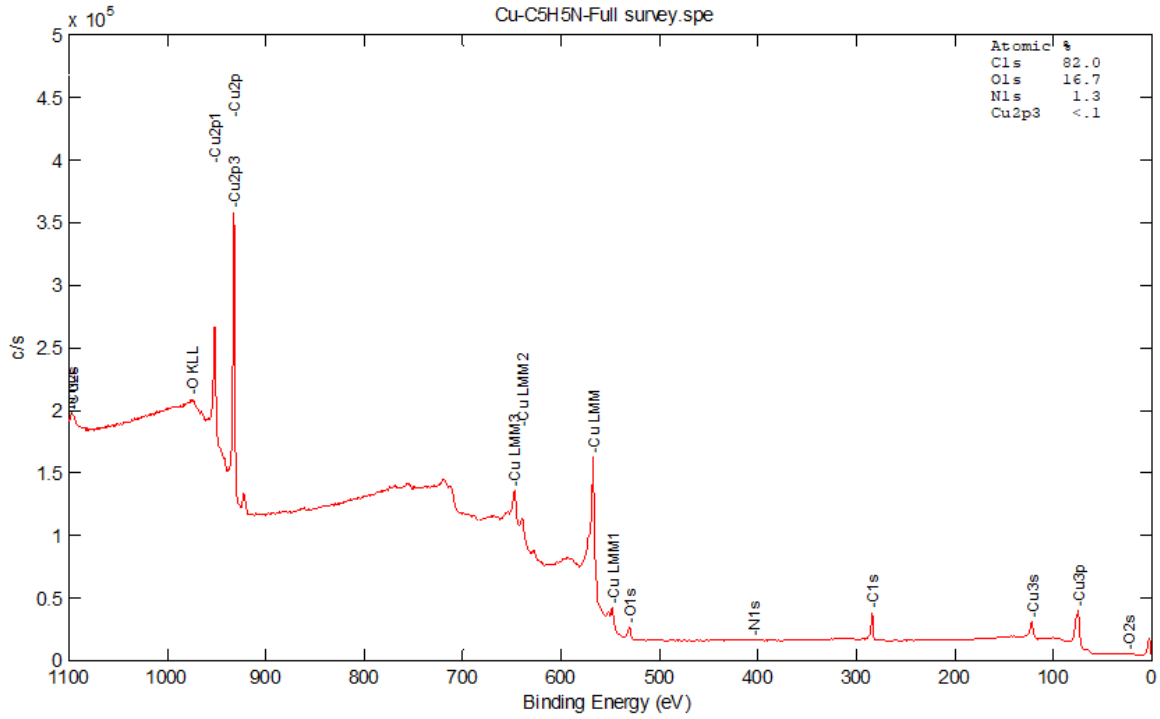

Figure 6.8: The full survey XPS analysis of the copper pyridine graphene sample.

The heavier elements, like transition metals, give rise to multiple peaks, because they have more electrons in different shells and orbitals. Lighter elements, like C, N and O have only a single peak called the '1s' peak, named after the electron shell and orbital. The O1s peak is not intended to be there, but is a result of the adsorption of moisture in the air when removed from the CVD vacuum chamber. H_2O molecules will loosely bind to the surface and cause charge transfer, effectively slightly p-doping the graphene as explained in section 2.4. The hydrogen atoms cannot be detected by XPS, but the oxygen atoms can, giving rise to the O1s peak. Another source for oxygen is the air present in the headspace of the bubbler, which will also get transported by the carrier gas, albeit very minor.

For the copper sample, a sizeable C1s peak is visible, the O1s peak is a bit smaller, and the N1s peak is so small, it's barely visible in the full survey. The XPS software, MultiPak, calculates the areas under the peaks, and divides them by the total area underneath all peaks together, to give an estimate on the atomic percentage of each element present. The nitrogen content is estimated at 1.3 at. %.

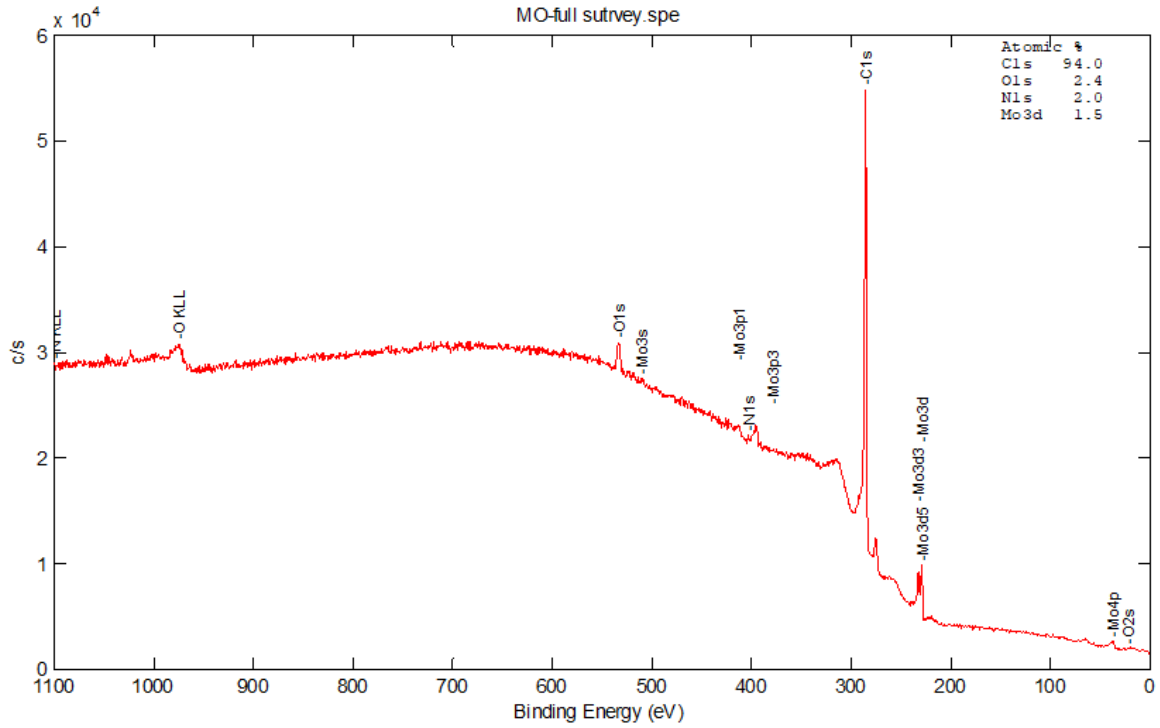

Figure 6.9: The full survey XPS analysis of the molybdenum pyridine graphene sample.

For the molybdenum sample, a very high C1s peak is observed, but notice the difference in vertical axis between figures 6.8 and 6.9, meaning the peaks are actually in the same order of magnitude. The O1s peak is relatively small in this sample, with also its estimated percentage way lower. The N1s peak is again barely visible, which is emphasized by the two Mo peaks flanking it, namely Mo3p1 and Mo3p3. The estimated nitrogen content is higher than the copper sample though, at 2.0 %. The molybdenum peaks are low in comparison with the graphene peaks, suggesting that this graphene is thicker than the graphene grown on the copper sample.

A high resolution scan was run for both of those samples, focusing specifically on the C1s and N1s peaks. The C1s peaks are shown in figure 6.10. As expected, the highest peak is at 284.8 eV in both cases, indicating the sp^2-hybridized C atoms in the graphene lattice. Three other peaks are fitted, at 286.2 eV, 288.5 eV and 291.1 eV, which is carbon with a different bonding, like sp^2 and sp^3 hybridized C-N bonds. While not exactly the numbers stated in section 4.6, those peaks suggest that nitrogen doping might be present, but we will have to look to the N1s peak to be sure, since it might also be oxygenated carbon.

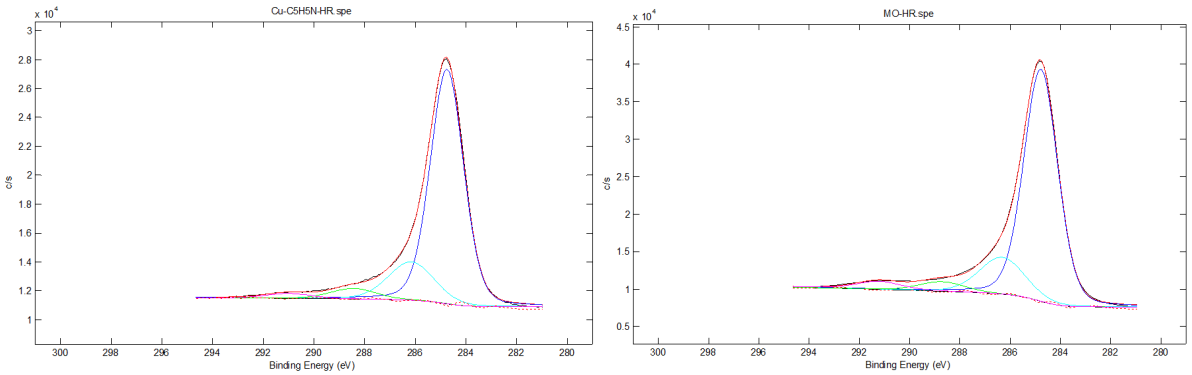

(a) C1s spectrum of the copper sample.

(b) C1s spectrum of the molybdenum sample.

Figure 6.10: C1s spectra of the XPS samples showing the four fitted subpeaks with different intensities.

Unfortunately, the N1s spectra of both samples had their own problems. Those spectra are small to begin with, which makes the fitting harder, because the signal is close to the noise level. The main issue for the copper sample was that this peak was shifted to higher energies, approximately 408 eV. A small shift is always used as a correction factor, because the surface of the sample gets charged during the measurement due to the negatively charged electrons being shot out of the sample. In this case the shift was already applied, and without the shift the N1s peak would end up at even higher energies. There are no nitrogen bonds above approximately 405 eV, so it was not possible to fit this peak.

For the Mo sample, the main problem are the two flanking peaks, which mask the shape of the N1s peak. Still, this peak could be fitted as a side lobe of the Mo3p3 peak, of which the result is shown in figure 6.11b. The main peak at 394.7 eV is that of the Mo3p3 bonds. The other two peaks are fitted at 397.5 eV and 399.0 eV, which corresponds approximately to the pyridinic and pyrrolic bonding of nitrogen. However, those peaks are very small and not really convincing next to the bigger Mo peak. This sample would benefit greatly from removing the Mo via etching, and then measuring again.

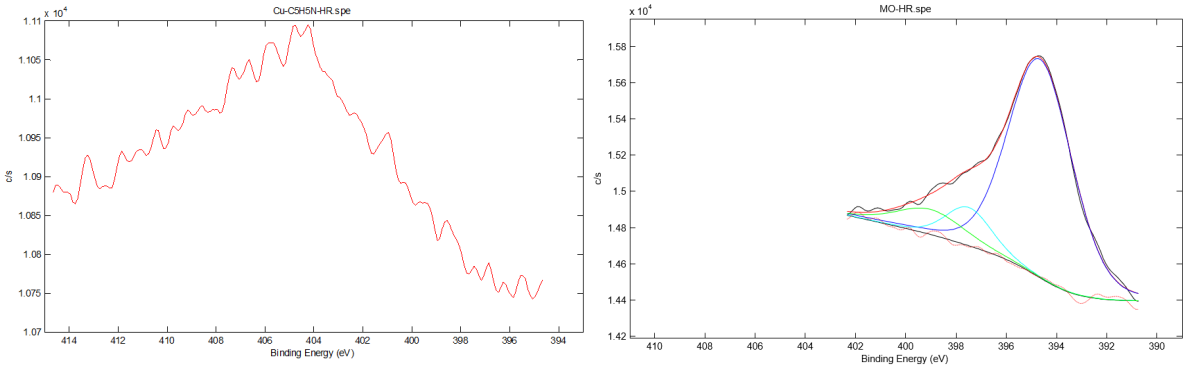

(a) N1s spectrum of the copper sample.

(b) N1s spectrum of the molybdenum sample.

Figure 6.11: N1s spectra of the XPS samples with the copper sample unable to be fitted.

The conclusion of this chapter is that in our setup, using pyridine as a precursor is preferred over the use of ammonia gas. The pyridine vapor can be injected in smaller quantities, to have more control over the graphene growth. It doesn't etch the catalyst, like ammonia did with copper and nickel, and it doesn't inhibit graphene growth, like ammonia did with molybdenum. According to the Raman spectra, good quality graphene can be grown on larger areas. The process window changes with the kind of sample that needs to be processed, so the CVD parameters and growth process are more complex for pyridine than for methane. This means that we cannot simply use one recipe for every sample we want to grow nitrogen-doped graphene on. The doping with nitrogen has not yet been confirmed, but is suggested by the XPS measurements. To fully confirm this, electrical measurements are necessary, but for this the pyridine CVD recipe needs to be tuned to be able to grow graphene on microstructures. If this works, back-gated transistors can be manufactured to confirm a shift in the Dirac point, and hence n- or p-type doping.

7

Conclusions and Future Work

7.1. Conclusion

Our ultimate goal of this research was to enhance the performance of graphene-based gas sensors, by doping the graphene with nitrogen impurities. The three sub goals stated in chapter 1 for achieving this goal, were optimizing the nitrogen-doped graphene CVD growth process, fabricating the graphene based gas sensors, and measuring the gas-sensing performance against NO_2 gas. Of those three goals, we only worked on the first one, which turned out to be harder and more time consuming than anticipated.

We did manage to grow a variety of graphene samples with different recepies, catalysts and precursors to build on top of the existing recepies using methane. Optimization was done by changing CVD parameters, doing Raman measurements and understanding what needs to be changed to get better results. A new chemical in the cleanroom, pyridine, was used to advance when it turned out that nitrogen-doped graphene could not be grown in our CVD setup using ammonia gas. Ammonia inhibits the growth of graphene on a Mo catalyst, and etches Cu and Ni catalysts, removing the graphene with it. With pyridine, graphene growth could be achieved, and the recipe was tuned till we could grow high quality graphene on both Mo and Cu catalysts.

Different characterization techniques were explored and tested on the produced samples, to be able to say something about the quality, structure and doping content. The used techniques included Raman spectroscopy, FTIR, EDX, scanning electron microscopy, back-gate measurements and XPS. The FTIR measurement was proven to be not suitable for measuring doping in graphene, but could definitely be a valuable asset when working with (r)GO to measure the different functional groups bonded to the material.

In the end, final tests in the form of electrical measurements and XPS were needed to confirm doping in graphene. The electrical measurements couldn't yet be performed, because growing graphene on a full wafer with prepatterned catalyst using pyridine required more experimental work. This was achieved in the end, and the wafers are now ready for testing. The XPS gave an inaccurate result because of two adjacent peaks of Mo in the spectrum, and so couldn't confirm the doping. Still, the growth of graphene on molybdenum using a nitrogen containing precursor is a novelty not previously reported in literature, that could potentially be an excellent addition in the field of gas sensing.

7.2. Future Work

A lot of work is still to be done on this topic. The next main hurdle to take is growing the pyridine on microstructures, made using a lithography process. For now, this doesn't yet work, and this needs investigation and subsequent testing. There should be a process window that allows the combination of pyridine and molybdenum to grow graphene. This might indeed be lowering the pyridine flow and/or the growth time, or alternatively changing gas mixture, or pretreating the catalyst surface. In any case,

if this works out, back-gate transistors can be manufactured, and measurements can be done to confirm nitrogen doping. Next to that the gas response can be tested, to see if the sensors have gotten more sensitive towards NO_2 gas.

Subsequently, different catalyst thicknesses can be tested on graphene quality, with probably thicker substrates producing thinner graphene, that is more useful for gas sensors. This should also be tried in combination with the transfer-free process, since this is one of the main benefits of using molybdenum. There is probably an optimum thickness that produces good quality graphene, but can still be used with a transfer-free process without losing all graphene.

Next to NO_2, other gases can be tested as well to measure their response. It is very well possible that some gas responses will be degraded compared to pristine graphene, while others will be improved, which adds to the selectivity of the sensor. The sensitivity, stability and speed should also be characterized. Also the recovery characteristics should be studied, to see if gases can fully desorb after a measurement, or that the help of a micro hot plate is necessary.

A way to make the sensors even more selective towards certain gases is functionalization. This is usually done by decorating the graphene with different amounts and types of nanoparticles, that will influence the adsorption and charge transfer of the gases to be measured. This is not the only option, and basically all design options made during sensor fabrication can influence the final gas sensitivity. This is very useful for creating an array of gas sensors that are all slightly different and will respond in their own unique way to different concentrations of gases or gas mixtures. In this way reading out such an array can create a kind of fingerprint of a gas, just like FTIR is doing this for certain powders or gels. This e-nose then allows us to have a whole library of gases and vapors that we can measure, and accurately detect, both in type and in concentration. This would open up a world of applications, and this is the type of device we ultimately want to develop.

References

[1] G. Deokar, J. Jin, U. Schwingenschlögl, and P. Costa, "Chemical vapor depoistion-grown nitrogen-doped graphene's synthesis, characterization and applications," *NPJ 2D materials and applications*, vol. 6, no. 14, 2022.

[2] J. Ma, *Gas sensors: materials and devices*. Institute of Physics Publishing, 2021.

[3] G. Gerasimov, *Graphene-based gas sensors*. Royal society of chemistry, 2017, pp. 133–152.

[4] R. Malik, V. Tomer, Y. Mishra, and L. Lin, "Functional gas sensing nanomaterials: A panoramic view," *Applied Physics Reviews*, vol. 7, 2020.

[5] R. Kumar, Mamta, R. Kumari, and V. N. Singh, "Sno2-based no2 gas sensor with outstanding sensing performance at room temperature," *Micromachines*, vol. 14, no. 4, p. 728, Mar. 2023. DOI: 10.3390/mi14040728.

[6] B. Vigna, P. Ferrari, F. Villa, E. Lasalandra, and S. Zerbini, *Silicon sensors and actuators, the Feynman roadmap*. Springer, 2022.

[7] C. Gautam, C. S. Tiwary, L. D. Machado, *et al.*, "Synthesis and porous h-bn 3d architectures for effective humidity and gas sensors," *RSC Adv.*, vol. 6, pp. 87 888–87 896, 91 2016. DOI: 10.1039/C6RA18833H. [Online]. Available: http://dx.doi.org/10.1039/C6RA18833H.

[8] H. Tian, H. Fan, J. Ma, *et al.*, "Pt-decorated zinc oxide nanorod arrays with graphitic carbon nitride nanosheets for highly efficient dual-functional gas sensing," *Journal of Hazardous Materials*, vol. 341, pp. 102–111, 2018, ISSN: 0304-3894. DOI: https://doi.org/10.1016/j.jhazmat.2017.07.056. [Online]. Available: https://www.sciencedirect.com/science/article/pii/S0304389417305654.

[9] H. Tang, L. N. Sacco, S. Vollebregt, H. Ye, X. Fan, and G. Zhang, "Recent advances in 2d/-nanostructured metal sulfide-based gas sensors: Mechanisms, applications, and perspectives," *J. Mater. Chem. A*, vol. 8, pp. 24 943–24 976, 47 2020. DOI: 10.1039/D0TA08190F. [Online]. Available: http://dx.doi.org/10.1039/D0TA08190F.

[10] "Allotropes of carbon." (Oct. 2024), [Online]. Available: https://en.wikipedia.org/wiki/Allotropes_of_carbon.

[11] A. H. Castro Neto, F. Guinea, N. M. R. Peres, K. S. Novoselov, and A. K. Geim, "The electronic properties of graphene," *Rev. Mod. Phys.*, vol. 81, pp. 109–162, 1 Jan. 2009. DOI: 10.1103/RevModPhys.81.109. [Online]. Available: https://link.aps.org/doi/10.1103/RevModPhys.81.109.

[12] D. A. Neamen, *Semiconductor physics and devices*, 4th ed. McGraw Hill Education, 2012.

[13] G. Deokar, J. Casanova-Cháfer, N. S. Rajput, *et al.*, "Wafer-scale few-layer graphene growth on cu/ni films for gas sensing applications," *Sensors and Actuators B: Chemical*, vol. 305, p. 127 458, 2020, ISSN: 0925-4005. DOI: https://doi.org/10.1016/j.snb.2019.127458. [Online]. Available: https://www.sciencedirect.com/science/article/pii/S0925400519316570.

[14] P. Recum and T. Hirsch, "Graphene-based chemiresistive gas sensors," *Nanoscale Adv.*, vol. 6, pp. 11–31, 1 2024. DOI: 10.1039/D3NA00423F.

[15] L. N. Sacco, H. Meng, and S. Vollebregt, "Humidity sensor based on multi-layer graphene (mlg) integrated onto a micro-hotplate (mhp)," in *2022 IEEE sensors*, 2022, pp. 1–4.

[16] F. Ricciardella, S. Vollebregt, R. Tilmann, *et al.*, "Influence of defect density on the gas sensing properties of multi-layered graphene grown by chemical vapor deposition," *Carbon Trends*, vol. 3, p. 100 024, 2021, ISSN: 2667-0569.

[17] Y. Zhang, Y. Chen, K. Zhou, *et al.*, "Improving gas sensing properties of graphene by introducing dopant and defects: A first-principles study," *Nanotechnology*, vol. 20, 2009.

[18] X. Wang, X. Li, L. Zhang, *et al.*, “N-doping of graphene through electrothermal reactions with ammonia,” *Science*, vol. 324, no. 5928, pp. 768–771, 2009. DOI: 10.1126/science.1170335. [Online]. Available: https://www.science.org/doi/abs/10.1126/science.1170335.

[19] S. Srivastava, P. K. Kashyap, V. Singh, T. D. Senguttuvan, and B. K. Gupta, “Nitrogen doped high quality cvd grown graphene as a fast responding no2 gas sensor,” *New J. Chem.*, vol. 42, pp. 9550–9556, 12 2018. DOI: 10.1039/C8NJ00885J. [Online]. Available: http://dx.doi.org/10.1039/C8NJ00885J.

[20] S. Srivastava, S. K. Jain, G. Gupta, T. D. Senguttuvan, and B. K. Gupta, “Boron-doped few-layer graphene nanosheet gas sensor for enhanced ammonia sensing at room temperature,” *RSC Adv.*, vol. 10, pp. 1007–1014, 2 2020. DOI: 10.1039/C9RA08707A. [Online]. Available: http://dx.doi.org/10.1039/C9RA08707A.

[21] R. C. Jaeger, *Introduction to microelectronic fabrication*, G. W. Neudeck and R. F. Pierret, Eds. Prentice Hall, 2002.

[22] F. Ricciardella, S. Vollebregt, E. Kurganova, A. Giesbers, M. Ahmadi, and P. Sarro, “Growth of multi-layered graphene on molybdenum catalyst by solid phase reaction with amorphous carbon,” *2D materials*, 2019. DOI: 10.1088/2053-1583/ab1518.

[23] D. Cai, S. Wang, P. Lian, *et al.*, “Superhigh capacity and rate capability of high-level nitrogen-doped graphene sheets as anode materials for lithium-ion batteries,” *Electrochimica Acta*, vol. 90, pp. 492–497, 2013, ISSN: 0013-4686. DOI: https://doi.org/10.1016/j.electacta.2012.11.105. [Online]. Available: https://www.sciencedirect.com/science/article/pii/S0013468612019263.

[24] T. V. Pham, J.-G. Kim, J. Y. Jung, *et al.*, “High areal capacitance of n-doped graphene synthesized by arc discharge,” *Advanced Functional Materials*, vol. 29, no. 48, p. 1 905 511, 2019. DOI: https://doi.org/10.1002/adfm.201905511. [Online]. Available: https://advanced.onlinelibrary.wiley.com/doi/abs/10.1002/adfm.201905511.

[25] L. Sun, L. Wang, C. Tian, *et al.*, “Nitrogen-doped graphene with high nitrogen level via a one-step hydrothermal reaction of graphene oxide with urea for superior capacitive energy storage,” *RSC Adv.*, vol. 2, pp. 4498–4506, 10 2012. DOI: 10.1039/C2RA01367C. [Online]. Available: http://dx.doi.org/10.1039/C2RA01367C.

[26] D. Deng, X. Pan, L. Yu, *et al.*, “Toward n-doped graphene via solvothermal synthesis,” *Chem. Mater*, vol. 23, pp. 1188–1193, Feb. 2011. DOI: 10.1021/cm102666r.

[27] Z. Lin, G. Waller, Y. Liu, M. Liu, and C.-P. Wong, “Facile synthesis of nitrogen-doped graphene via pyrolysis of graphene oxide and urea, and its electrocatalytic activity toward the oxygen-reduction reaction,” *Advanced Energy Materials*, vol. 2, no. 7, pp. 884–888, 2012. DOI: https://doi.org/10.1002/aenm.201200038. eprint: https://advanced.onlinelibrary.wiley.com/doi/pdf/10.1002/aenm.201200038. [Online]. Available: https://advanced.onlinelibrary.wiley.com/doi/abs/10.1002/aenm.201200038.

[28] D. Wei, Y. Liu, Y. Wang, H. Zhang, L. Huang, and G. Yu, “Synthesis of n-doped graphene by chemical vapor deposition and its electrical properties,” *Nano letters*, vol. 9, pp. 1752–1758, 5 2009.

[29] M. Rybin, A. Pereyaslavtsev, T. Vasilieva, *et al.*, “Efficient nitrogen doping of graphene by plasma treatment,” *Carbon*, vol. 96, pp. 196–202, 2016, ISSN: 0008-6223. DOI: https://doi.org/10.1016/j.carbon.2015.09.056. [Online]. Available: https://www.sciencedirect.com/science/article/pii/S0008622315302748.

[30] M. Son, S.-S. Chee, S.-Y. Kim, *et al.*, “High-quality nitrogen-doped graphene films synthesized from pyridine via two-step chemical vapor deposition,” *Carbon*, vol. 159, pp. 579–585, 2020, ISSN: 0008-6223.

[31] Z. Zhai, H. Shen, J. Chen, X. Li, and Y. Jiang, “Direct growth of nitrogen-doped graphene films on glass by plasma-assisted hot filament cvd for enhanced electricity generation,” *Journal of materials chemistry A*, vol. 7, 2019.

[32] Z. Luo, S. Lim, Z. Tian, *et al.*, “Pyridinic n doped graphene: Synthesis, electronic structure, and electrocatalytic property,” *Journal of Materials Chemistry*, vol. 21, pp. 8038–8044, 22 2011.

[33] Z. Jin, J. Yao, C. Kittrel, and J. M. Tour, "Large-scale growth and characterizations of nitrogen-doped monolayer graphene sheets," *ACS Nano*, vol. 5, no. 5, pp. 4112–4117, 2011, PMID: 21476571. DOI: 10.1021/nn200766e.

[34] Y.-P. Lin, Y. Ksari, D. Aubel, *et al.*, "Efficient and low-damage nitrogen doping of graphene via plasma-based methods," *Carbon*, vol. 100, pp. 337–344, 2016, ISSN: 0008-6223. DOI: https://doi.org/10.1016/j.carbon.2015.12.094. [Online]. Available: https://www.sciencedirect.com/science/article/pii/S0008622315305601.

[35] A. L. M. Reddy, A. Srivastava, S. R. Gowda, H. Gullapalli, M. Dubey, and P. M. Ajayan, "Synthesis of nitrogen-doped graphene films for lithium battery application," *ACS Nano*, vol. 4, no. 11, pp. 6337–6342, 2010, PMID: 20931996. DOI: 10.1021/nn101926g.

[36] A. Cabrero-Vilatela, R. Weatherup, P. Braeuninger-Weimer, S. Caneva, and S. Hofmann, "Towards a general growth model for graphene cvd on transition metal catalysts," *Nanoscale*, vol. 8, 2016.

[37] F. Ricciardella, S. Vollebregt, T. Polichetti, B. Alfano, E. Massera, and P. M. Sarro, "High sensitive gas sensors realized by a transfer-free process of cvd graphene," in *2016 IEEE sensors*, 2016, pp. 1–3.

[38] F. Ricciardella, S. Vollebregt, T. Polichetti, B. Alfano, E. Massera, and P. M. Sarro, "An innovative approach to overcome saturation and recovery issues of cvd graphene-based gas sensors," in *2017 IEEE sensors*, 2017, pp. 1–3.

[39] L. N. Sacco, A. Dobrowolski, B. Boshuizen, *et al.*, "Controlling the number of layers of mo-grown cvd graphene through the catalyst thickness," *Diamond and Related Materials*, vol. 154, p. 112 195, 2025, ISSN: 0925-9635. DOI: https://doi.org/10.1016/j.diamond.2025.112195. [Online]. Available: https://www.sciencedirect.com/science/article/pii/S0925963525002523.

[40] Y. Seekaew, N. Tammanoon, A. Tuantranont, T. Lomas, A. Wisitsoraat, and C. Wongchoosuk, "Conversion of carbon dioxide into chemical vapor deposited graphene with controllable number of layers via hydrogen plasma pre-treatment," *Membranes*, vol. 12, 2022.

[41] F. Ricciardella, S. Vollebregt, T. Polichetti, *et al.*, "Effects of graphene defects on gas sensing properties towards no2 detection," *Nanoscale*, vol. 9, pp. 6085–6093, 18 2017.

[42] T. Liang, C. Luan, H. Chen, and M. Xu, "Exploring oxygen in graphene chemical vapor deposition synthesis," *Nanoscale*, vol. 9, pp. 3719–3735, 11 2017. DOI: 10.1039/C7NR00188F. [Online]. Available: http://dx.doi.org/10.1039/C7NR00188F.

[43] F. Weich, J. Widany, and T. Frauenheim, "Paracyanogen-like structures in high-density amorphous carbon nitride1this paper was preserved at the european materials research society 1997 meeting, symposium a: Fullerenes and carbon based materials, strasbourg, france, june 1997.1," *Carbon*, vol. 37, no. 4, pp. 545–548, 1999, ISSN: 0008-6223.

[44] A. Capasso, T. Dikonimos, F. Sarto, *et al.*, "Nitrogen-doped graphene films from chemical vapor deposition of pyridine: Influence of process parameters on the electrical and optical properties," *Beilstein Journal of Nanotechnology*, vol. 6, pp. 2028–2038, 2015, ISSN: 2190-4286. DOI: 10.3762/bjnano.6.206.

[45] Y. Jin, B. Hu, Z. Wei, *et al.*, "Roles of h2 in annealing and growth times of graphene cvd synthesis over copper foil," *J. Mater. Chem. A*, vol. 2, pp. 16 208–16 216, 38 2014. DOI: 10.1039/C4TA02557A. [Online]. Available: http://dx.doi.org/10.1039/C4TA02557A.

[46] D. M. Dobkin and M. K. Zuraw, *Principles of chemical vapor deposition*. Kluwer academic publishers, 2003.

[47] F. Ricciardella, S. Vollebregt, T. Polichetti, B. Alfano, E. Massera, and P. Sarro, "Low temperature cvd grown graphene for highly selective gas sensors working under ambient conditions †," vol. 1, Aug. 2017. DOI: 10.3390/proceedings1040445.

[48] W.-J. Su, H.-C. Chang, S.-i. Honda, P.-H. Lin, Y.-S. Huang, and K.-Y. Lee, "Nitrogen plasma-treated multilayer graphene-based field effect transistor fabrication and electronic characteristics," *Physica E: Low-dimensional Systems and Nanostructures*, vol. 92, pp. 41–46, 2017.

[49] "How much vapor goes out?" (2021), [Online]. Available: https://www.enigmatic-consulting.com/semiconductor_processing/CVD_Fundamentals/reactors/Bubbler_simple_model.html.

[50] AN53174, "Characterizing graphene with raman spectroscopy," Thermo scientific, application note, 2019.

[51] A. C. Ferrari, J. C. Meyer, V. Scardaci, *et al.*, "Raman spectrum of graphene and graphene layers," *Phys. Rev. Lett.*, vol. 97, p. 187 401, 18 Oct. 2006. DOI: 10.1103/PhysRevLett.97.187401. [Online]. Available: https://link.aps.org/doi/10.1103/PhysRevLett.97.187401.

[52] A. C. Ferrari, "Raman spectroscopy of graphene and graphite: Disorder, electron–phonon coupling, doping and nonadiabatic effects," *Solid State Communications*, vol. 143, no. 1, pp. 47–57, 2007, Exploring graphene, ISSN: 0038-1098. DOI: https://doi.org/10.1016/j.ssc.2007.03.052. [Online]. Available: https://www.sciencedirect.com/science/article/pii/S0038109807002967.

[53] J. v. Wingerden, *Hitachi regulus su8230 sem manual*, Else Kooij Laboratory, Aug. 2023.

[54] M. Kumar, K. Thangaian, G. Kalita, P. Ragupathy, T. Narayanan, and D. Pattanayak, "On the large capacitance of nitrogen doped graphene derived by a facile route," *RSC Advances*, vol. 4, Aug. 2014. DOI: 10.1039/C4RA04927F.

[55] A. Misra, P. K. Tyagi, M. Singh, and D. Misra, "Ftir studies of nitrogen doped carbon nanotubes," *Diamond and Related Materials*, vol. 15, no. 2, pp. 385–388, 2006, Proceedings of the Applied Diamond Conference/NanoCarbon 2005, ISSN: 0925-9635. DOI: https://doi.org/10.1016/j.diamond.2005.08.013. [Online]. Available: https://www.sciencedirect.com/science/article/pii/S0925963505003146.

[56] A. M. Vasilica Țucureanu and A. M. Avram, "Ftir spectroscopy for carbon family study," *Critical Reviews in Analytical Chemistry*, vol. 46, no. 6, pp. 502–520, 2016. DOI: 10.1080/10408347.2016.1157013.

[57] W. Herres and J. Gronholz, *Understanding ftir data processing*, Bruker Analytische Messtechnik GmbH.

[58] Bruker.com. "Guide to infrared spectroscopy." (2022), [Online]. Available: https://www.bruker.com/en/products-and-solutions/infrared-and-raman/ft-ir-routine-spectrometer/what-is-ft-ir-spectroscopy.html#:~:text=There%20are%20three%20main%20measurement,(ATR)%2C%20and%20Reflection. (visited on 02/21/2025).

[59] Piketech, *Hatr accessory installation and user guide*, PIKE technologies, inc., Jan. 2013.

[60] F. Schwierz, "Graphene transistors," *Nature nanotechnology*, May 2010.

[61] "A systematic study of the stability, electronic and optical properties of beryllium and nitrogen co-doped graphene," *Carbon*, vol. 129, pp. 207–227, 2018, ISSN: 0008-6223. DOI: https://doi.org/10.1016/j.carbon.2017.12.014.

[62] D. Joly. "Monte carlo simulation of electron trajectory in solids." (2003), [Online]. Available: https://casino.espaceweb.usherbrooke.ca/ (visited on 12/17/2024).

[63] F. T. Ulaby and U. Ravaioli, *Fundamentals of Applied Electromagnetics*, S. Disanno and R. Kernan, Eds. Pearson, 2015.

[64] T. Tran, V. A. Pham, P. Le, T. Nguyen, and V. Tran, "Synthesis of amorphous silica and sulfonic acid functionalized silica used as reinforced phase for polymer electrolyte membrane," *Adv. Nat. Sci.: Nanosci. Nanotechnol.*, vol. 4, p. 045 007, Dec. 2013. DOI: 10.1088/2043-6262/4/4/045007.

[65] W. Zheng, T. P. Cotter, P. Kaghazchi, *et al.*, "Experimental and theoretical investigation of molybdenum carbide and nitride as catalysts for ammonia decomposition," *Journal of the American Chemical Society*, vol. 135, no. 9, pp. 3458–3464, 2013, PMID: 23350903. DOI: 10.1021/ja309734u. [Online]. Available: https://doi.org/10.1021/ja309734u.

[66] B. Fang, M. Yang, C. Zhang, *et al.*, "Molybdenum carbide phase effects in heterogeneous catalytic ammonia synthesis," *Chemical Engineering Science*, vol. 259, p. 117 834, 2022, ISSN: 0009-2509. DOI: https://doi.org/10.1016/j.ces.2022.117834. [Online]. Available: https://www.sciencedirect.com/science/article/pii/S0009250922004183.

[67] H. Gao, L. Song, W. Guo, *et al.*, “A simple method to synthesize continuous large area nitrogen-doped graphene,” *Carbon*, vol. 50, no. 12, pp. 4476–4482, 2012, ISSN: 0008-6223. DOI: https://doi.org/10.1016/j.carbon.2012.05.026. [Online]. Available: https://www.sciencedirect.com/science/article/pii/S0008622312004551.

[68] J. F. Bao, N. Kishi, and T. Soga, “Synthesis of nitrogen-doped graphene by the thermal chemical vapor deposition method from a single liquid precursor,” *Materials Letters*, vol. 117, pp. 199–203, 2014, ISSN: 0167-577X. DOI: https://doi.org/10.1016/j.matlet.2013.11.125. [Online]. Available: https://www.sciencedirect.com/science/article/pii/S0167577X13016510.

[69] H. Memon, K. Bartle, J.M.Taylor, and A. Williams, “The shock tube pyrolysis of pyridine,” *International journal of energy research*, vol. 24, pp. 1141–1159, 2000.

[70] I. Vlassiouk, M. Regmi, P. Fulvio, *et al.*, “Role of hydrogen in chemical vapor deposition growth of large single-crystal graphene,” *ACS Nano*, vol. 5, no. 7, pp. 6069–6076, 2011, PMID: 21707037. DOI: 10.1021/nn201978y.

[71] R. J. Koch, M. Weser, W. Zhao, *et al.*, “Growth and electronic structure of nitrogen-doped graphene on ni(111),” *Phys. Rev. B*, vol. 86, p. 075 401, 7 Aug. 2012. DOI: 10.1103/PhysRevB.86.075401. [Online]. Available: https://link.aps.org/doi/10.1103/PhysRevB.86.075401.

A

Black Magic recepies

The standard graphene recepy (with methane gas) used in EKL can be found below.

```
COMM Ar Ar H2 CH4
VALV 1 OPEN
FLOW 3 OFF
TUNE PCON Fully open
PCON ON 1.0 1.0
WAIT PRES < 0.10
FLOW 2 ON 1000
WAIT TIME > 60
FLOW 2 OFF
WAIT PRES < 0.10
FLOW 2 ON 1000
WAIT TIME > 60
FLOW 2 OFF
WAIT PRES < 0.05
VALV 1 CLOSE
FLOW 6 ON 1000
FLOW 1 ON 500
TUNE PCON Graphene 25mbar
PCON ON 25.0 1.0
TUNE HTTC zero power
TUNE TOPH zero power
SENS SF 10
HEAT ON 550.0 125.0
TOPH ON 550.0 125.0
TUNE HTSF Graphene 550C SF
TUNE TOPH Graphene 450C
WAIT TEMP > 535.0
WAIT TIME > 60
TUNE HTSF Graphene 750C SF
TUNE TOPH Graphene 650C
HEAT ON 725.0 50.0
TOPH ON 725.0 50.0
WAIT TEMP > 710.0
WAIT TIME > 90
TUNE HTSF Graphene 1100C SF
TUNE TOPH Graphene 1000C
HEAT ON 935.0 30.0
TOPH ON 1000.0 30.0
WAIT TEMP > 925.0
WAIT TIME > 1200
TUNE HTSF Graphene 1100C Stable SF
HEAT ON 935.0 30.0
```

```
FLOW 2 ON 960
FLOW 6 ON 40
WAIT TIME > 15
FLOW 3 ON 25
WAIT TIME > 1200
FLOW 3 OFF
HEAT ON 350.0 600.0
TOPH ON 350.0 600.0
WAIT TEMP < 350.0
FLOW 6 OFF
SENS TC 600
HEAT OFF
TOPH OFF
TUNE PCON Graphene 10mbar
PCON ON 10.0 1.0
FLOW 1 ON 500
FLOW 2 ON 500
VALV 1 CLOSE
WAIT TEMP < 200.0
PCON OFF
VALV 1 OPEN
WAIT TEMP < 150.0
FLOW 2 OFF
FLOW 1 OFF
WAIT PRES < 0.50
```

The programs on the black magic are an assembly-like language with each line giving an instruction to the CVD reactor control software. There are 12 different operation commands:

- **COMM** - a comment that will open in a pop-up window
- **VALV** - open or close one of the valves
- **FLOW** - open or close one of the six MFCs and set the flow rate
- **TUNE** - send a specific set of parameters to the PID controller
- **PCON** - turn the pressure controller on/off and set its value
- **WAIT** - wait for a given time or temperature before continuing
- **SENS** - switch to one of the temperature sensors
- **HEAT** - turn the bottom heater on/off and set the temperature and rate of change
- **TOPH** - turn the top heater on/off and set the temperature and rate of change
- **LOOP** - create a loop that will run a specified amount of times
- **ALAR** - set an alarm that triggers an action when a process goes out of bounds
- **PLAS** - turn on/off the plasma generator and set the voltage for the generator

All recepies created in this thesis follow a similar pattern, with a flushing part, a heating up stage, growth section and cooling down stage. All recipes are logged in a separate file to be able to check if the actual temperatures/pressures/flow rates are equal or close to their setpoints. If the reactor was not used for more than two hours, a cleaning recipe was run first to purge the chamber with hydrogen at high temperature.

B

Raman matlab script

The Matlab scipt for curve fitting Raman spectra is shown below.

```
%Uses a 3 Lorentzian fit to analyse graphene on Mo (poly2 baseline extraction)

clear all

cd 'C:\Users\bram9\OneDrive\Documenten\Graduation Project Sten\Matlab\Raman data'

%[filename, filedirectory] = uigetfile ('*.txt', 'Select Raman data:');
%file = strcat(filedirectory,filename);
files = dir('*.txt');

mkdir results;

storename = input('In which file do you want to store the fitting parameters?
    [fitresults.txt]: ', 's');
if isempty(storename)
   storename = 'fitresults.txt';
end

cd results;
message = 'Fit of Raman spectrum with linear baseline removal using 8 Lorentzians and 2
    Gaussians';
dlmwrite(storename, message, 'delimiter', '', 'newline', 'pc');
cd ..;

skipall = input('Do you want to automatically accept all fitting results? y/n [n]: ', 's');
if isempty(skipall)
   skipall = 'n';
end

%% Actual readout of the data files
for i = 1:length(files)
   %Retreive data
   filename = files(i).name;
   DATA = dlmread(filename, '\t');
   freq = DATA(:,1);
   spec = DATA(:,2);

   % --- Create fit "baseline"

   % Apply exclusion rule "Spectra area 3"
   if length(freq)~=2650
       error('Exclusion rule ''%s'' is incompatible with ''%s''.','Spectra area 3','freq');
```

```
end
ex2_ = true(length(freq),1);
ex2_([(1:301) (1136:1935) (2546:2650)]) = 0;
fo2_ = fitoptions('method','LinearLeastSquares','Robust','On');
ok2_ = isfinite(freq) & isfinite(spec);
if ~all( ok2_ )
    warning( 'GenerateMFile:IgnoringNansAndInfs', ...
        'Ignoring NaNs and Infs in data' );
end
set(fo2_,'Exclude',ex2_(ok2_));
ft2_ = fittype('poly2');

% Fit this model using new data
if sum(~ex2_(ok2_))<2 %% too many points excluded
    error('Not enough data left to fit ''%s'' after applying exclusion rule
        ''%s''.','baseline','Spectra area 3')
else
    cf2_ = fit(freq(ok2_),spec(ok2_),ft2_,fo2_);
end

% Or use coefficients from the original fit:
%if 0
%    cv_ = { 0.13369924049934909, 125.28750762357522};
%    cf_ = cfit(ft_,cv_{:});
%end

%Now generate and substract the obtained linear baseline
baseline = feval(cf2_,freq);
rm_spec = spec - baseline;

%Obtain maximum of G-peak
f_1500 = find(freq > 1499 & freq < 1501);
f_1800 = find(freq > 1799 & freq < 1801);
[g_mag,g_index] = max(rm_spec(f_1800:f_1500));

%Normalize spectrum to G-peak
clean_spec = rm_spec./g_mag;

%Start generated fit script
f_ = clf;
figure(f_);
%set(f_,'Units','Pixels','Position',[467 144 688 483]);
legh_ = []; legt_ = {}; % handles and text for legend
xlim_ = [Inf -Inf];   % limits of x axis
ax_ = axes;
set(ax_,'Units','normalized','OuterPosition',[0 0 1 1]);
set(ax_,'Box','on');
grid(ax_,'on');
axes(ax_); hold on;

% --- Plot data originally in dataset "norm_spec vs. freq"
freq = freq(:);
clean_spec = clean_spec(:);
h_ = line(freq,clean_spec,'Parent',ax_,'Color',[0.333333 0 0.666667],...
    'LineStyle','none', 'LineWidth',1,...
    'Marker','.', 'MarkerSize',12);
xlim_(1) = min(xlim_(1),min(freq));
xlim_(2) = max(xlim_(2),max(freq));
legh_(end+1) = h_;
legt_{end+1} = 'clean_spec vs. freq';
```

```
% Nudge axis limits beyond data limits
if all(isfinite(xlim_))
    xlim_ = xlim_ + [-1 1] * 0.01 * diff(xlim_);
    set(ax_,'XLim',xlim_)
else
    set(ax_, 'XLim',[66.338840000000005, 3635.8451599999999]);
end

% --- Create fit "fit 1"
fo_ = fitoptions('method','NonlinearLeastSquares','MaxFunEvals',1000,'Lower',[0 0 0 1300
     1550 2600 0.1 0.1 0.1],'Upper',[Inf Inf Inf 1400 1600 2800 Inf Inf Inf]);
ok_ = isfinite(freq) & isfinite(clean_spec);
if ~all( ok_ )
    warning( 'GenerateMFile:IgnoringNansAndInfs', ...
        'Ignoring NaNs and Infs in data' );
end
st_ = [0.1 1 1 1330 1580 2650 50 10 10 ];
set(fo_,'Startpoint',st_);
ft_ = fittype('a1/(1+((x-b1)/(c1/2))^2) + a2/(1+((x-b2)/(c2/2))^2) +
     a3/(1+((x-b3)/(c3/2))^2)',...
    'dependent',{'y'},'independent',{'x'},...
    'coefficients',{'a1', 'a2', 'a3', 'b1', 'b2', 'b3', 'c1', 'c2', 'c3'});

% Fit this model using new data
[cf_, quality] = fit(freq(ok_),clean_spec(ok_),ft_,fo_);

% Or use coefficients from the original fit:
%if 0
%    cv_ = { 0.0090070897439802518, 0.3652511518653046, 0.017530516381767693,
     0.99783675849908737, 0.11807640371766899, 0.044329032220910961, 0.93600336222924874,
     0.06355737979872754, 0.058737822544813273, 1161.6555928405469, 1352.2501105783977,
     1468.7899601174461, 1582.0822523422937, 1619.8229984609836, 2455.1588355395629,
     2704.1029619173314, 2944.7024687317107, 3235.6086573066568, 71.016712335890077,
     24.599732860293244, 22.209566244062753, 17.505247911008528, 11.790862408964765,
     31.037709652934844, 32.407162860497664, 43.306241495775218, 30.313285864582593};
%    cf_ = cfit(ft_,cv_{:});
%end

% Plot this fit
h_ = plot(cf_,'fit',0.95);
legend off; % turn off legend from plot method call
set(h_(1),'Color',[1 0 0],...
    'LineStyle','-', 'LineWidth',2,...
    'Marker','none', 'MarkerSize',6);
legh_(end+1) = h_(1);
legt_{end+1} = 'fit 1';

% Plot fits
coeff = coeffvalues(cf_);

f_d = coeff(1)./(1+((freq-coeff(4))./(coeff(7)/2)).^2);
f_g = coeff(2)./(1+((freq-coeff(5))./(coeff(8)/2)).^2);
f_gp = coeff(3)./(1+((freq-coeff(6))./(coeff(9)/2)).^2);

plot(freq, f_d, 'g', freq, f_g, 'g', freq, f_gp, 'g');

% Done plotting data and fits. Now finish up loose ends.
hold off;
leginfo_ = {'Orientation', 'vertical', 'Location', 'NorthEast'};
h_ = legend(ax_,legh_,legt_,leginfo_{:}); % create legend
set(h_,'Interpreter','none');
```

```
    xlabel(ax_,'');           % remove x label
    ylabel(ax_,'');           % remove y label

    %Display quality of fit
    disp(quality);

    %If desired ask user to accept fit
    if skipall == 'n'
        reply = input('Do you accept the fit? y/n [y]: ', 's');
        if isempty(reply)
            reply = 'y';
        end
    else
        reply = 'y';
    end

    if reply == 'y'
        %Retreive the fitting parameters and write out data
        coefficients = coeffvalues(cf_);
        fit_par = [coefficients(1,1:3)' coefficients(1,4:6)' coefficients(1,7:9)'];

        cd results;
        samplename = strrep(filename, '.txt', '');
        dlmwrite(storename, samplename, '-append', 'roffset', 1, 'delimiter', '', 'newline',
            'pc');
        dlmwrite(storename, fit_par, '-append', 'delimiter', '\t', 'precision', 6, 'newline',
            'pc');

        writename = strrep(filename, '.txt', '-fit.txt');
        dlmwrite(writename, fit_par, 'delimiter', '\t', 'precision', 6, 'newline', 'pc');

        writename2 = strrep(filename, '.txt', '-norm.txt');
        dlmwrite(writename2, [freq clean_spec], 'delimiter', '\t', 'precision', 6, 'newline',
            'pc');
        cd ..;
    end
end
```

This script was written by Sten Vollebregt. It uses 3 lorentzian functions to fit the 3 dominant peaks in the Raman spectrum of graphene. Because lorentzians have a single peak, and a defined width, this allows us to extract the exact locations of the 3 graphene peaks, their intensities, and their full-width at half maximum (FWHM) values. It can process multiple files with Raman data at once, and will visually show the suggested fit over the original Raman graph. The user can then either accept or reject each individual fit, and extract all the data in a single file.

C

XPS measurement setup

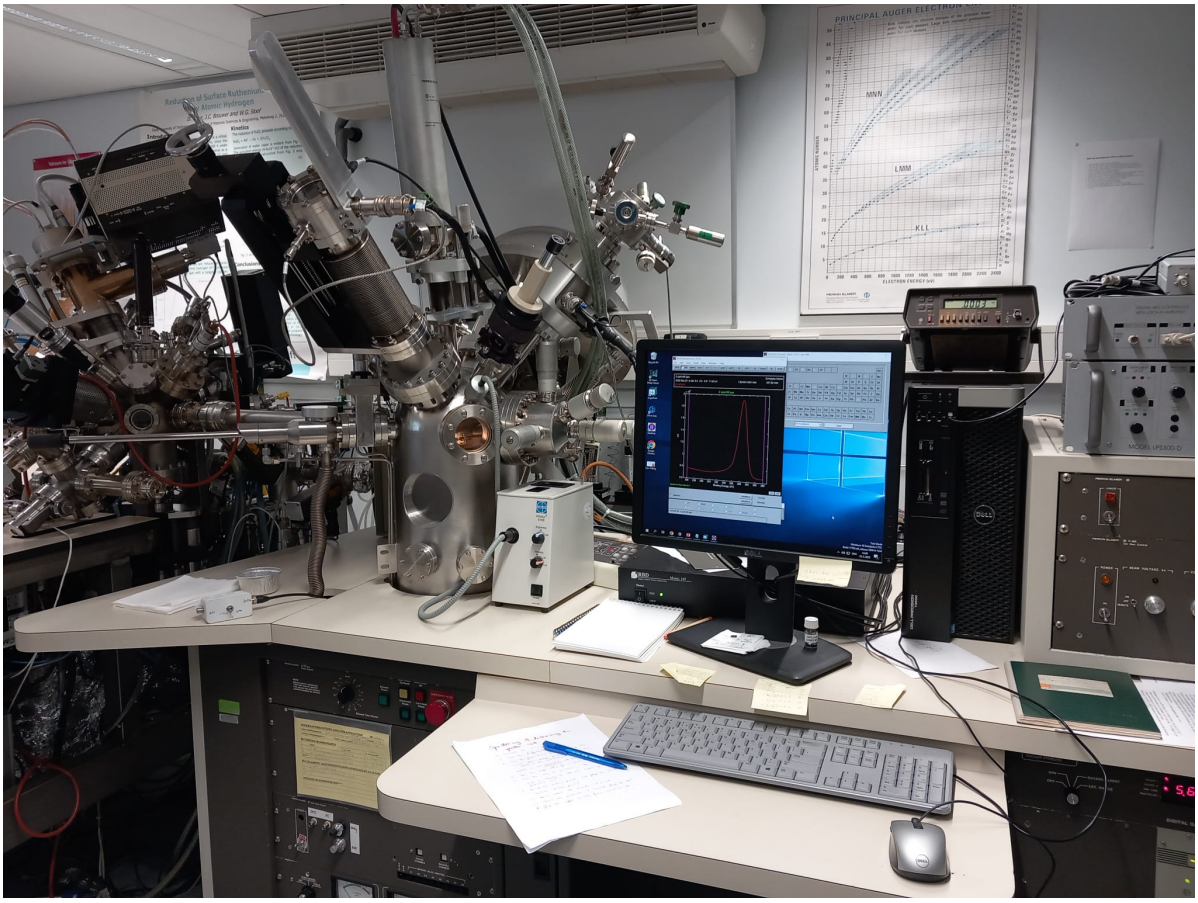

Figure C.1: The complete XPS measurement setup

The XPS setup was located in a different faculty, at the materials research laboratory. Samples could be loaded with a loadlock, since the chamber itself operated under ultrahigh vacuum. The results could be collected, viewed and fitted with the MultiPak data reduction software for XPS and AES, build on the MATLAB software. The samples themselves needed to be under 1.5 by 1.0 cm to be able to fit on a sample chuck. The system was available to us for two days, in which only two high resolution scans could be run. The settings for the survey and high resolution scans can be found in the image below.

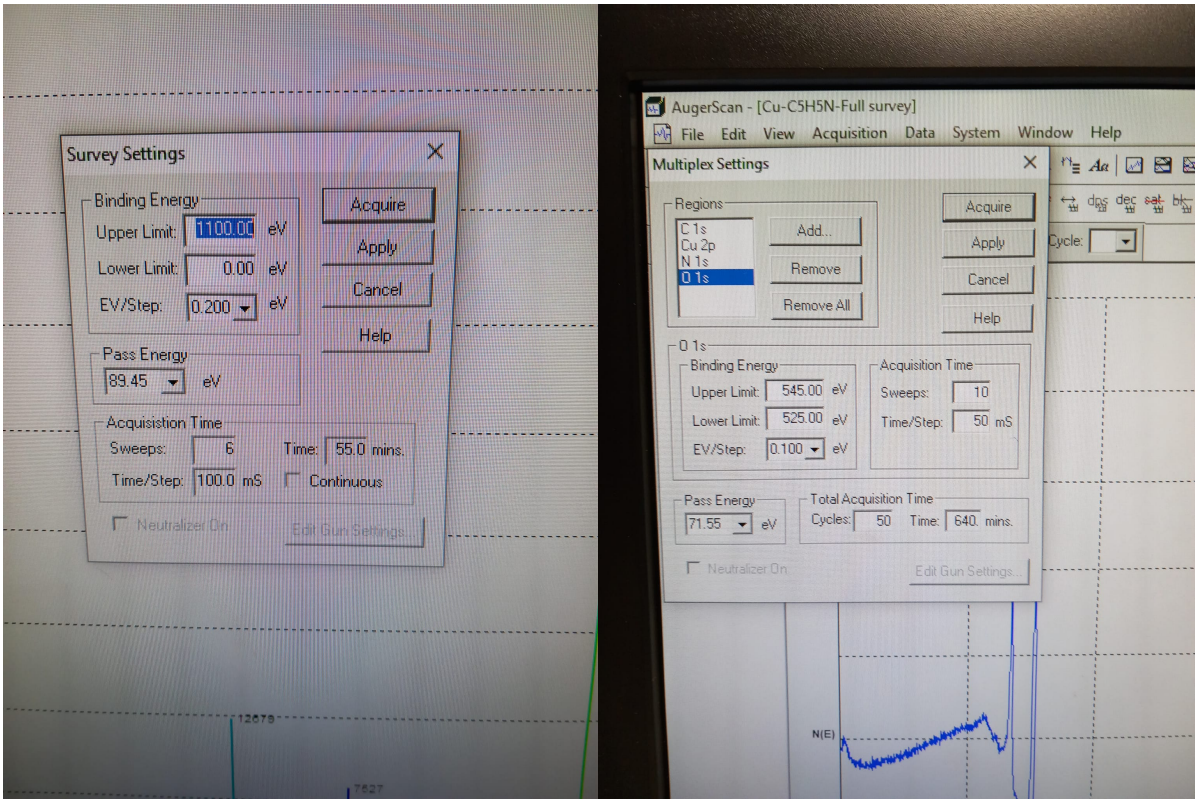

(a) **(b)**

Figure C.2: XPS settings for the survey scan [left] and the high resolution scan [right]

D

Raman measurement spectra

In this appendix all spectra of the samples that gave a Raman signal are shown. Since some samples worked better with different settings of the Raman spectrometer, not all samples have exactly the same settings, but roughly all use 50 or 100% laser power, either 10, 30 or 60 seconds exposure time, and are measured in the center of the sample at different spots.

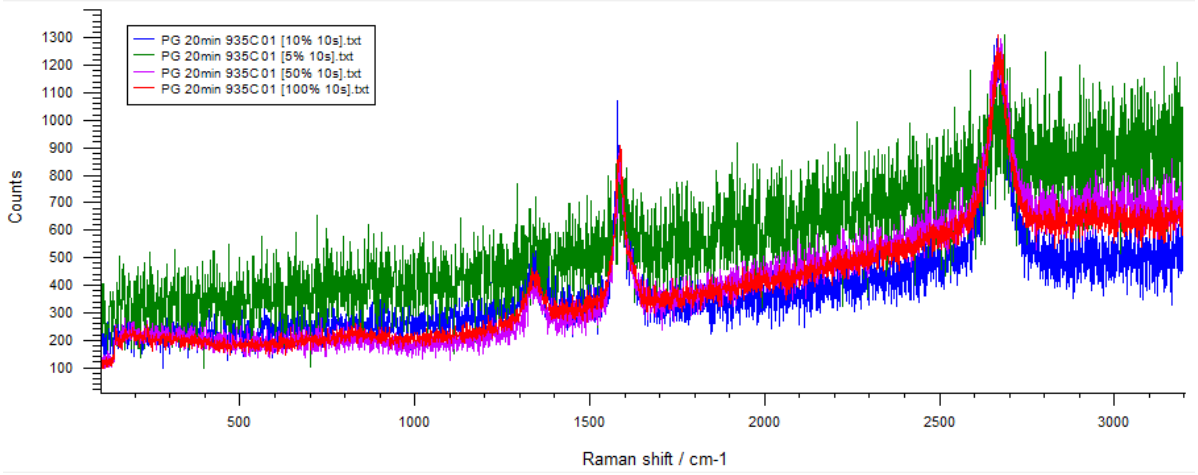

Figure D.1: Sample M1.1

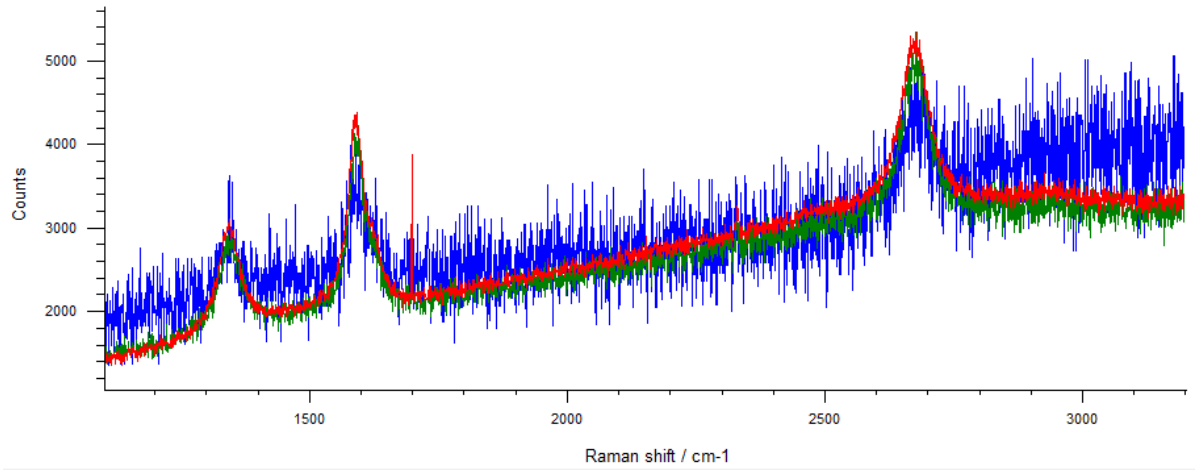

Figure D.2: Sample M1.3

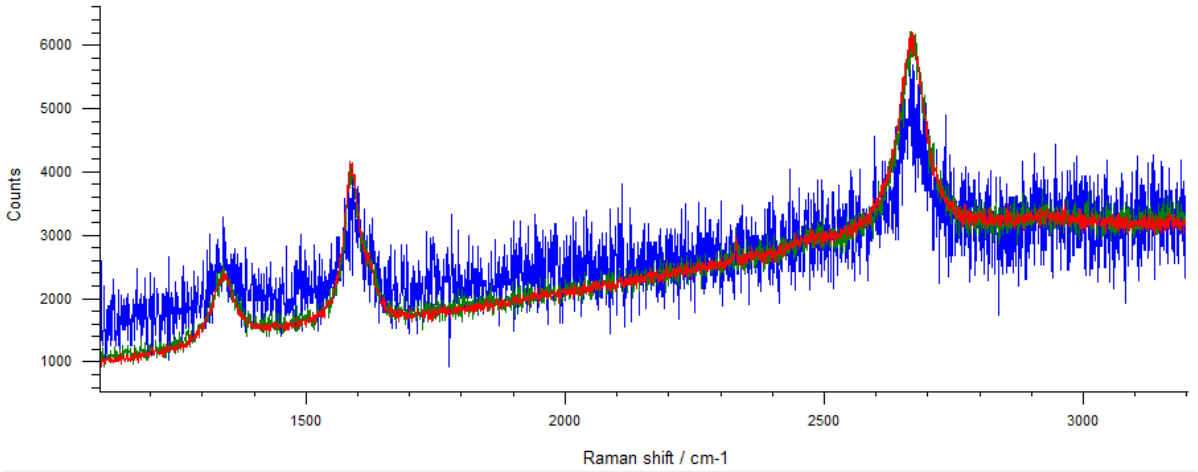

Figure D.3: Sample M1.6

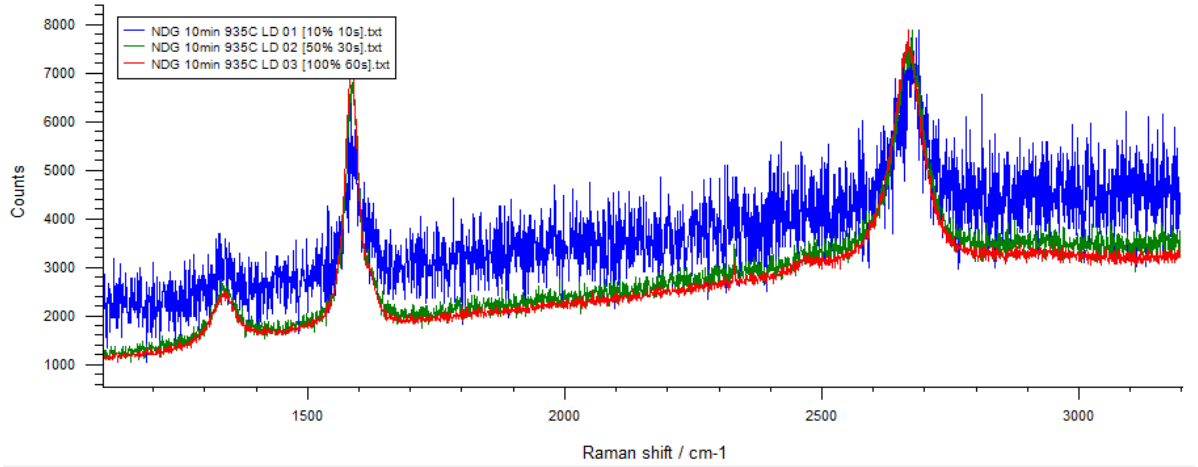

Figure D.4: Sample M1.7

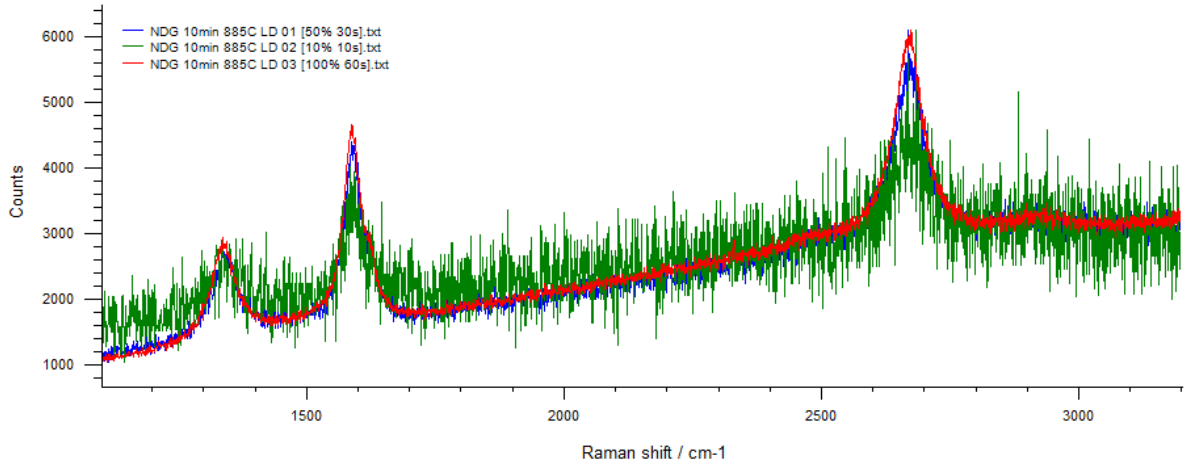

Figure D.5: Sample M1.8

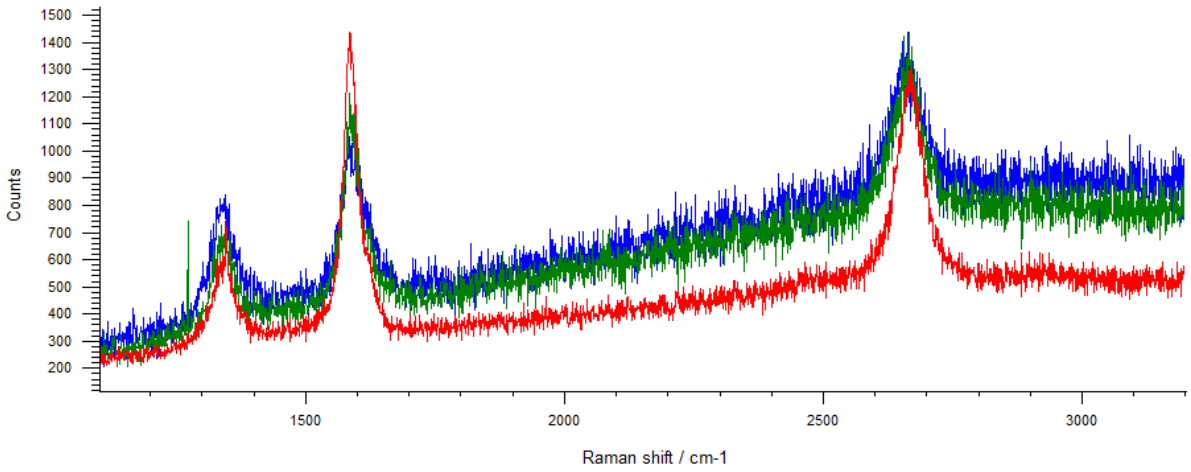

Figure D.6: Sample M2.2

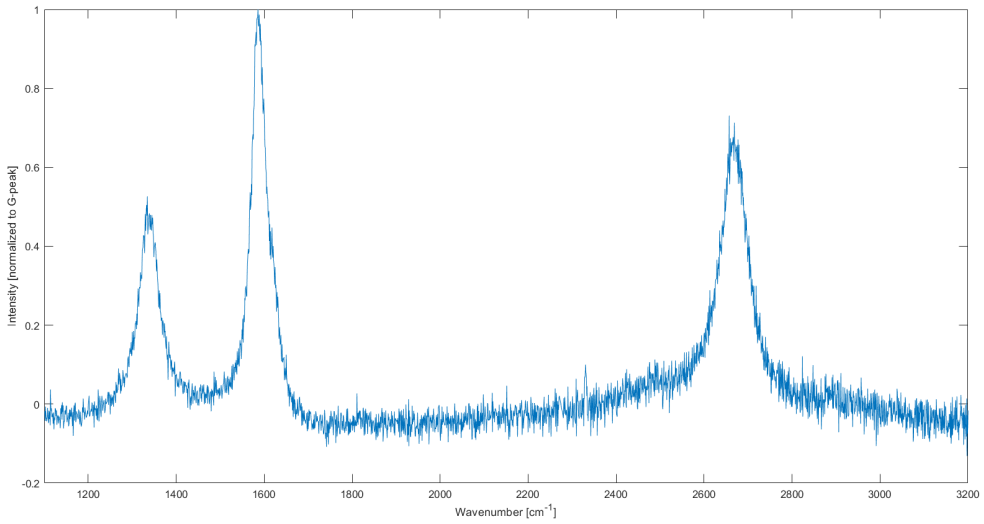

Figure D.7: Sample M2.3

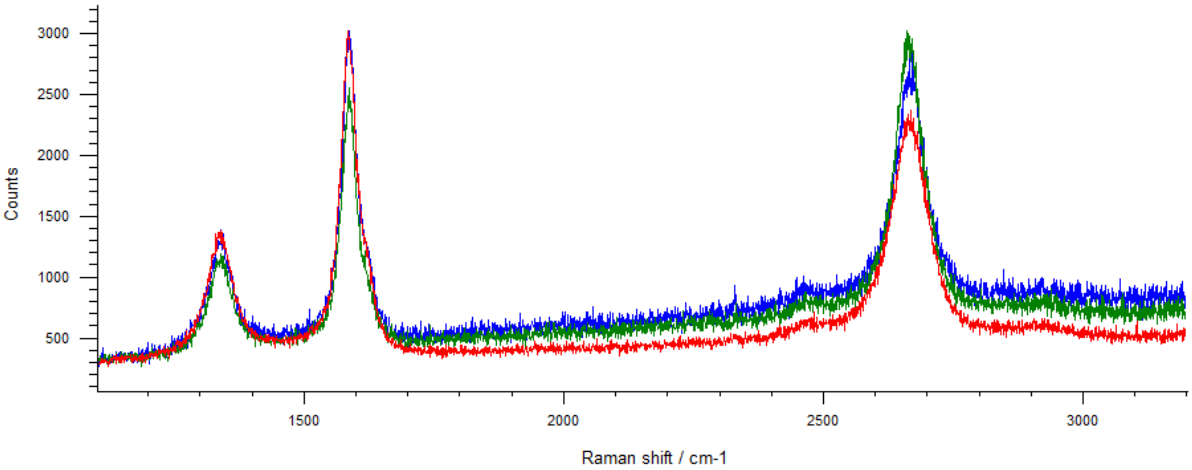

Figure D.8: Sample M2.4

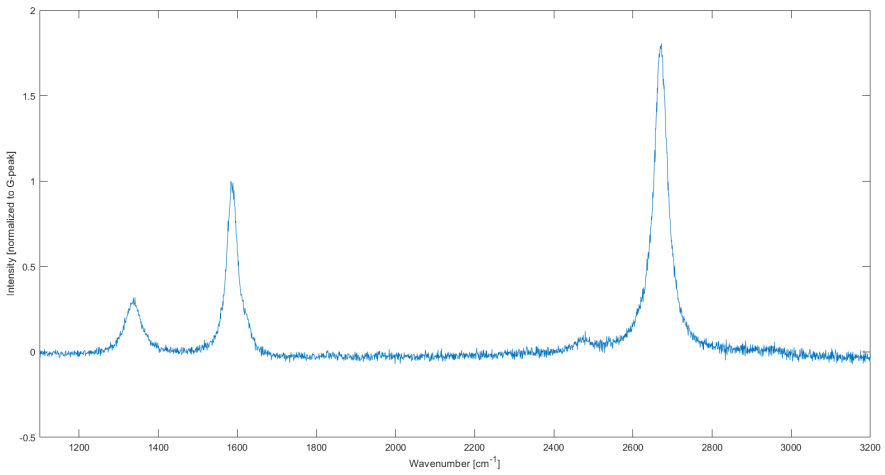

Figure D.9: Sample M2.5a

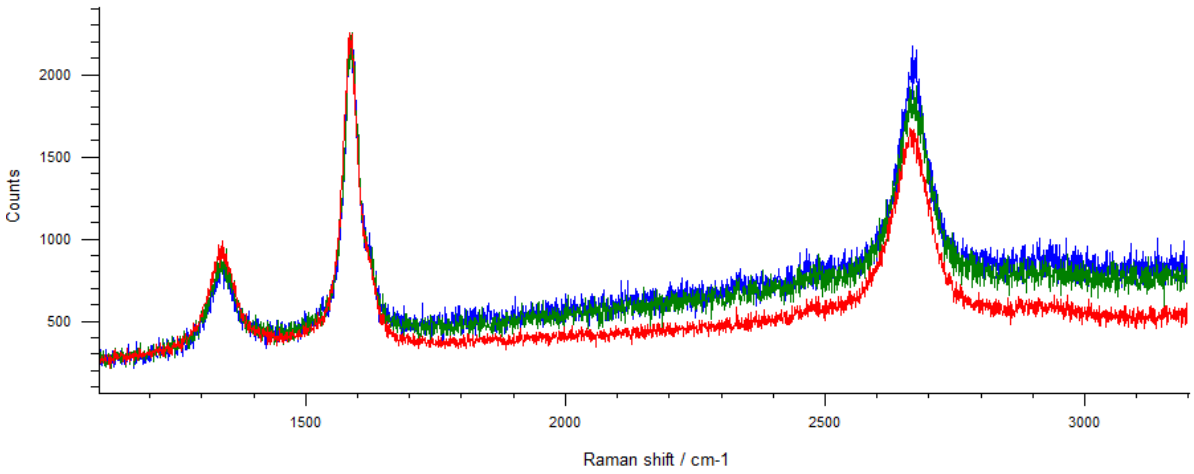

Figure D.10: Sample M2.5b

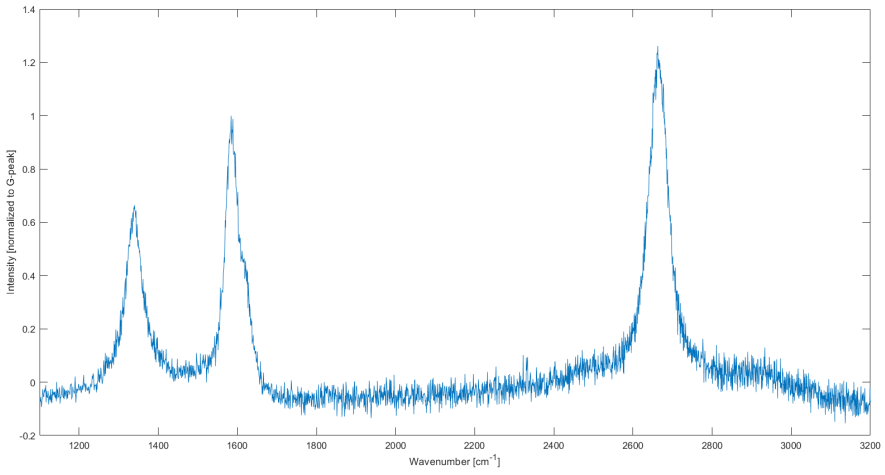

Figure D.11: Sample M2.6b

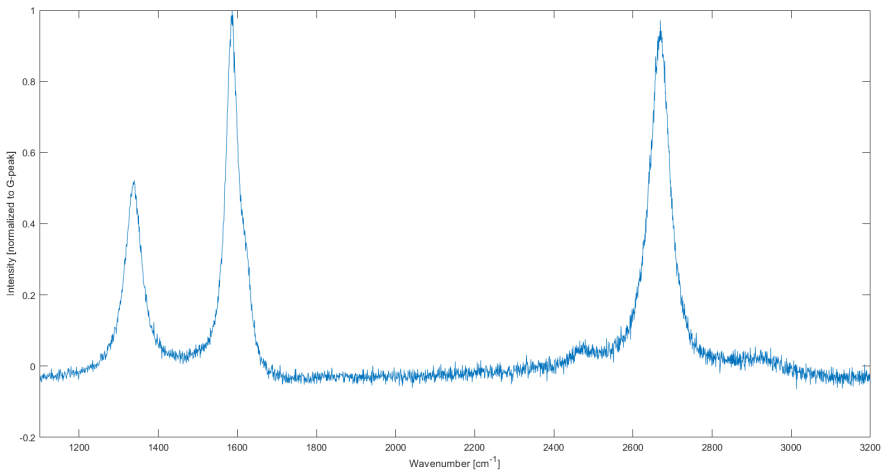

Figure D.12: Sample M2.7a

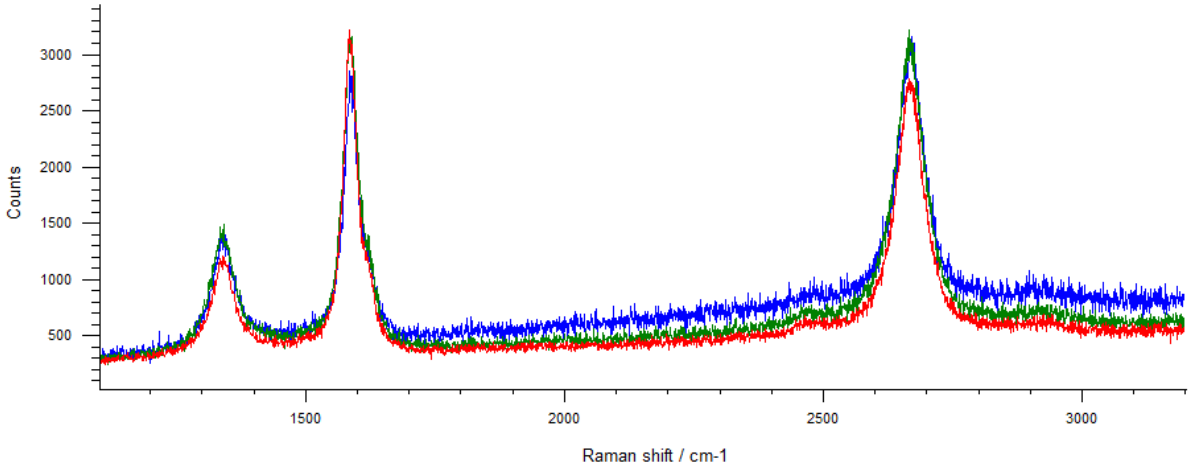

Figure D.13: Sample M2.7b

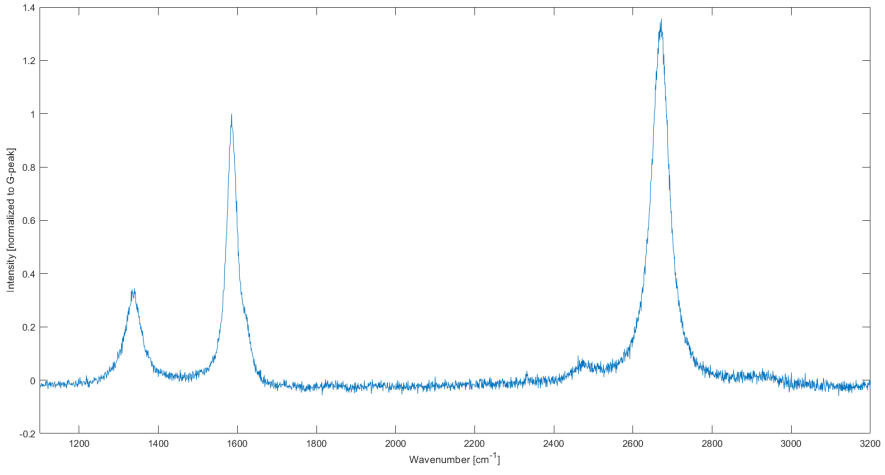

Figure D.14: Sample M2.8a

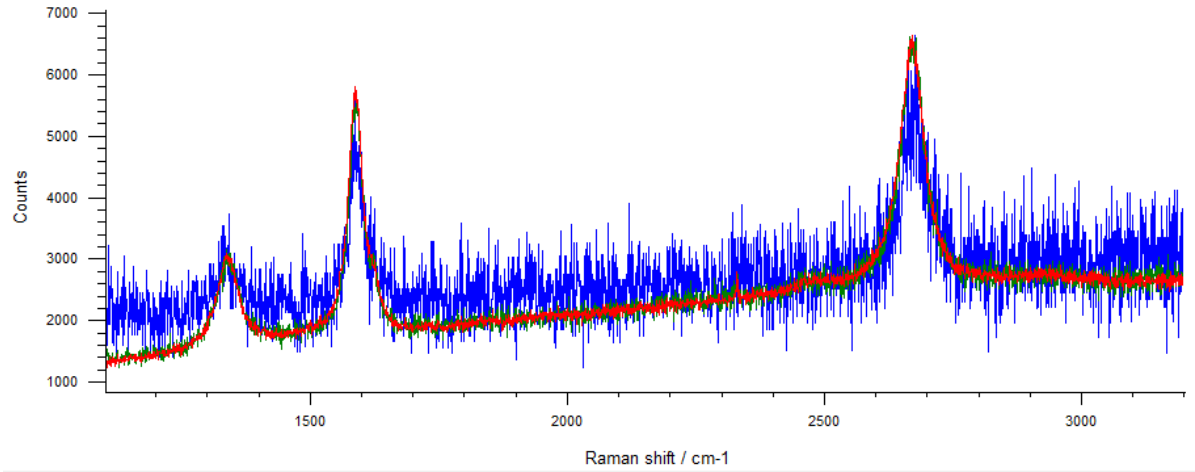

Figure D.15: Sample M3.1a

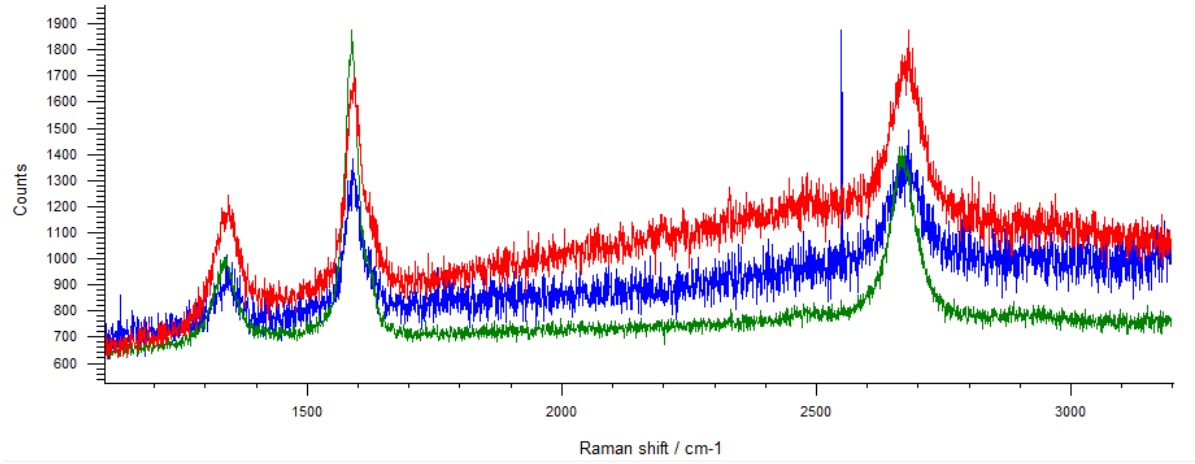

Figure D.16: Sample M3.1b

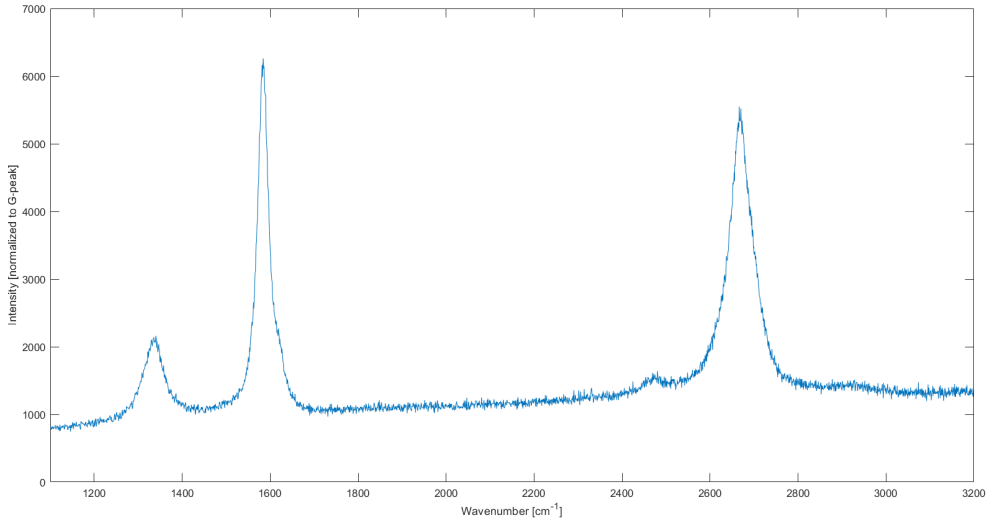

Figure D.17: Sample M3.2a

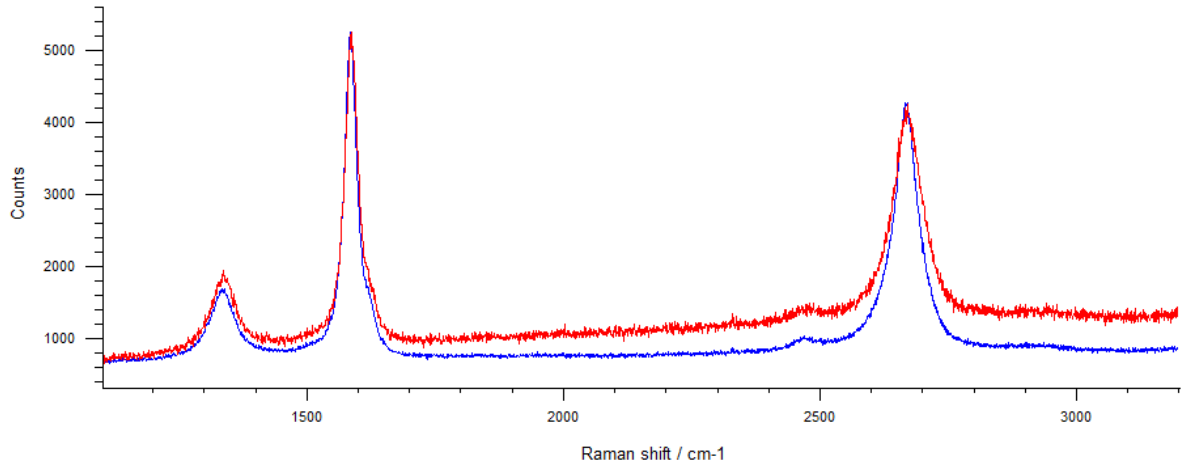

Figure D.18: Sample M3.2b

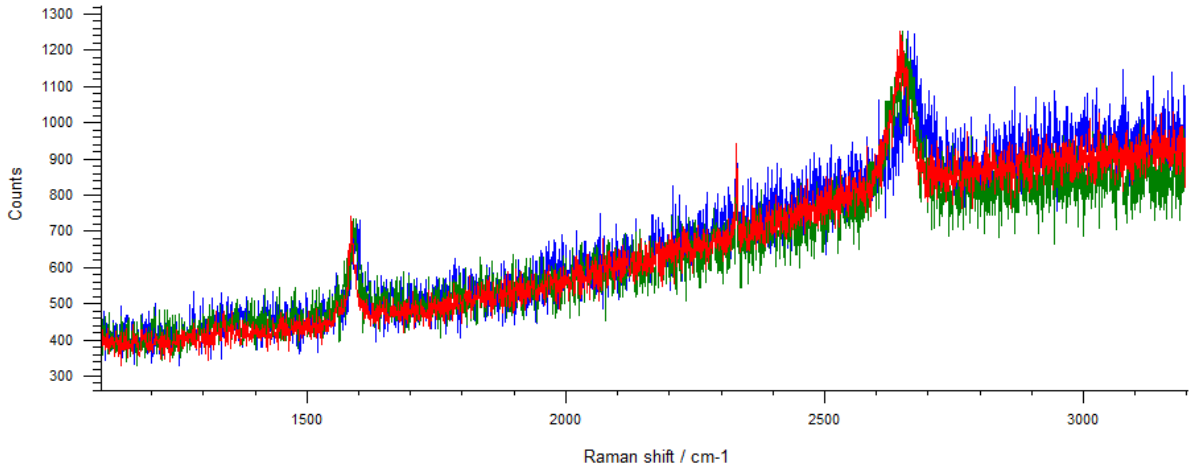

Figure D.19: Sample C1.1

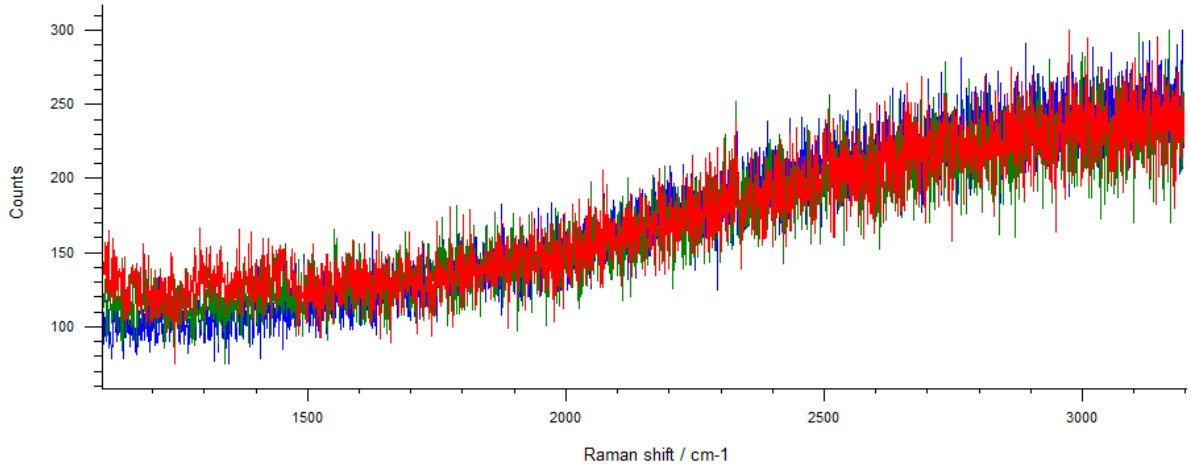

Figure D.20: Sample C1.2

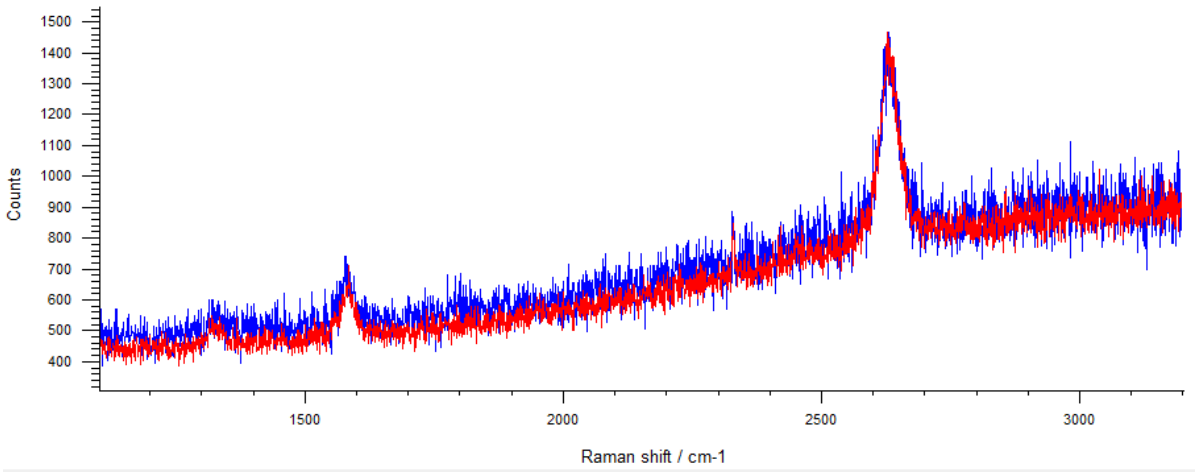

Figure D.21: Sample C1.3

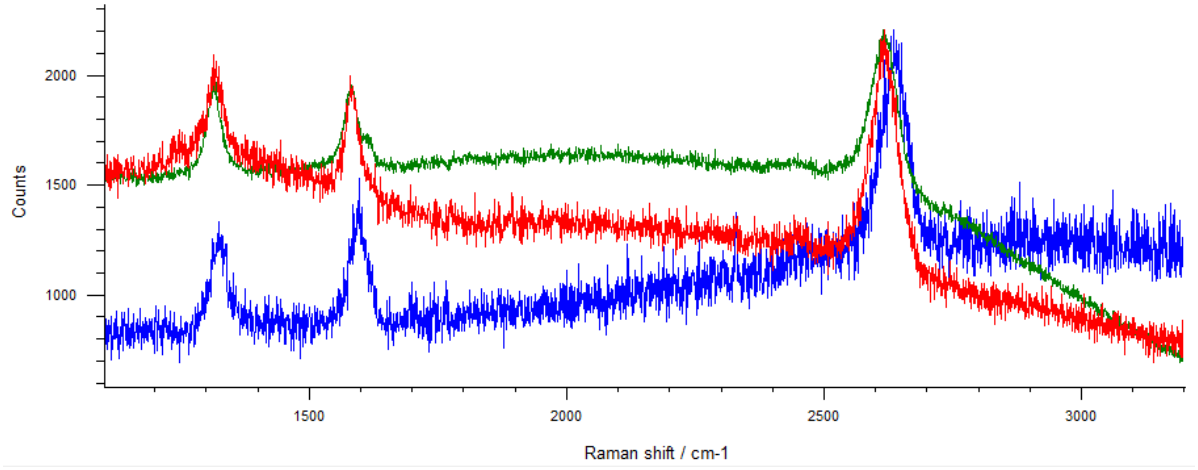

Figure D.22: Sample C1.4

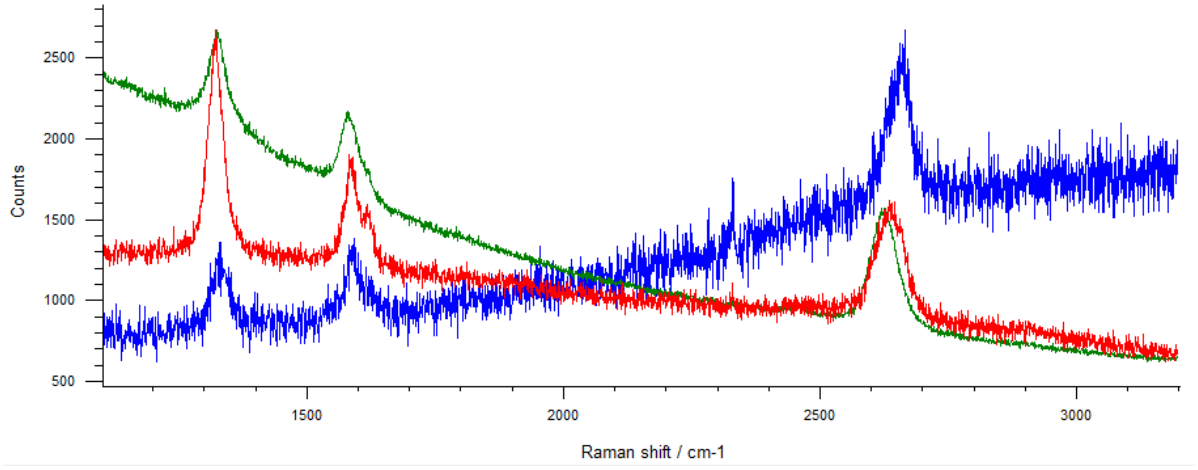

Figure D.23: Sample C1.5

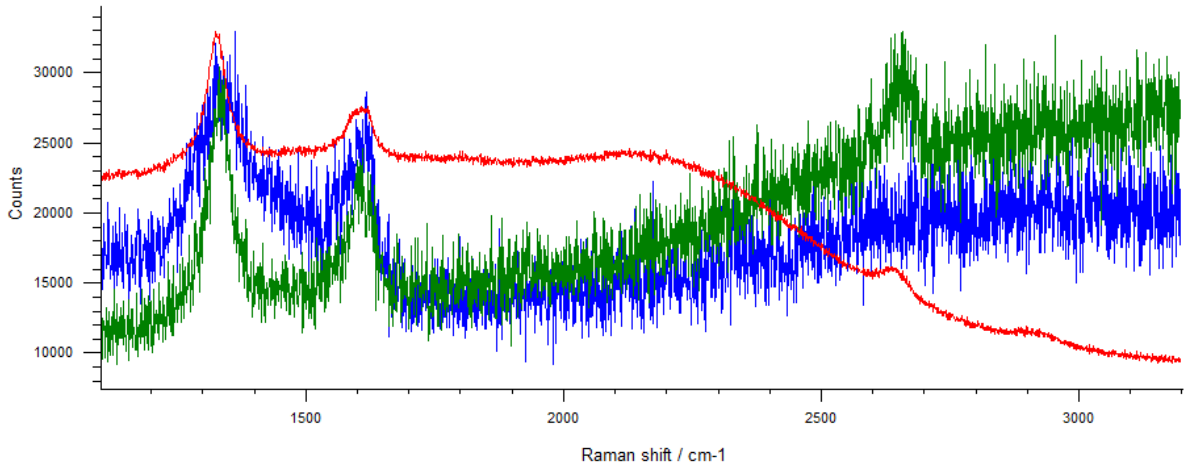

Figure D.24: Sample C1.6

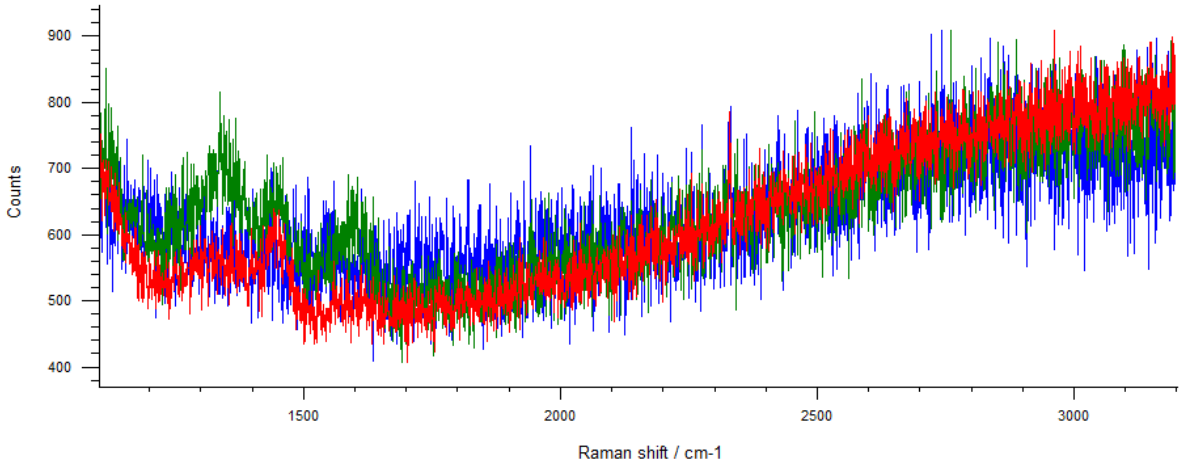

Figure D.25: Sample C1.7

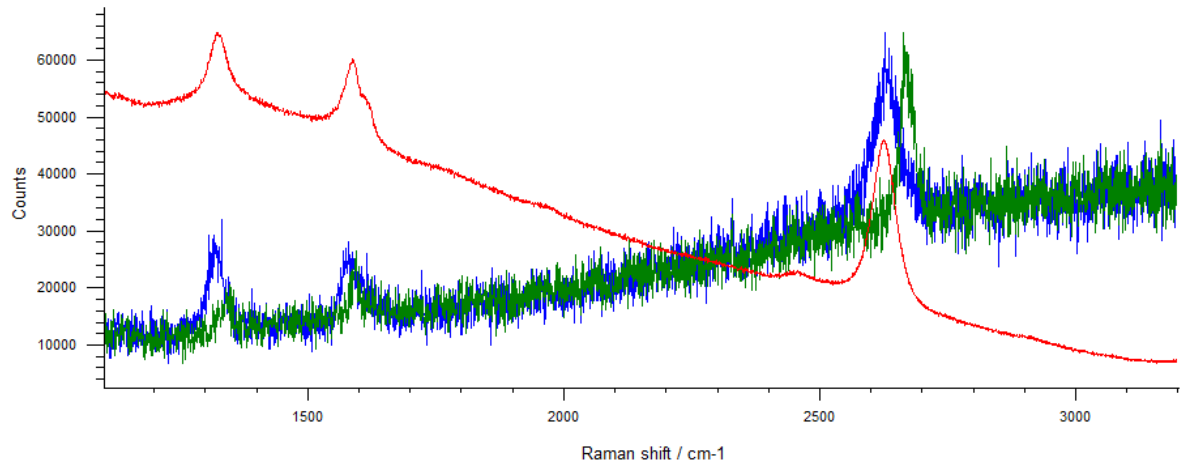

Figure D.26: Sample C1.8

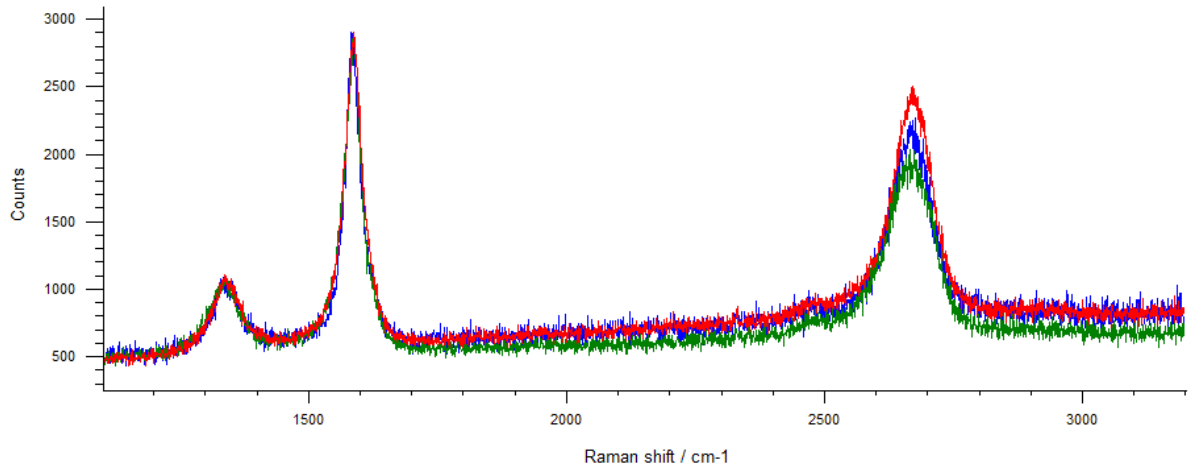

Figure D.27: Sample N1.1

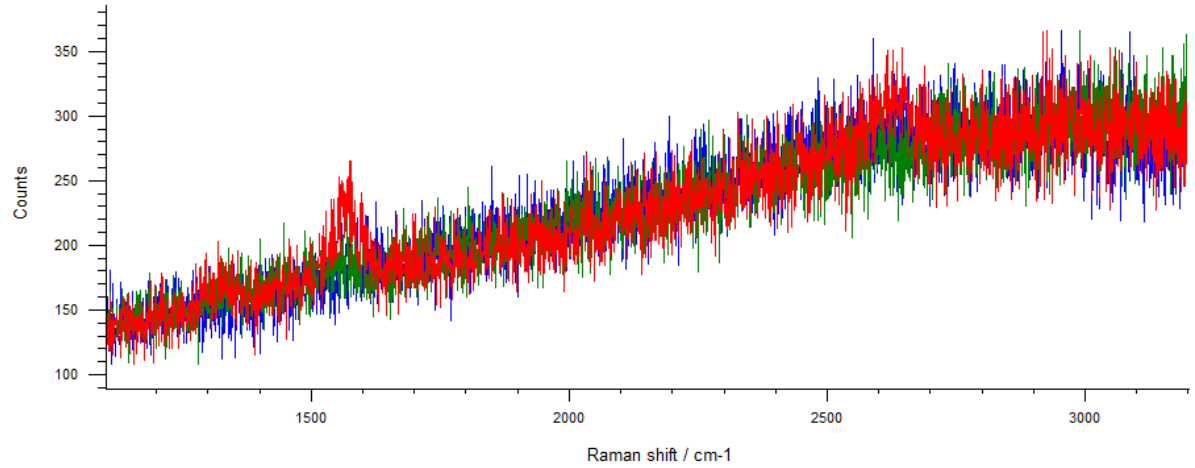

Figure D.28: Sample N1.2

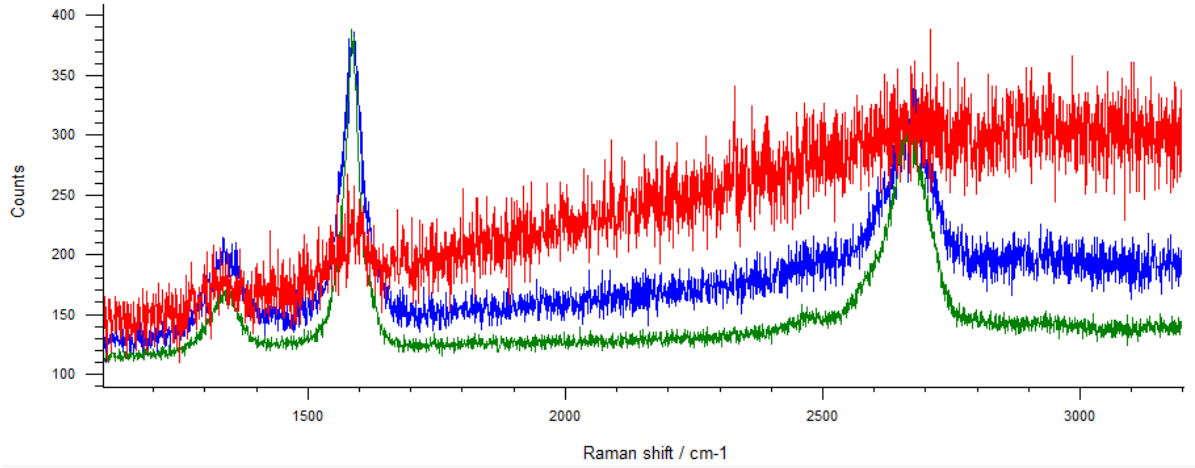

Figure D.29: Sample N1.3

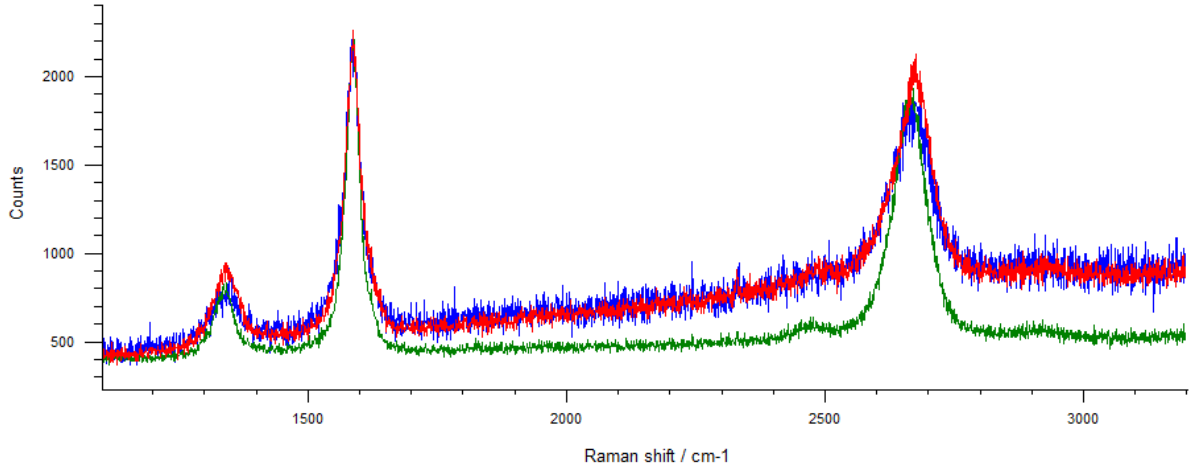

Figure D.30: Sample N1.4

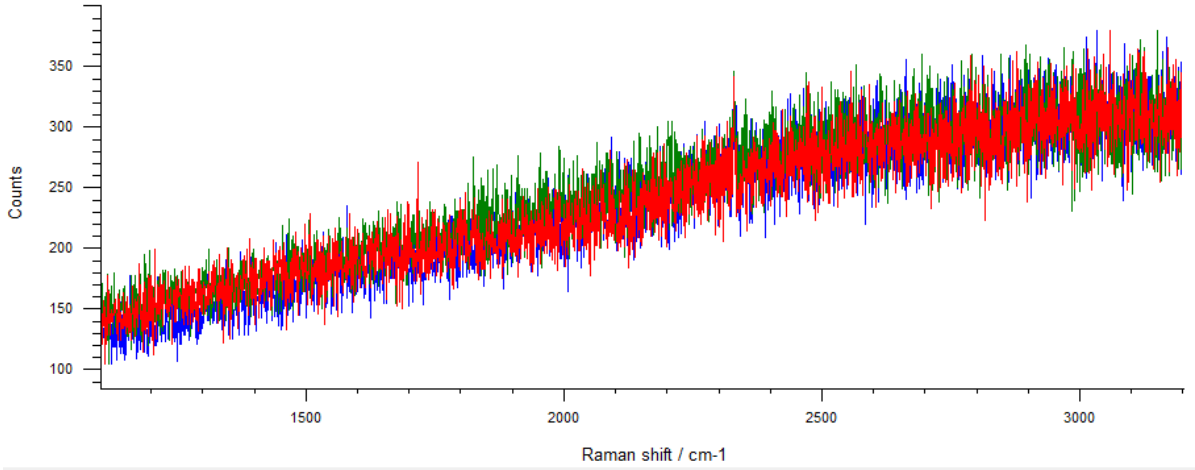

Figure D.31: Sample N1.5

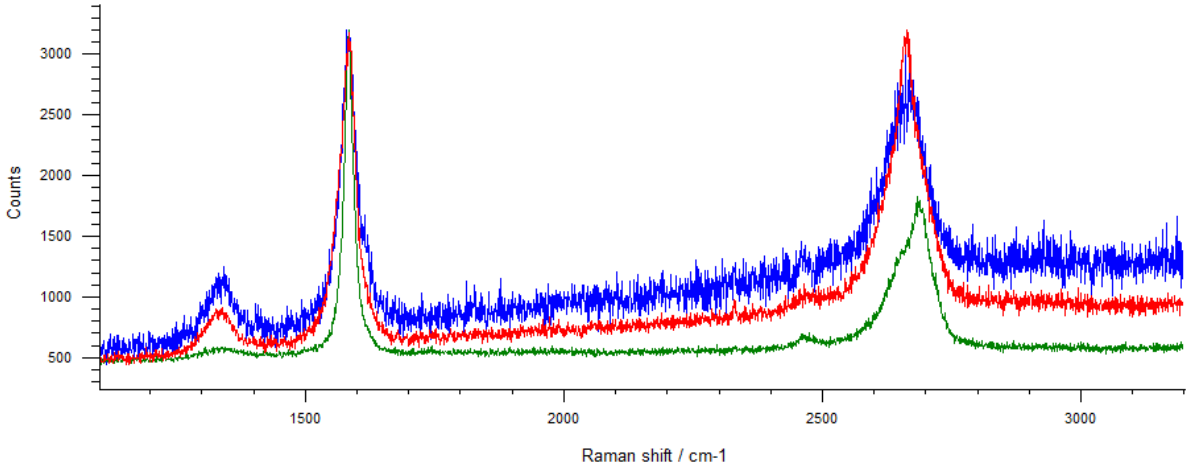

Figure D.32: Sample N1.6

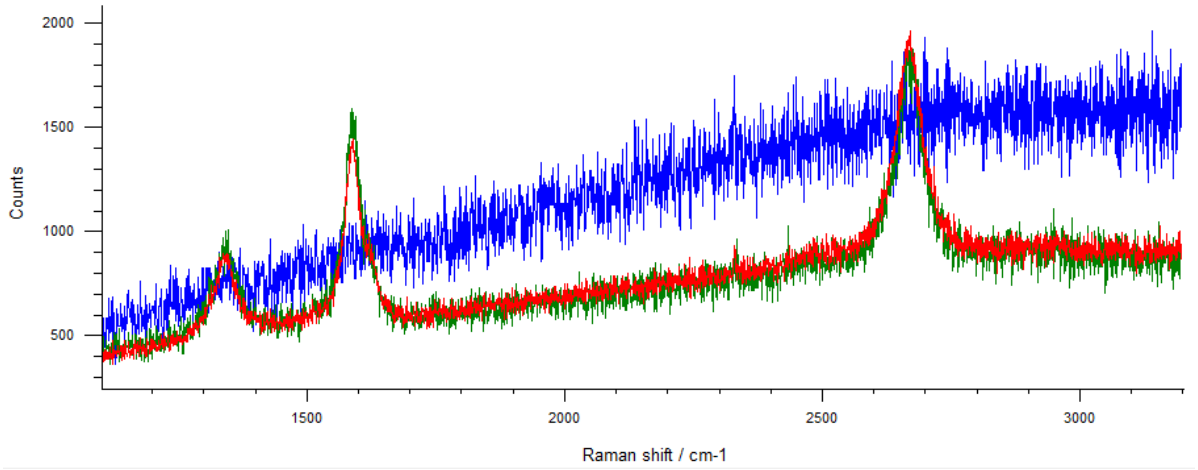

Figure D.33: Sample MP1.4

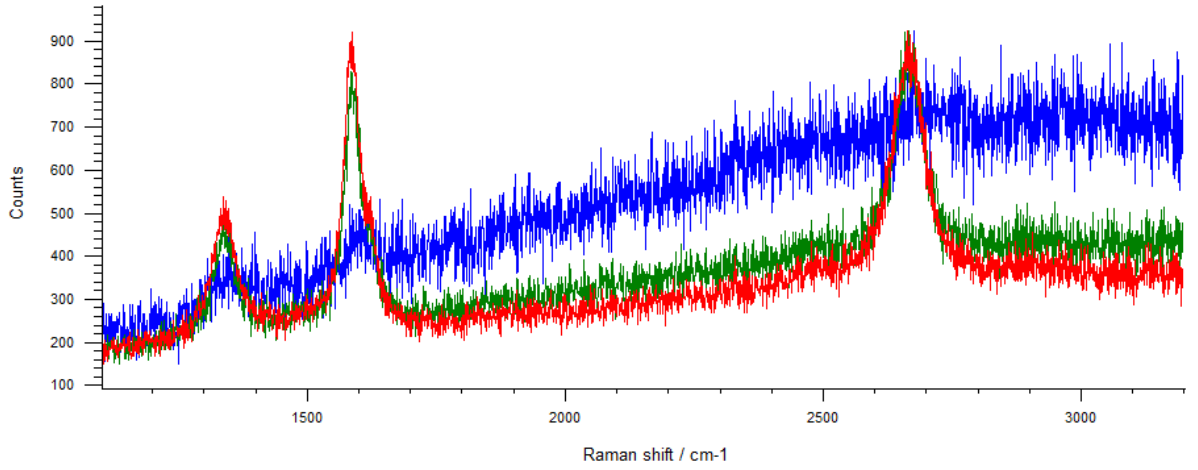

Figure D.34: Sample MP1.5

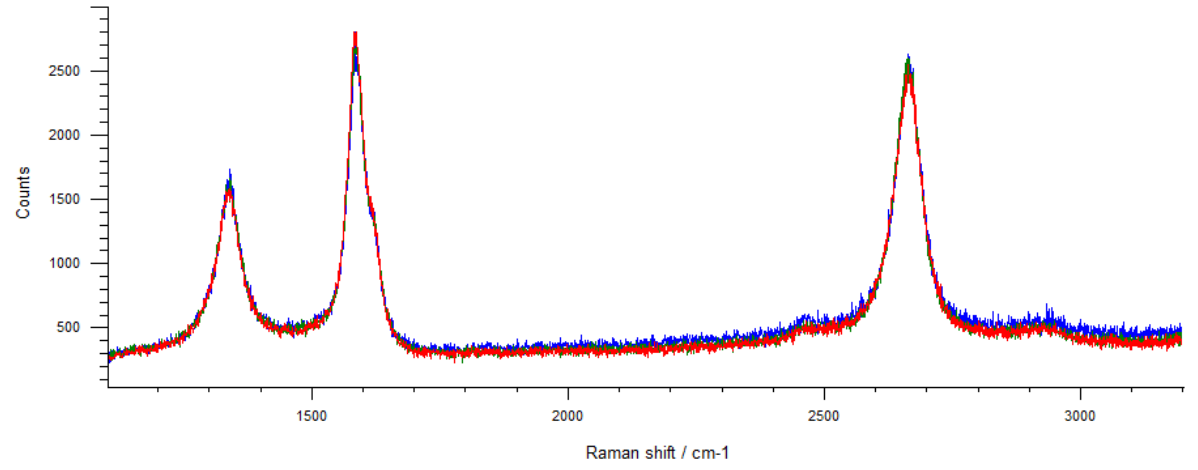

Figure D.35: Sample MP1.6

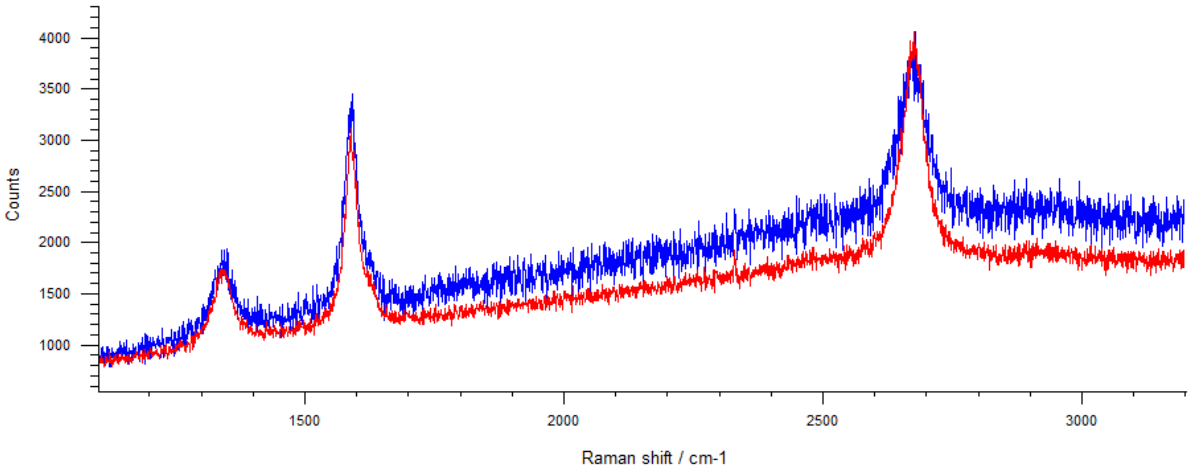

Figure D.36: Sample MP1.9

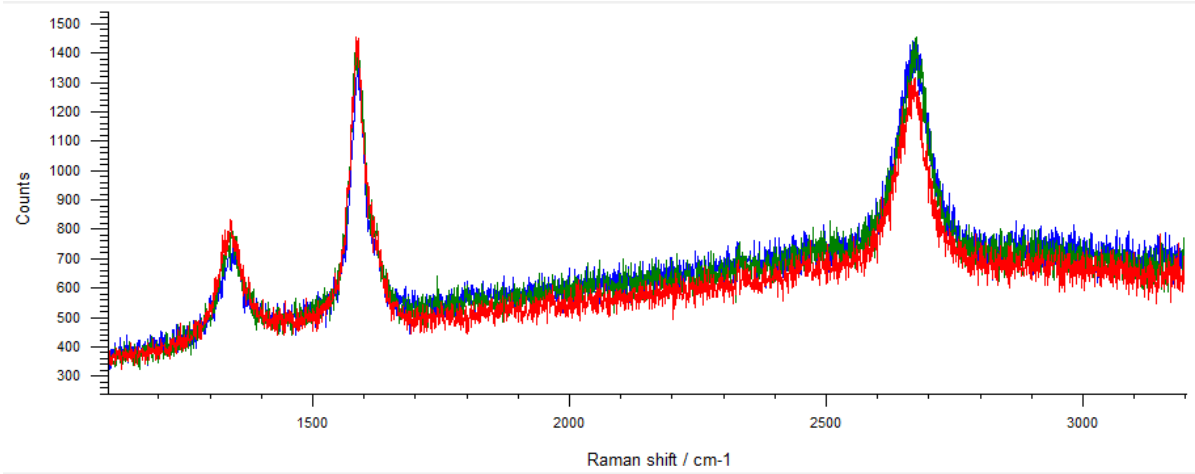

Figure D.37: Sample MP1.10

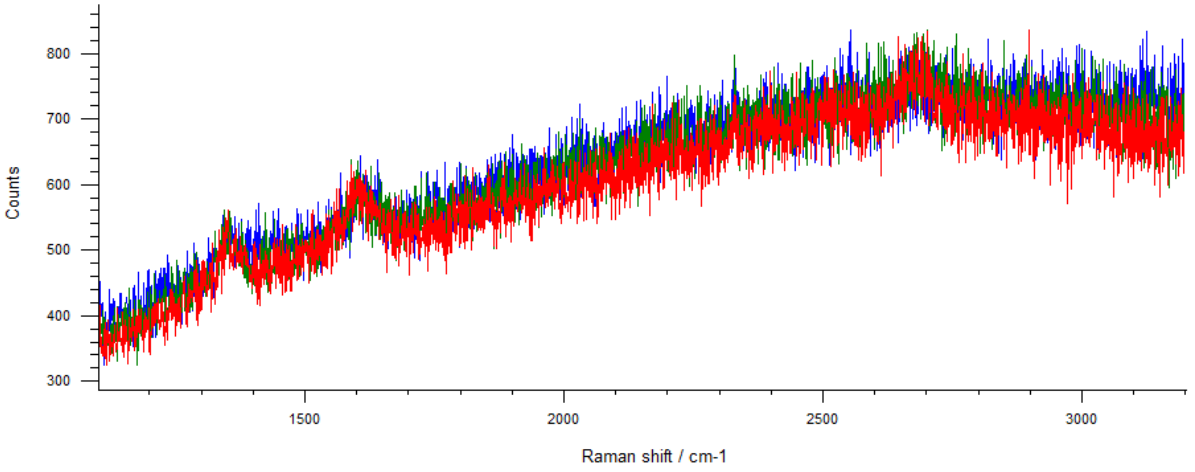

Figure D.38: Sample MP2.1

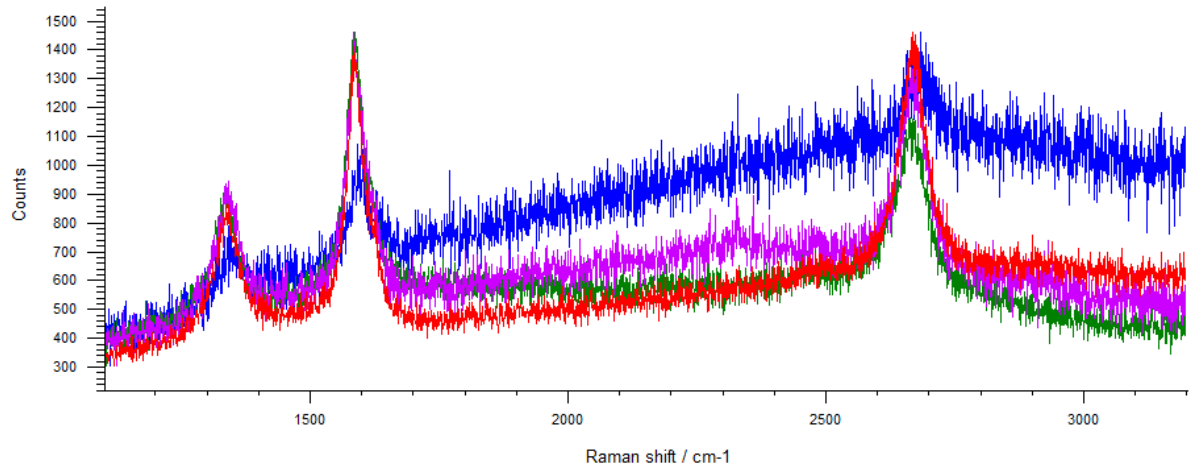

Figure D.39: Sample MP2.2

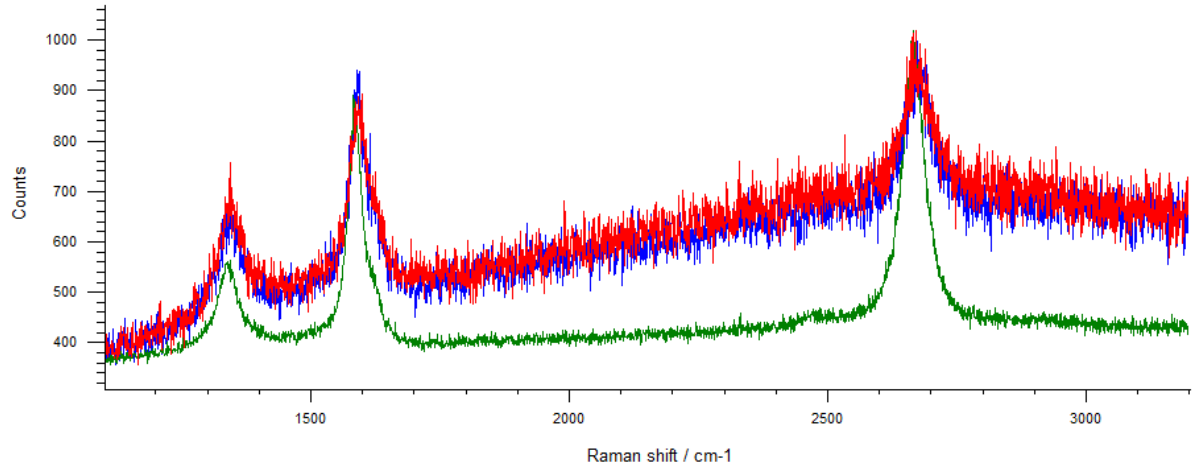

Figure D.40: Sample MP2.3

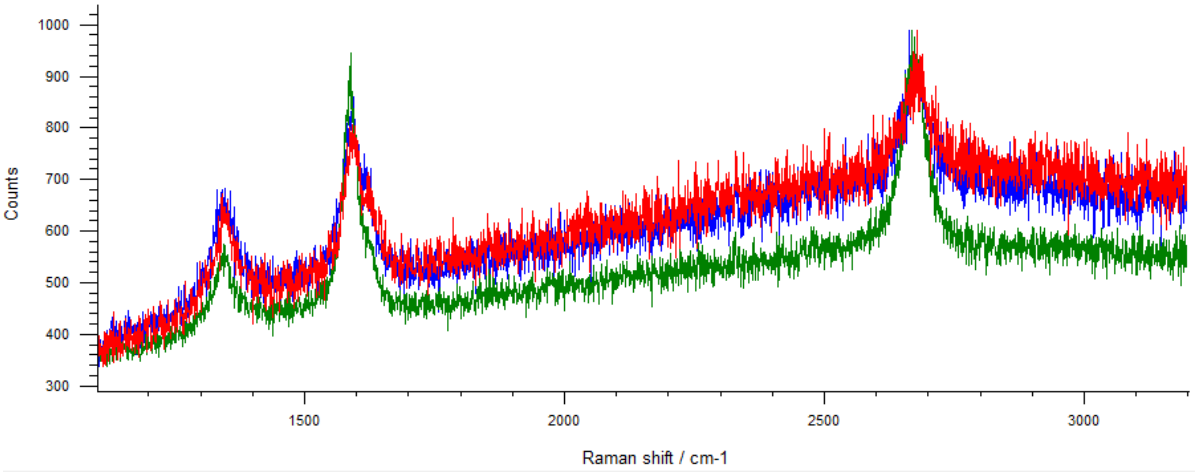

Figure D.41: Sample MP2.4

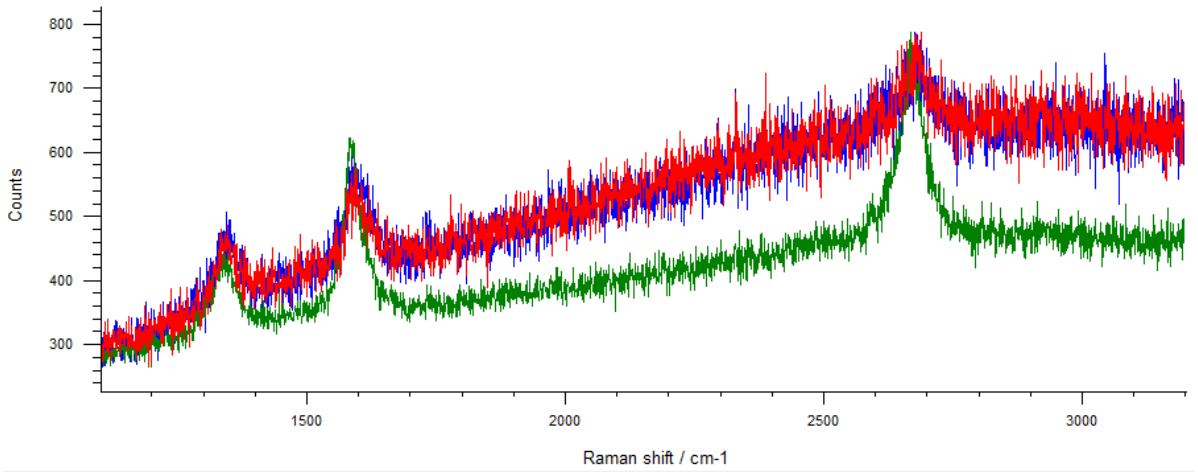

Figure D.42: Sample MP2.5

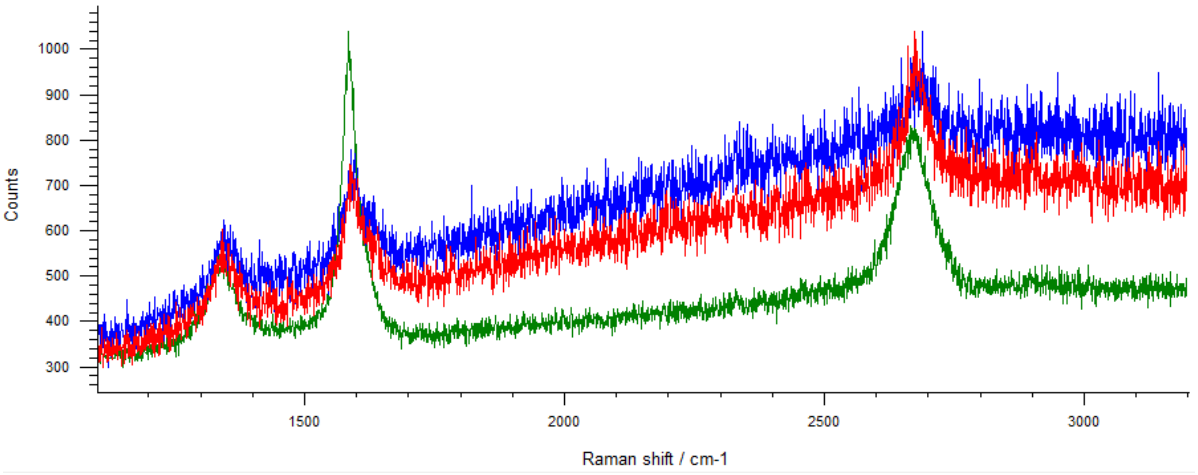

Figure D.43: Sample MP2.6

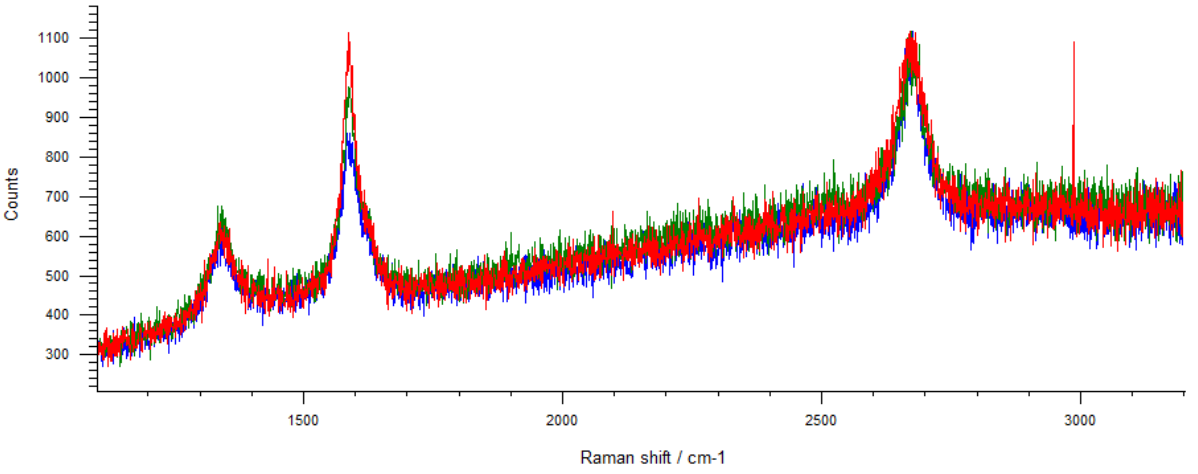

Figure D.44: Sample MP2.8

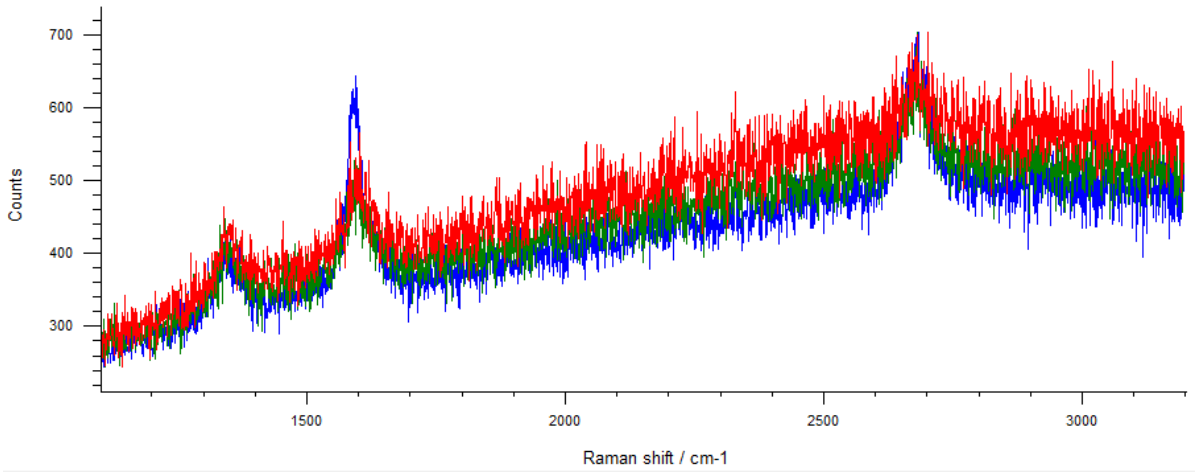

Figure D.45: Sample MP2.10

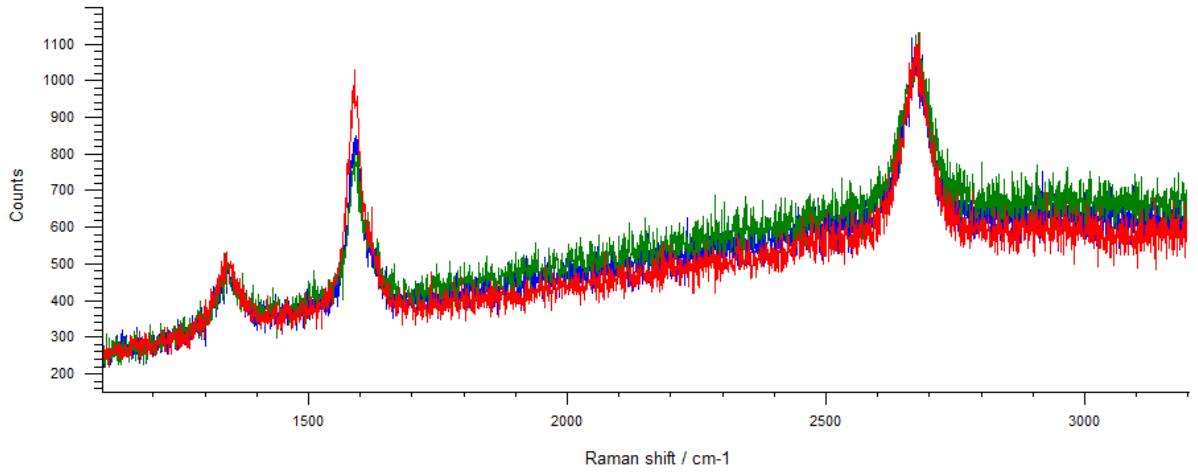

Figure D.46: Sample MP2.11

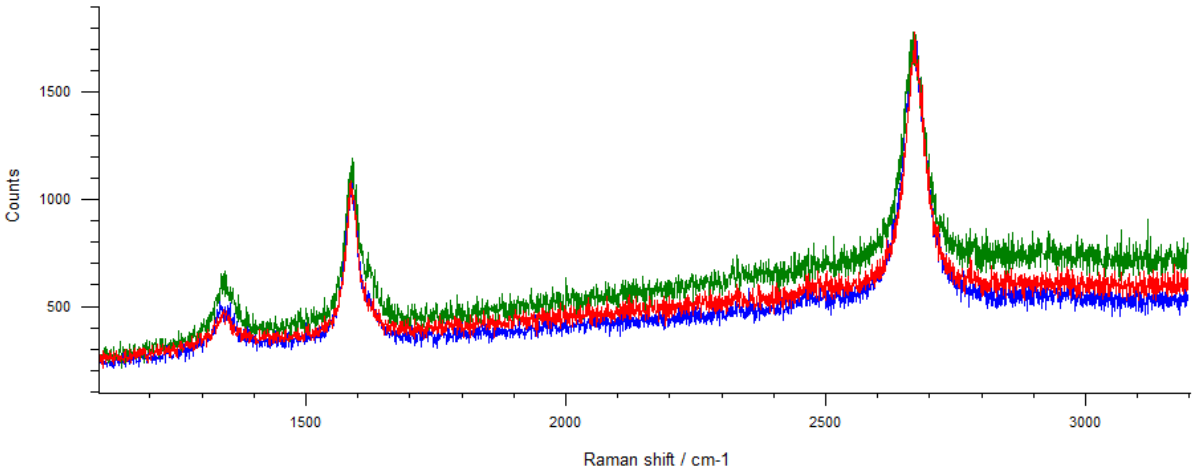

Figure D.47: Sample MP2.12

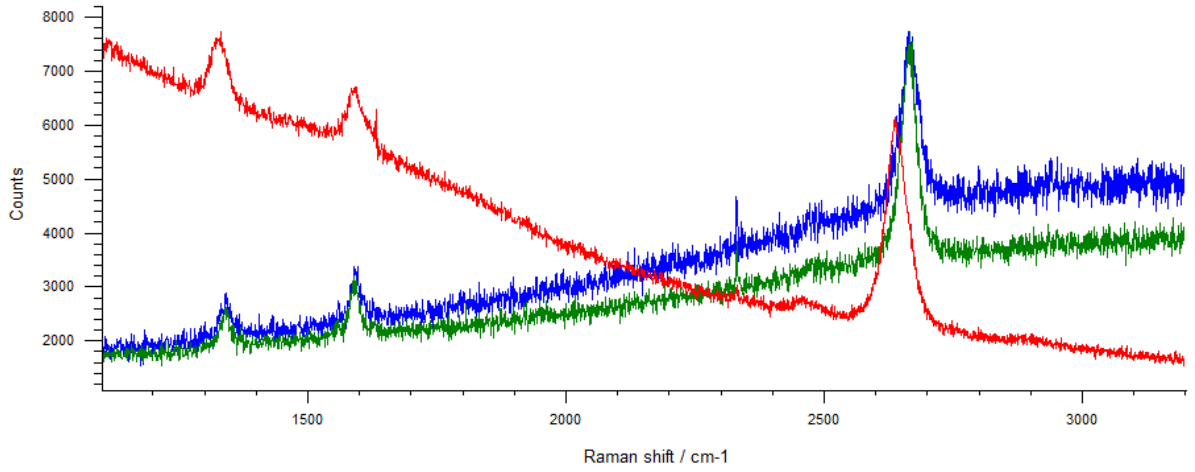

Figure D.48: Sample CP1.1

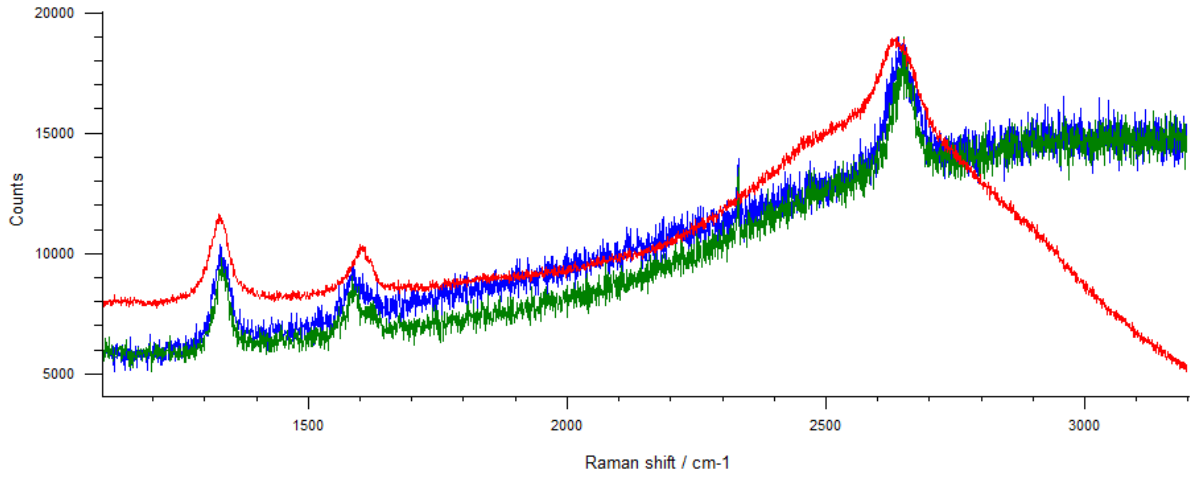

Figure D.49: Sample CP1.2

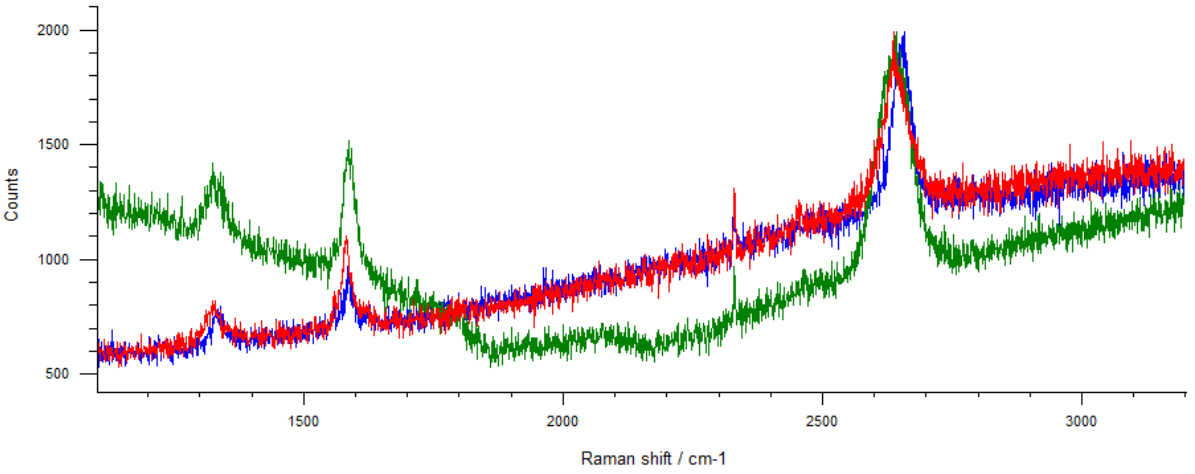

Figure D.50: Sample CP1.3

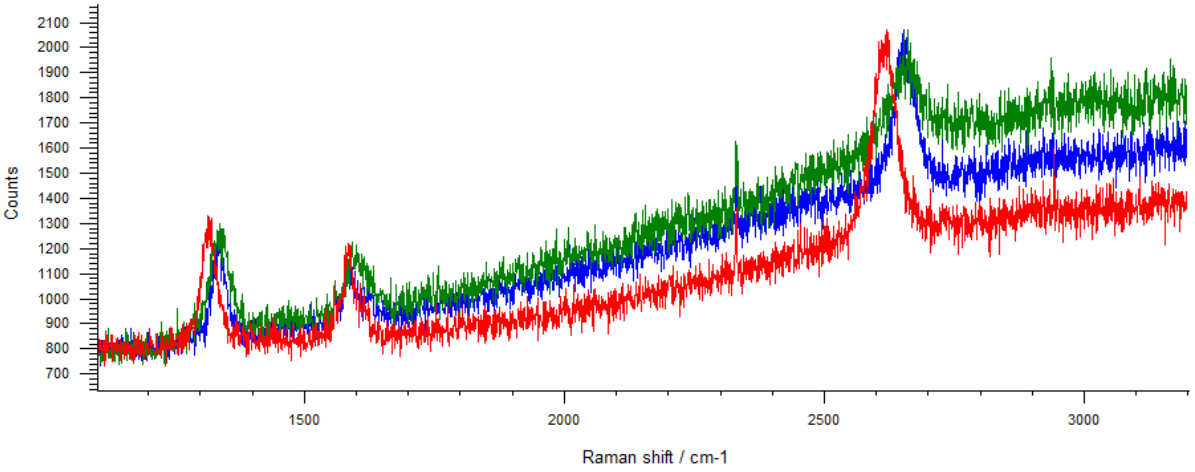

Figure D.51: Sample CP1.4

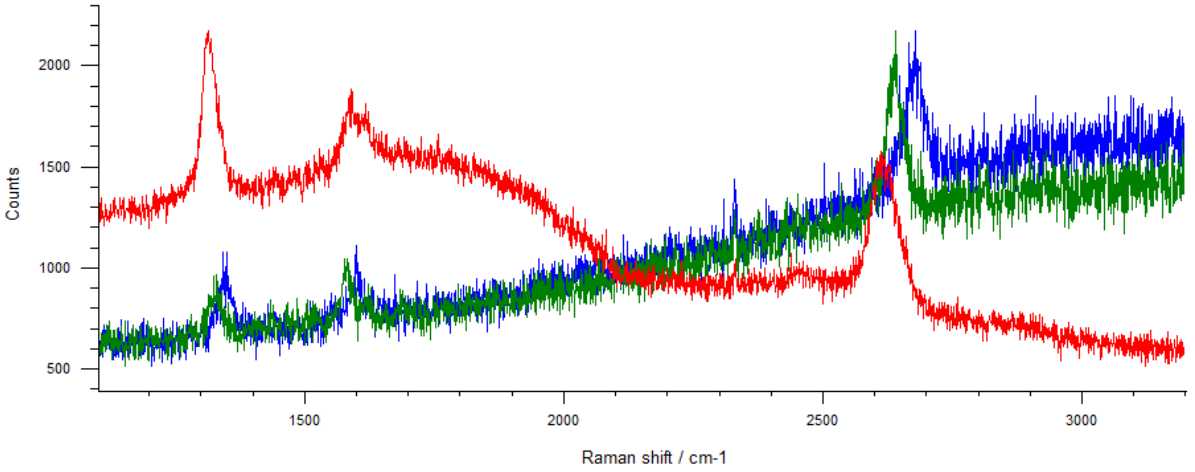

Figure D.52: Sample CP1.5

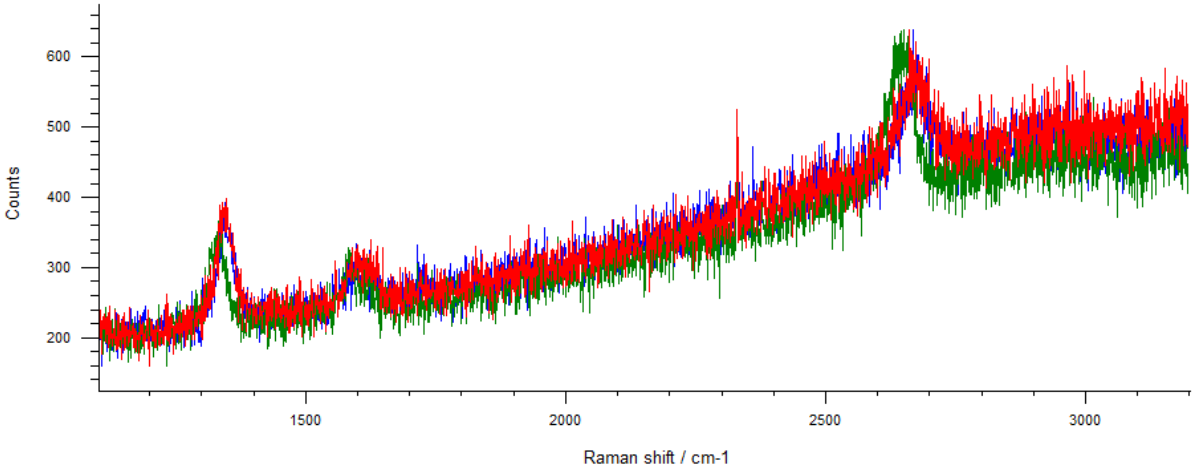

Figure D.53: Sample CP1.6

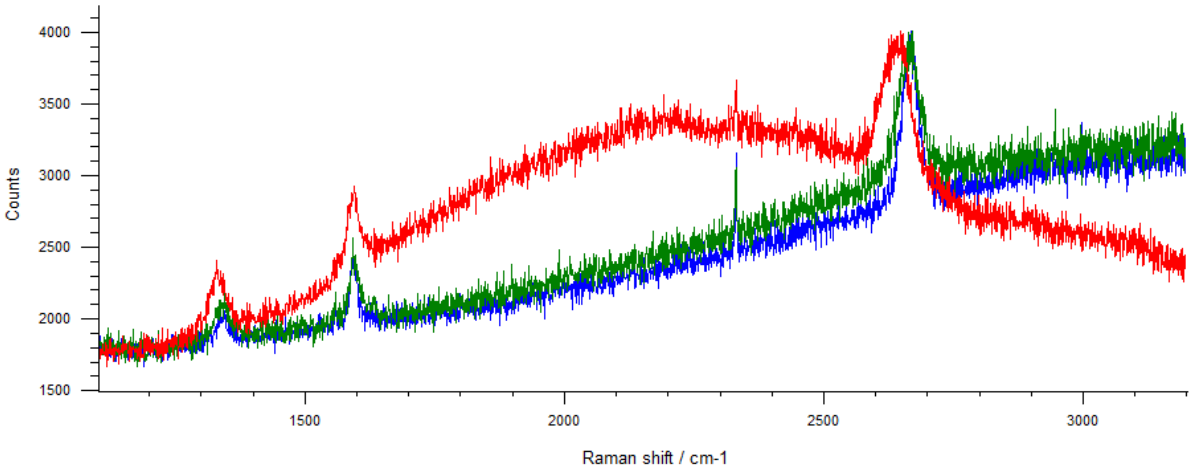

Figure D.54: Sample CP1.7

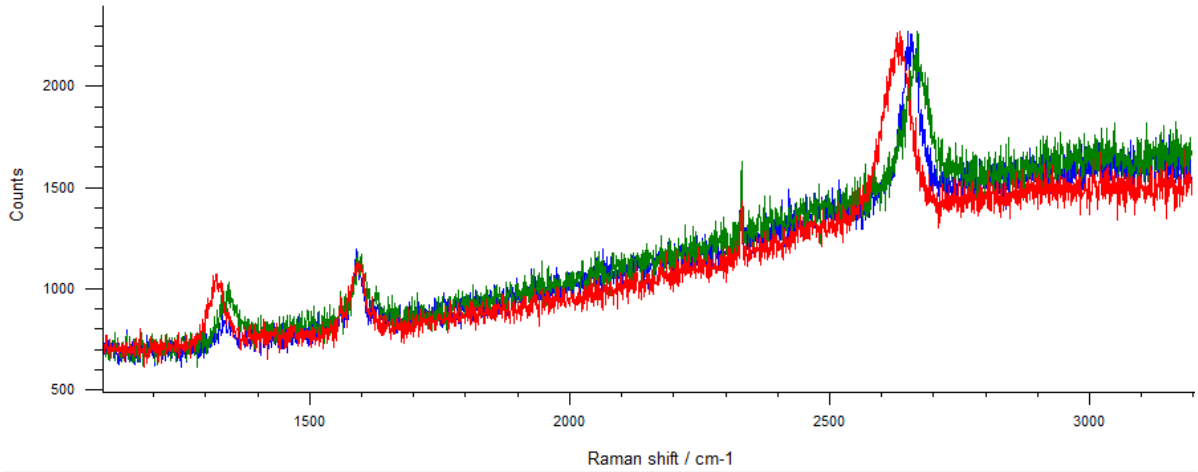

Figure D.55: Sample CP1.8

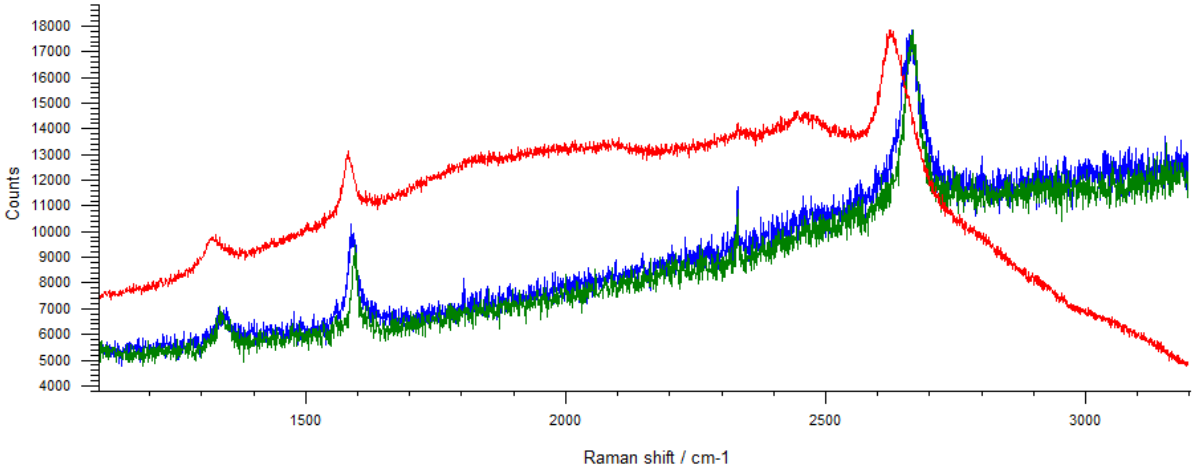

Figure D.56: Sample CP1.9

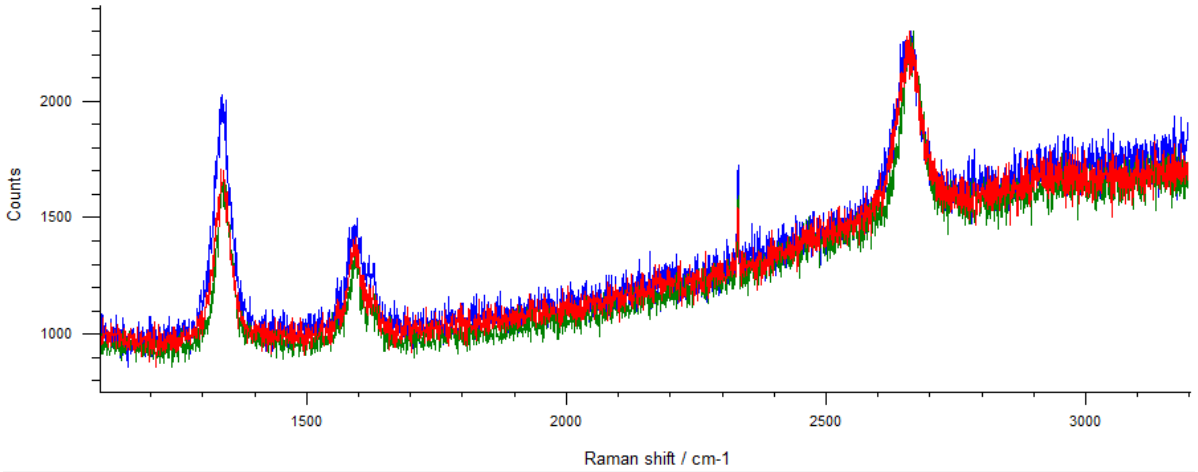

Figure D.57: Sample CP1.10

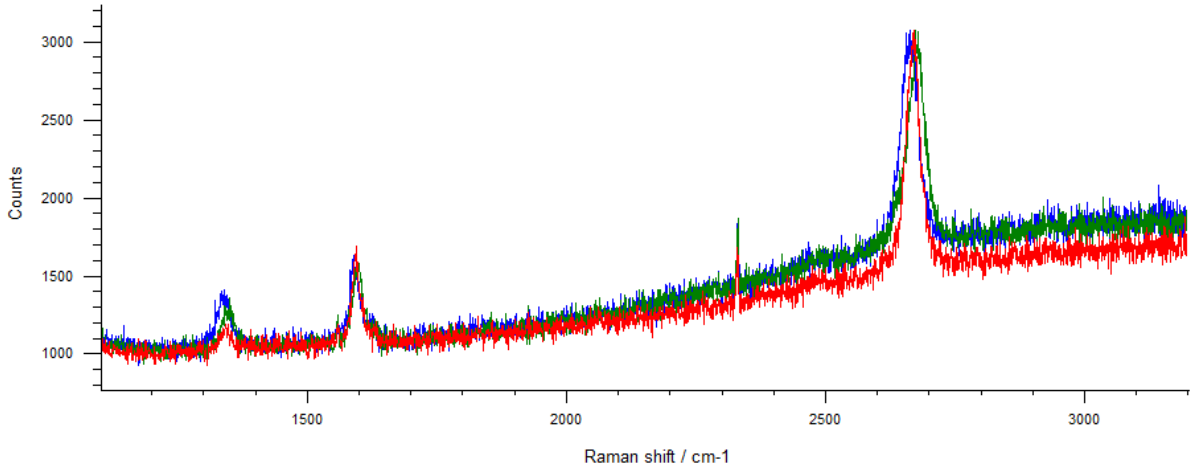

Figure D.58: Sample CP1.11

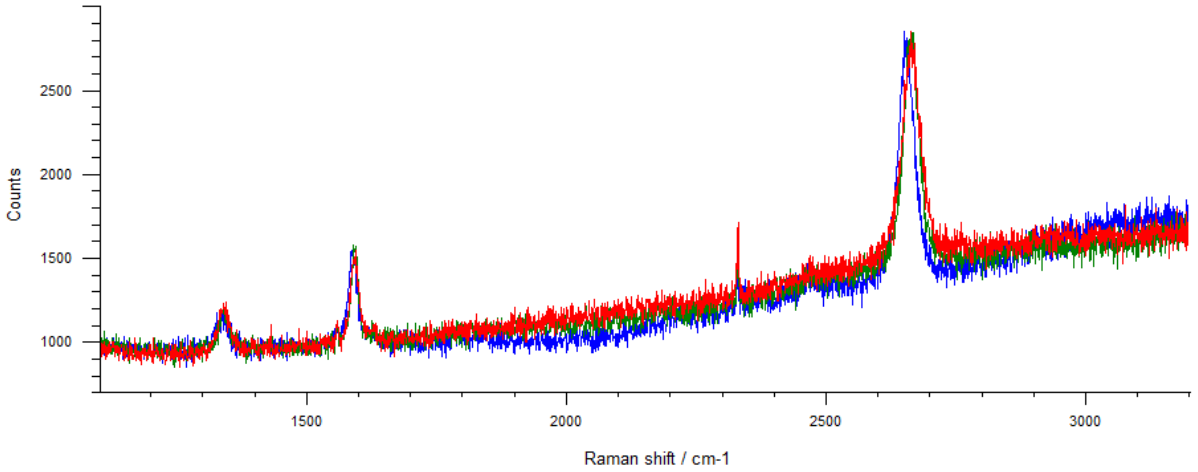

Figure D.59: Sample CP1.12